الجمهورية الجزائرية الديمقراطية الشعبية

République Algérienne Démocratique et Populaire

Ministère de L'Enseignement Supérieur et de la Recherche Scientifique



UNIVERSITÉ SETIF 1 FERHAT ABBAS

FACULTÉ DE TECHNOLOGIE

THÈSE

Présentée au Département d'Electrotechnique

Pour l'obtention du diplôme de

DOCTORAT

Domaine : Sciences et Technologie

Filière: Electrotechnique **Option: Réseaux Electriques**

Par

M. GUETTAF Nacereddine

THÈME

Modélisation du mécanisme de chargement électrique dans les séparateurs électrostatiques

Soutenue le 10/03/2026 devant le Jury:

M. BAYADI Abdelhafid	**Professeur**	**Univ. Sétif 1Ferhat Abbas**	**Président**
M. NOURI Hamou	**Professeur**	**Univ. Sétif 1Ferhat Abbas**	**Directeur de thèse**
M. ZEGHLOUL Thami	**Professeur**	**Univ. Poitiers - France**	**Co-Directeur**
M. GHERBI Ahmed	**Professeur**	**Univ. Sétif 1Ferhat Abbas**	**Examinateur**
M. MOULAI Hocine	**Professeur**	**Univ. S.T. Houari Boumediene**	**Examinateur**
M. BOUMOUS Samira	**MCA**	**Univ. M.C. Messaidia Souk Ahras**	**Examinatrice**

الجمهورية الجزائرية الديمقراطية الشعبية

Democratic and Popular Republic of Algeria

Ministry of Higher Education and Scientific Research

Université Ferhat ABBAS Sétif 1

UNIVERSITY SETIF 1 FERHAT ABBAS

FACULTY OF TECHNOLOGY

THESIS

Presented to the Department of Electrical Engineering

To obtain the diploma of

DOCTORATE

Field: Science and Technology

Sector: Electrical Engineering **Option: Electrical Networks**

By

M. GUETTAF Nacereddine

THEME

Modeling of the electrical charging mechanism in electrostatic separators

Defended on 10/03/2026 before the Jury:

M. BAYADI Abdelhafid	**Professeur**	**Univ. Setif 1 Ferhat Abbas**	**Chair of committee**
M. NOURI Hamou	**Professor**	**Univ. Setif 1 Ferhat Abbas**	**Supervisor**
M. ZEGHLOUL Thami	**Professor**	**Univ. Poitiers - France**	**Co- Supervisor**
M. GHERBI Ahmed	**Professor**	**Univ. Setif 1Ferhat Abbas**	**Examiner**
M. MOULAI Hocine	**Professor**	**Univ. S.T. Houari Boumediene**	**Examiner**
M. BOUMOUS Samira	**PHD**	**Univ. M.C. Messaidia Souk Ahras**	**Examiner**

DEDICATION

I hereby dedicate this work:

To my dear parents,

To my dear brothers, sister and wife,

To my entire family,

To all those who know me near or far.

THANKS

Firstly, I am thankful to “ALLAH”, the Almighty, for granting me the strength to continue, as well as the audacity to overcome all difficulties to complete this work.

I am very grateful to Mr. NOURI Hamou, Professor at the University of Setif 1 Ferhat Abbas, who supervised me and believed in my abilities throughout this thesis. His help and advice were invaluable in finalizing this work. I express my sincere thanks to him for his patience, availability, generosity, understanding and efficiency, which allowed me to complete this work, as well as for often sharing his vast experience with me.

My thanks also go to the thesis co-director Mr. ZEGHLOUL Thami, Professor at the University of Poitiers - France, for having provided good direction and supervision This work.

I express my gratitude to Mr. BAYADI Abdelhafid, Professor at the University of Setif 1 Ferhat Abbas, for agreeing to judge this work and for doing me the honor of chairing the defense jury.

I express my gratitude to Mr. GHERBI Ahmed, Professor at the University of Setif 1 Ferhat Abbas, Mr. MOULAI Houcine, Professor at the University of Sciences and Technology Houari Boumediene of Algiers and Mrs. BOUMOUS Samira, PHD at the University of Souk Ahras, for having agreed to examine this work and to participate in the defense jury.

My sincere thanks, to my dear teachers without exception, my loved ones for their encouragement and for their support and presence at my side. Without forgetting my colleagues, in the field of research and during the formation at the Setif university.

Finally, I extend my sincere thanks to all those who have contributed, directly or indirectly, to the completion of this work.

Summary

DEDICATION i
THANKS ii
SOMMARY iii
LIST OF FIGURES iv
LIST OF TABLES v
LIST OF ACRONYMS AND SYMBOLS vi

GENERAL IINTRODUCTION 1

CHAPTER I
GENERAL INFORMATION ON ELECTROSTATIC SEPARATION

I.1 Introduction 4
I.2 Problem of waste electrical and electronic equipment 4
I.3 Environmental impacts of non-recycled WEEE 6
I.3.1 Soil and water pollution 8
I.3.2 Air quality degradation 8
I.3.3 Loss of natural resources 8
I.4 Impact of WEEE recycling on the circular economy 9
I.5 Electrostatic separator 9
I.5.1 Physical mechanisms of electrical charging of powdered materials 10
I.5.2 Corona effect 11
I.5.2.1 Description 11
I.5.2.2 Charging devices 13
I.5.3 Electrostatic induction 14
I.5.3.1 Description 14
I.5.3.2 Charging devices 15
I.5.4 Triboelectric effect 16
I.5.5 Electrostatic separation installations for powdered materials 18
I.5.5.1 Conveyor belt tribo-electrostatic separator 18
I.5.5.2 Multifunction electrostatic conveyor belt separator 18
I.5.5.3 Tribo-aero-electrostatic separator with two metal disks 20
I.5.5.4 Electrostatic separator with two vertical electrodes 21
I.6 Conclusion 22

CHAPTER II
STUDY THE CORONA DISCHARGE PARAMETERS

II.1 Introduction 23
II.2 Corona discharge physics 23
II.3 Corona discharge mechanism 24
II.4 Different types of corona discharge 26
II.4.1 Positive corona 27
II.4.2 Negative corona 29
II.5 Numerical simulation of corona discharge in the point-plane configuration 30
II.5.1 Geometric description 30
II.5.2 Solution method flow chart 31
II.5.3 Results and discussion 32
II.5.3.1 Mesh grid 32
II.5.3.2 Electric potential 32
II.5.3.3 Electric field 33
II.5.3.4 Electric displacement 34
II.5.3.5 Current density 36
II.5.3.6 Space charge density 37
II.6 Conclusion 39

CHAPTER III
MODELING THE SEPARATION OF FINE PARTICLES BY CORONA EFFECT

III.1 Introduction 40
III.2 Principle of electrostatics applied to air filtration and material separation 40
III.3 Mathematical modelling 42
III.3.1 Geometric description of the problem 42
III.3.2 Governing equations 43
III.3.3 Boundary conditions 43
III.3.4 Proposed method of analysis 43
III.3.5 Matrix formulations of the finite element method 45
III.4 Results and discussion 46
III.4.1 Numerical determination of the mesh grid 47

III.4.2 Electric potential 48
III.4.3 Electric field 48
III.4.4 Current density 49
III.4.5 Space charge density 50
III.4.6 Particle charging 51
III.4.7 Migration velocity 53
III.4.8 Collection efficiency 55
III.5 Conclusion 57

CHAPTER IV

INVESTIGATION OF PARTICALES TRAJECTORIES IN MULTIFONCTIONAL ELECTROSTATIC SEPARATOR

IV.1 Introduction 59
IV.2 Multifunctional electrostatic separator description 59
IV.3 Numerical modeling 62
IV.3.1 Photovoltaic panel modeling 62
IV.3.2 Electrical field modeling 63
IV.3.3 Modeling the particles trajectories 63
IV.4 Results and discussion 64
IV.4.1 Photovoltaic characteristics 66
IV.4.2 Electric field variation 68
IV.4.2.1 Electrical charging zone 70
IV.4.2. Electrostatic separation zone 71
IV.4.3 Trajectories of the charged particles in the separation zone 73
IV.5 Conclusion 76

GENERAL CONCLUSION 77

BIBLIOGRAPHIC REFERENCES 79

List of figures

Figure 1.1: Example of waste electrical and electronic equipment 4
Figure 1.2: Example of electronic component waste 5
Figure 1.3: Materials used in a mobile phone 6
Figure 1.4: Attraction and repulsion Forces between two charged particles 11
Figure 1.5: Generation an electronic avalanche of corona discharge 12
Figure 1.6: Principle of corona effect an electrostatic separation 13
Figure 1.7: Different types of corona electrodes: (a): needle electrode; (b): wire electrode 14
Figure 1.8: Principle of electrostatic induction an electrostatic separation. 15
Figure 1.9: Electrostatic separator with elliptical electrode 15
Figure 1.10: Electrostatic separator with rotating electrode 16
Figure 1.11: The triboelectric effect and the exchange of electric charge between two charges. 16
Figure 1.12: Continuously operating multi-helix triboelectric charging device 17
Figure 1.13: Cyclone charging device 17
Figure 1.14: Tribocharged Belt Separator 18
Figure 1.15: Multifunctional electrostatic separator 19
Figure 1.16: Two-rotating disk-type tribo-aero-electrostatic separator 21
Figure 1.17: Electrostatic tribo-aero separator with two vertical electrodes 21
Figure 2.1: Topology of the corona discharge 24
Figure 2.2: Mechanism of bipolar corona 26
Figure 2.3: Different configurations producing corona discharge 27
Figure 2.4: Description of the positive corona discharge 27
Figure 2.5: Bright aspect of the positive corona discharge 28
Figure 2.6: Photographer of a positive streamer : (a) U = 20 kV, (a) U = 46 kV 28
Figure 2.7: Description of negative corona discharge 29
Figure 2.8: Photographer of a negative streamer : (a) U = 20 kV, (a) U = 46 kV 29
Figure 2.9: Bright appearance of the negative corona discharge 30
Figure 2.10: Geometry of the discharge point - plane 31
Figure 2.11: Flow chart used in simulation 31
Figure 2.12: Generated grid for an electrostatic separator 32
Figure 2.13: Electric potential distribution 33
Figure 2.14: Electric potential at the ground plane for different voltage 33

Figure 2.15: Electric Field distribution 34
Figure 2.16: Electric field at the ground plane for different voltage..... 34
Figure 2.17: Electric field displacement distribution. 35
Figure 2.18: Electric field displacement at the ground plane for different voltage 35
Figure 2.19: Current density distribution 36
Figure 2.20: Current density at the ground plane for different voltage 36
Figure 2.21: Corona discharge current-voltage characteristic 37
Figure 2.22: Space charge density distribution 37
Figure 2.23: Space charge density at the ground plane for different voltage..... 38
Figure 2.24: Space charge density varaition at the ground plane 38
Figure 3.1: Assembly system of electrostatic precipitator 42
Figure 3.2: Flowchart of the different stages of the numerical solution 44
Figure 3.3: Generated mesh grid 47
Figure 3.4: Electric Potential distribution 48
Figure 3.5: Variation of electric field..... 49
Figure 3.6: Variation of current density 50
Figure 3.7: Variation of space charge density..... 51
Figure 3.8: Variation of particle charging: (a) Dust, (b) Dielectric, (c) Semiconductor..... 52
Figure 3.9: Variation of migration velocity: (a) Dust, (b) Dielectric, (c) Semiconductor 54
Figure 3.10: Collection efficiency variation: (a) Dust, (b) Dielectric, (c) Semiconductor 56
Figure 4.1: Global system of multifunctional electrostatic separator used 60
Figure 4.2: Simplified circuit for converting photovoltaic energy into high voltage 61
Figure 4.3: Single-diode model of photovoltaic cell..... 62
Figure 4.4: Simulation model of photovoltaic panel created in Matlab/Simulink..... 66
Figure 4.5: The photovoltaic panel block under Matlab/Simulink 67
Figure 4.6: The I-V characteristics of 14 modules of type ET-M572185 at 25°C..... 67
Figure 4.7: The P-V characteristics of 14 modules of type ET-M572185 at 25°C..... 68
Figure 4.8: The distribution of electric field at the electric charging zone.. 69
Figure 4.9: The distribution of electric field at the separation zone.. 70
Figure 4.10: Electric field variation at the conveyor..... 70
Figure 4.11: Electric field variation at the conveyor for different applied voltages 71
Figure 4.12: Electric field variation at the conveyor for different distances 71

Figure 4.13: Electric field variation at the ground for different applied voltages..... 72
Figure 4.14: Electric field variation at the ground for different distances 72
Figure 4.15: Trajectories variation with applied voltages for particle of size 2 mm 73
Figure 4.16 Trajectories variation with different distances for particle of size 2 mm 74
Figure 4.17: Trajectories variation with applied voltages for particle of size 4 mm 74
Figure 4.18: Trajectories variation with different distances for particle of size 2 mm..... 75
Figure 4.19: Trajectories variation particles of size 2 mm and 4 mm at 30 kV and 80 mm..... 75

List of tables

Tableau 1.1: Substances and health effects..... 7
Tableau 3.1: Permittivity and rigidity of materials used in simulation..... 47
Tableau 4.1: Photovoltaic parameters of an ETSolar photovoltaic module 65
Tableau 4.2: Configuration dimensions..... 65

List of acronyms and symbols

DC: Direct Current.

EEE: Electrical Electronic Equipment.

ES : Electrostatic Separator.

ESP: Electrostatic Precipitator.

FEM : Finite Element Method.

HV : High Voltage.

MC : Method of Characteristics.

MM : Monte Carlo Method.

PMMA : PolyMethyl Methacrylate.

PP : PolyPropylene.

PV : Photovoltaic.

WEEE : Waste Electrical Electronic Equipment.

a : Particle acceleration.

A :Area of the collecting electrode.

C_f : Coefficient of friction.

C_u : Cunningham Slip correction factor.

d : Distance.

d_p: Particle diameter.

D :Electrical displacement.

E : Electrical field.

E_{Peek} : Peek field.

E_x: Horizontal components of field.

E_y : Vertical components of field.

F: Force of attraction or repulsion.

F_{aero}: Aerodynamic force.

F_{ele}: Electrostatic force.

F_g:Gravitational force.

g: Gravitational constant.

I: Electric current.

I_0 : Saturation current of the diode.

I_d : Current at the diode junction.

I_p : Current in the resistor R_p.

I_{ph} : Photo-current

I_{pv} : PV Output current.

J : Current density.

k_B : Boltzmann constant.

K_n : Knudsen number.

m_p : Masse of the charged particles.

n : Ideality coefficient of the cell.

n_i : Number of interpolation nodes.

N_i: shape functions.

N_p: Number of cells in parallel.

N_s: Number of cell in series.

p : Position.

q: electron charge.

Q: Total charge.

Q_g : Gas flow rate.

Q_p : Charge of the charged particles.

Q_1, Q_2: Charges.

r: The separation distance.

r_p: Radius of the charged particles.

R_p : Parallel resistance of the photovoltaic cell.

R_s : Series resistance of the photovoltaic cel.

S : Area.

T : Temperature.

v : velocity.

v_x, v_y : Components of particle velocity.

V: High voltage of the active electrode.

V_{pv} : Output voltage of the photovoltaic cell.

w_{th} : Migration velocity.

z : Gas dynamic viscosity.

δ: Relative density of the air.

ε_r : Specific permittivity.

ε_0 : Permittivity of free space.

η_e, η_s: Concentrations at the inlet and outlet of the precipitator.

λ : Gas means free path.

λ_i : Interpolation functions.

μ : Ion mobility.

ρ : Space charge density.

ρ_a : Density of the air.

ρ_v : volume charge density.

τ_q : Charging time constant.

Δt : Time step.

$\emptyset$: Electrical potential.

GENERAL

INTRODUCTION

Pollution, according to the Larousse dictionary, refers to the degradation of the environment by substances, waste, or various nuisances. While some phenomena can be natural, such as a volcanic eruption, pollution today largely results from human activities. It corresponds to the introduction into the air, water, soil, or ecosystems of elements that exceed tolerance thresholds and disrupt their functioning. Whether physical (noise, light, radioactivity, etc.), chemical (pesticides, heavy metals, plastics, etc.), diffuse, or point-source, pollution is multifaceted, with various forms interacting with one another. It thus exerts a major pressure on the environment, omnipresent in our daily lives. Overexploitation increases, and ecosystems can no longer keep up. Waste and pollution therefore accumulate in the air, land, and water. Pollution threatens our health. Released into the air, water, and soil, it causes significant economic losses. The exponential increase in the world's population in recent years has been accompanied by rapid industrialization. Mobility has developed alongside the overconsumption of resources… Emissions of various pollutants have also multiplied.

New technologies integrated into modern devices have led to a significant increase in electrical and electronic equipment. This equipment has become a major source of waste, the fastest growing in the world [1,2].

According to recent statistics, the amount of waste from electrical and electronic equipment is estimated at approximately eight times the world's population, or 22.3% [3]. Plastics represent between 10% and 30% of the total amount of this waste [4]. Consequently, the increasing amount of plastic generated creates an urgent need to manage this waste after its end of life. Therefore, waste recycling has become a key issue for reducing the risks of air and soil pollution, limiting the depletion of natural resources, alleviating oil shortages, increasing the demand for raw materials, and addressing the significant challenges our planet faces today and in the future [5].

Currently, the recycling of plastics and polymers is experiencing significant growth and its importance has increased considerably. Various alternatives have been developed for managing this waste: optical sorting [6-8], flotation [9-12], and electrostatic separation [13-15], the subject of our research.

Electrostatic separation is a process for sorting and selecting plastics, metals, and semiconductors depending on their charging characteristics.

This process comprises two distinct steps which take place sequentially: the charging of the mixture or powdered components by the following mechanisms:

- ✓ corona discharge,
- ✓ electrostatic induction,

- ✓ triboelectric effect, and electrostatic separation under an intense electric field.

Various devices have been designed and implemented to charge granules and powders for separation under an electromagnetic field, depending on the applied voltage and the acquired charge. Numerous studies have been conducted by European, American, Canadian, Algerian, Japanese, and Romanian laboratories in the field of separation and filtration, notably the results obtained are very satisfactory with millimeter-sized granular mixtures [16]. However, few studies have focused on the separation of mixtures of powdered materials (submillimeter particles), such as ores and agri-food products [17]. Current research on the electrostatic separation of mixtures of granular and powdered materials aims to control the movement of charged particles as a function of aerodynamic forces.

The objective of our study is to demonstrate the specific characteristics of the electrostatic separation of granular and powdered materials. Our research focuses primarily on the following points:

- ✓ Study and analysis of particle trajectories in the electrostatic separator whose power supply is based on photovoltaic energy,
- ✓ Modeling of the separation of conducting, semiconducting, and insulating materials as a function of their permittivities and conductivities.

This thesis is structured into four main chapters followed by a general conclusion. The first chapter is devoted to the state of the art in electrostatic discharge, describing various physical mechanisms involved in its formation and development. The apparent forms of discharge manifestation depending on the nature of the voltage applied to the active electrode are also reviewed, as well as the construction and operating principles of certain electrostatic separation systems.

The second chapter focuses on numerical simulation using COMSOL Multiphysics software, employing the finite element method to study and analyze corona discharge parameters. Namely electric potential, electric field, electric displacement, current density, and space charge density, in different configurations.

Chapter three focuses on modeling and simulating the separation of powders used in the materials recycling industry with corona discharge as the charging mechanism.

Chapter four is reserved for the simulation of the trajectory of particles after ionization by field and by triboelectricity. We used the Euler-Cromer method to simulate the movement of charged particles inside the separation system.

The thesis concludes with a general summary of the work carried out, highlighting the main contributions and outlining the promising future directions opened up by this research.

CHAPTER I

General information on electrostatic separation

I.1 Introduction

Electrostatic separation is a separation technique that has become increasingly popular due to the availability of new equipment that expands the range of separation types offered. It is a cost-effective process due to its low capital and operating costs and the fact that it does not use any chemicals that could impact the environment. Separating recycled materials such as plastics, copper, and aluminum is an economical technology and a way to combat environmental pollution.

This chapter presents general information on the applications of electrostatic separation in various fields. By classifying electrostatic separators according to their charging method and sorting equipment type, it presents recent advances in this field and discusses future prospects. The principles of separators using corona charging and induction charging are described in this section. The separation methods are generally applied to materials with large differences in conductivity.

I.2 Problem of waste electrical and electronic equipment

The problem of waste electrical and electronic equipment (WEEE) is a growing global environmental crisis (Figure 1.1), characterized by massive production (62 million metric tons in 2022), a low recycling rate (22%), and the release of toxic substances (lead, mercury) into the environment, harming human health and ecosystems.



Figure 1.1. Example of waste electrical and electronic equipment

The environmental impact of a product refers to its effects, disturbances, and positive or negative modifications to the environments, that is, to the biophysical and human environments. To assess the environmental impacts of a product (or a service, a sector, a process, etc.), an analysis of all stages of its life cycle is necessary: the acquisition of raw materials and energy sources, transportation, and distribution.

This waste contains precious materials (gold, copper) that are lost, leading to economic losses and increased mining, while informal practices (burning, landfilling) aggravate pollution and health risks, particularly in developing countries.

WEEE refers to end-of-life electrical and electronic equipment, including telephones, computers, household appliances, and digital equipment.

When these devices become unusable, they often contain (Figure 1.2):

- Precious components: gold, copper, silver, and other rare metals.
- Toxic substances: mercury, lead, cadmium, and flame retardants.
- The Plastics that can release dangerous chemicals when burned.

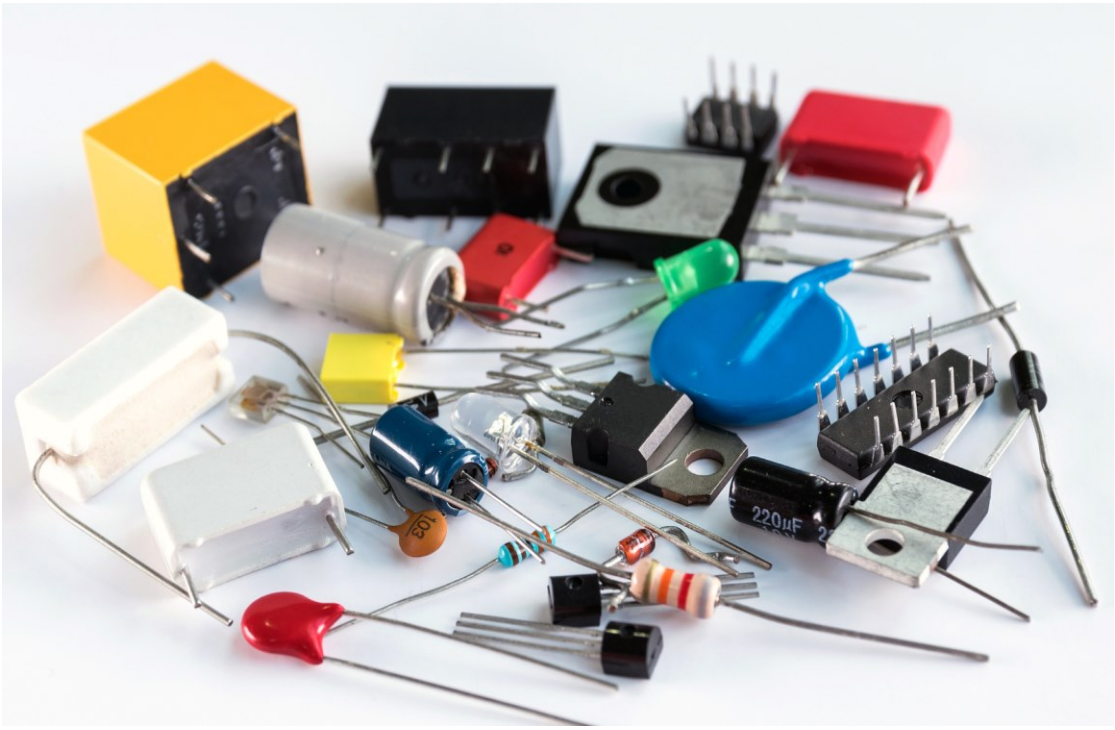

Figure 1.2. Example of electronic component waste

Although grouped under a single category of devices, electrical equipment is made of a wide variety of materials. The complexity of this assembly is a common characteristic of EEEs.

It is therefore very difficult to accurately represent this complexity. A desktop computer weighing around 30 kg is made of thirty different materials, such as plastics, aluminum, lead, gold, copper, barium, nickel, zinc, iron, silver, and so on.

In a simple mobile phone, there can be between 500 and 1000 substances as shown in Figure 1.3.

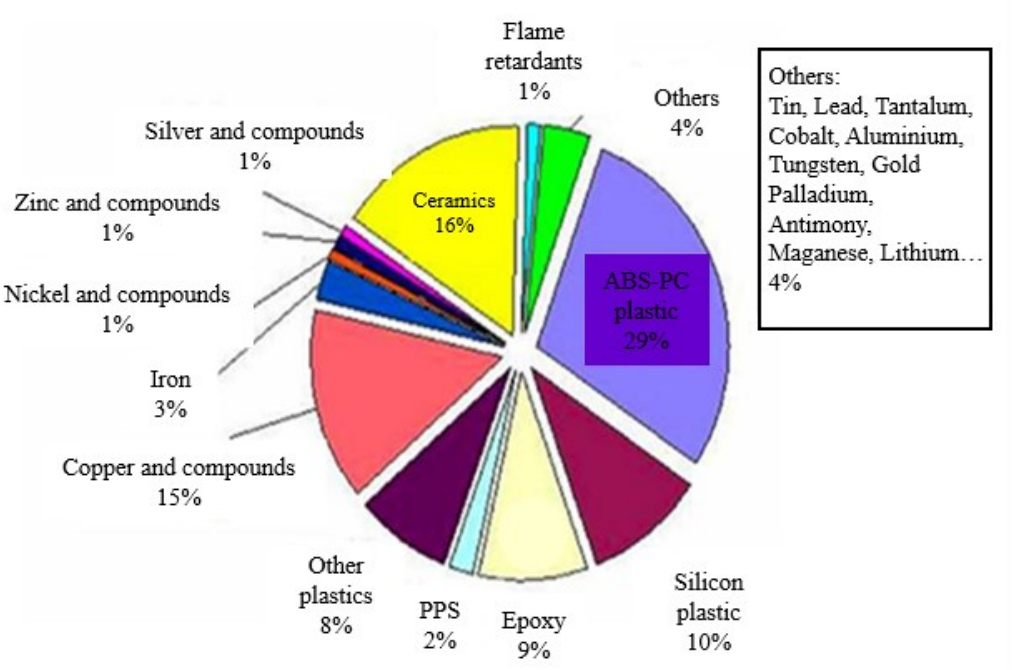

Figure 1.3. Materials used in a mobile phone [18]

It is difficult to find highly precise data regarding the composition of electrical equipment due to the wide variety of equipment and the confidentiality of process data. However, their composition can be classified into materials that pose environmental hazards (refrigerants, batteries and accumulators, cathode ray tubes, capacitors, liquid crystal displays, mercury relays or switches, cables, printer cartridges and toners, etc.) and non-hazardous materials. The latter include plastics, ferrous metals, and rare and precious metals, which are essential elements in the manufacture of new equipment brought to market due to their specific properties.

I.3 Environmental impacts of non-recycled WEEE

WEEE has an unavoidable impact on our planet. Every year, millions of tons of this waste are produced, containing toxic substances and valuable materials. If poorly managed, WEEE poses serious threats to the environment and human health.

The health and environmental risks posed by electrical equipment are linked to the substances it contains (Table 1.1).

Table 1.1. Substances and health effects [18]

Substances	Health effects	Current presence
Brominated flame retardants	Although less studied than polycyclic chlorinated derivatives, their toxicity is likely similar. They are thus suspected of having endocrine-disrupting, neurotoxic, and reproductive toxic properties.	Printed circuit boards, Connectors, Plastic coatings, Cables.
Cadmium and its compounds	Toxicity depends in particular on the solubility of the compounds. Some are classified as toxic (inhalation and ingestion), carcinogenic (Cat. 2), mutagenic (Cat. 2), and toxic to reproduction (fertility and development (Cat. 2). After inhalation, toxic effects can be observed on the kidneys and bones (demineralization), as well as lung and prostate cancers.	Printed circuit board components, Cathode ray tubes, PVC stabilizers.
Lead and its inorganic compounds	Lead compounds are classified as harmful by inhalation and ingestion, accumulating in the body and toxic to reproduction (fertility and development (Cat. 1). These compounds affect numerous organs, including the blood, nervous system, and kidneys. Carcinogenic effects are also suspected.	Printed circuit board soldering, Cathode ray tube glass components, Soldering and glass for fluorescent tubes.
Nickel and its compounds	Some compounds in nickel are classified as skin allergens and carcinogens when inhaled. Their effects depend in part on their solubility. They can cause skin allergies, rhinitis, and asthma. Sinus and bronchial cancers have also been reported with certain uses.	Batteries
Mercury and its inorganic compounds	Mercury is classified as toxic by inhalation. It accumulates in the body. The effects of repeated exposure primarily affect the nervous system.	Thermostats, Sensors, Relays and switches; Fluorescent lamps.
Beryllium and its compounds	They are classified as highly toxic by inhalation and ingestion, irritants to the skin, eyes, and respiratory tract, and skin allergens. Finally, they are classified as carcinogenic by inhalation (Cat. 2). Even at very low concentrations, they can cause serious damage to the bronchi and lungs of allergic and/or irritant origin (berylliosis).	Motherboards, Printed circuit board connectors, Monitors, Relays, Switches, X-ray tube windows.

The main areas affected by waste are described below:

I.3.1 Soil and water pollution

Land is a vital resource for humanity, like air and water. Soil degradation, or the loss of soil productivity for the present and future, is a global challenge that is intimately linked to essential aspects of human security and well-being: food, employment, health, and livelihoods.

When WEEE is improperly disposed of (landfilled or incinerated), heavy metals such as lead and mercury seep into the soil and contaminate groundwater. This pollution affects not only local ecosystems but also the human populations who consume this water.

Water pollution is characterized by the presence of microorganisms, chemicals, and industrial waste. It can affect rivers, groundwater, and brackish water, as well as rainwater, dew, snow, and polar ice.

The different sources of pollution are:

- Industry: including chemical discharges such as hydrocarbons released by industries, as well as wastewater from factories.
- Agriculture: including animal waste, pesticides, and fertilizers. They then seep into the soil until they reach groundwater, or they run off into surface water.
- Domestic: including wastewater from toilets, cosmetics or cleaning products, paints, used motor oil.
- Accidental: spillage of toxic products into the natural environment, which disrupts the ecosystem.

I.3.2 Air quality degradation

These are emissions resulting from inadequate or nonexistent waste management. Food waste and landfills are significant sources of methane, a greenhouse gas with a Global Warming Potential (GWP) 25 times greater than that of carbon dioxide, which disrupts ecosystem services. Rapid and unsustainable urbanization, coupled with lagging waste management infrastructure, exacerbates air pollution, responsible for 6.7 million deaths annually.

These pollutants cause respiratory problems, worsen the greenhouse effect, and harm the environment, making responsible waste management (sorting, recycling) crucial for cleaner air.

I.3.3 Loss of natural resources

Environmental and social standards recognize that the protection and preservation of biodiversity and the sustainable management of biological natural resources are fundamental to sustainable development. Biodiversity refers to the variability among living organisms from all sources, including, among others, terrestrial, marine, and other aquatic ecosystems and the

ecological complexes of which they are part. This includes diversity within and between species, as well as diversity of ecosystems. Because biodiversity often underpins ecosystem services valued by humans, adverse effects on biological diversity can negatively impact these services.

WEEE contains valuable materials such as gold, copper, and platinum. When these strategic resources are not recycled, they are lost, leading to increased mining and further exacerbating the environmental impact.

I.4 Impact of WEEE recycling on the circular economy

In a circular economy model, waste electrical and electronic equipment (WEEE) must be considered an important source of secondary raw materials. Due to problems related to primary mining, market price fluctuations, material depletion and limited access to resources, it has become necessary to improve the extraction of secondary resources and reduce pressure on virgin materials. By recycling WEEE, countries could at least safely and sustainably limit their material demand [19].

From a materials design perspective, WEEE is highly complex. Waste electrical and electronic equipment (WEEE) contains up to 69 chemical elements from the periodic table, including precious metals (e.g., gold, silver, copper, platinum, palladium, ruthenium, rhodium, iridium, and osmium), critical raw materials (e.g., cobalt, palladium, indium, germanium, bismuth, and antimony), and non-critical metals such as aluminum and iron.

Therefore, before manufacturing new products from this waste, each material must be separated using modern separation technologies.

I.5 Electrostatic separator

The charging method varies depending on the equipment and application. An attraction or repulsion system proportional to this charge enables particle separation. The materials must be completely dry [20,21].

This section presents a state-of-the-art overview of the applications of electrostatic separation technology.

By classifying the separation according to their charging method and sorting equipment type, it outlines recent advances in this field and discusses future prospects.

Electrostatic separation is a separation method based on the differential attraction or repulsion of charged particles under the influence of a very intense electric field [22,23].

In the case of electrostatic separations, the principal separation force is given by:

$$\boldsymbol{F_e = q \cdot E} \quad (1.1)$$

Where *f* is the force, *q* is the charge, and *E* is the electric field. In reality, secondary forces such as gravity, air current force, etc., must also be taken into account. However, the two parameters *E* and *q* are essential for understanding electrostatic separations [24].

In the case where a tribocharger is used, the charge developed on the particles is the attractive force between a charged particle and an electrode surface. It can be given by the following relation:

$$\boldsymbol{F_{DEP} \propto \frac{dE}{dr}} \quad (1.2)$$

Where *dE/dr* represents the field gradient and *r* indicates the separation distance between the electrodes.

In planar electrostatic separators, the field gradient is uniform, and the force does not vary with position.

In a non-uniform field, the attractive force varies with the position of the charged particle within the region of influence.

In all cases, a minimum separation distance between the electrodes must be maintained to avoid the formation of electric arcs.

I.5.1 Physical mechanisms of electrical charging of powdered materials

The electrostatic separation is a generic term for an important class of technologies used for sorting selections of powdery materials by application of electric forces acting on particles that have different characteristics, which are charged or polarized, and which are found in particles, and in intense electric fields [25,26] on the order of 1.0 kV/mm which are required, and that the development of electrostatic separation technologies and equipment has always been synchronous with advances in high-voltage engineering [27]. These electric forces are based on Charles Coulomb's law, which established the expression of the force *F* of attraction or repulsion that results between two bodies having the charges Q_1 and Q_2, located at a distance *d* from one relative to the other:

$$F = \frac{Q_1 \cdot Q_2}{4\pi \cdot \varepsilon_0 \cdot d^2} \quad (1.3)$$

Like charges repel each other, whereas opposite charges attract (Figure 1.4).

There are physical mechanisms capable of imparting electric charges to powdery materials for the purpose of separating them in the presence of a high field.

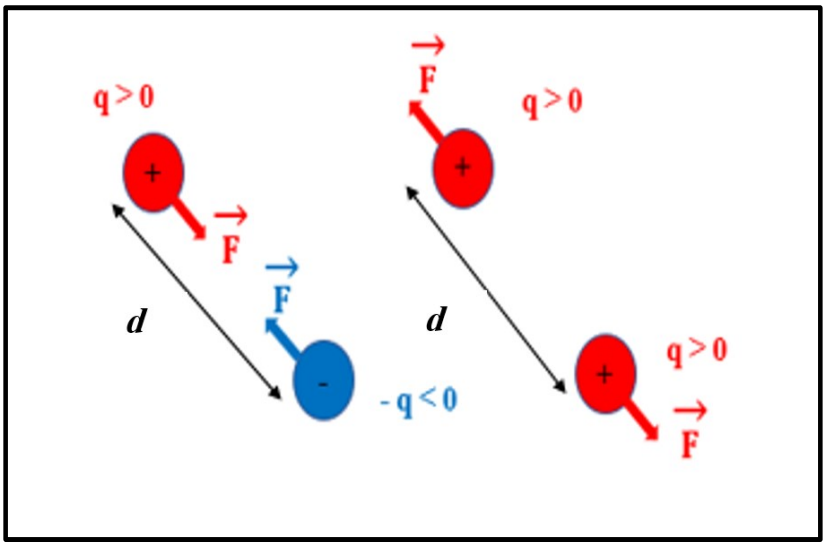

Figure 1.4. Attraction and repulsion forces between two charged particles

There is a part of this chapter that will be devoted to the theory of electrostatic separation and the electrical charging mechanisms of granular and powdery materials.

Electrostatic separation of powdery mixture materials is possible if the constituents of this one carry different electric charges. Three different physical mechanisms are commonly used to charge powdery materials for separation in an intense electric field: the corona effect, electrostatic induction, and triboelectric effect [28-30].

I.5.2 Corona effect

In recent years, corona discharge has become widely applicable in several active sectors, and has been the subject of several scientific researches. It is used in several industrial processes. Such as dust precipitation (electrostatic precipitators) [31], the manufacture of plastic and textile films [32], gas pollution control, and electrically charging insulators in plate form, as well as in the processes of electrophotography and electrostatic separation of granular mixtures.

I.5.2.1 Description

The corona effect is one of the essential phases in electrical discharges, and its most striking consequence is the ionization of air in a zone of very intense field produced between two metal electrodes: one, called active, is generally represented in the form of a point or a wire of small diameter and is connected to a power supply of several kilovolts; the other, passive, is a metal plate or grid that connects to the ground. Near the active electrode, the voltage varies greatly over a short distance, creating a high field, which is responsible for the natural ionization of the

air. The corona effect results from the phenomenon of electronic avalanche, which takes place near the active electrode regardless of the polarity applied to it (Figure 1.5).

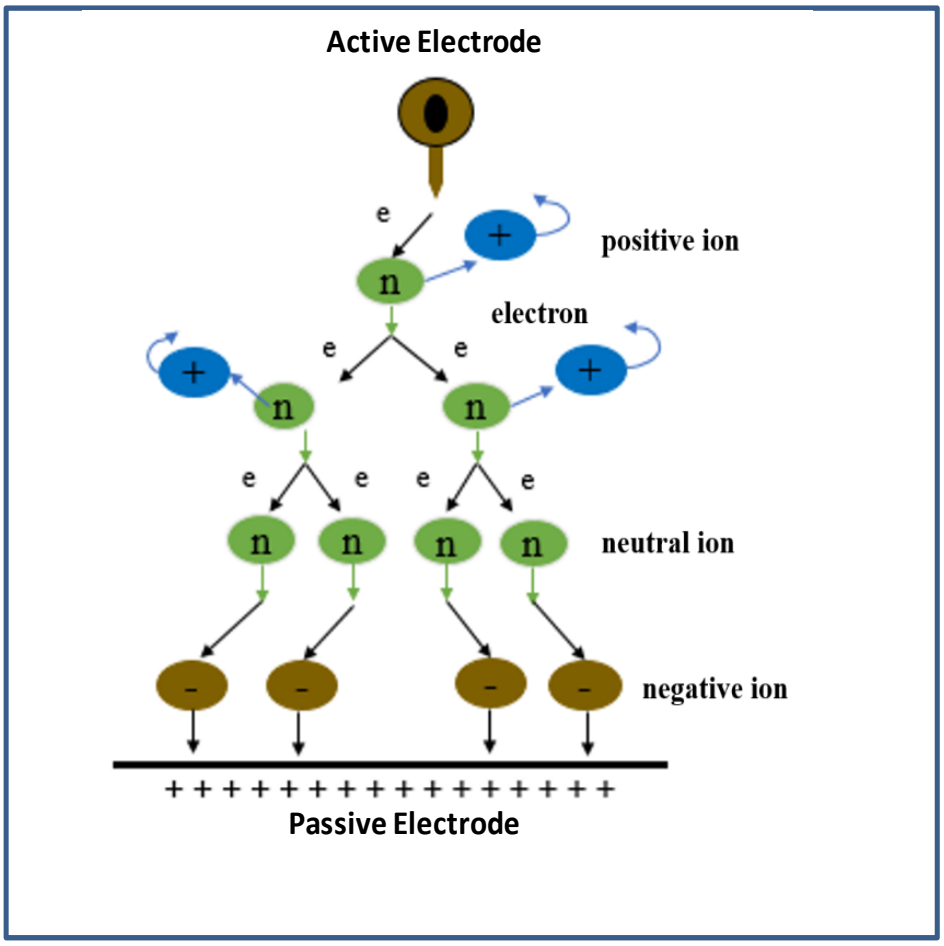

Figure 1.5. Generation an electronic avalanche of corona discharge

The released electrons will collide with the air molecules present in space; these molecules release one or more electrons carrying a high level of energy. These electrons continue their trajectory towards the opposite-polarity passive electrode, colliding with other gas molecules and thus multiplying their number. The molecules having released electrons have become positive ions and are therefore attracted by the active electrode. In this way, they regain an electron and become neutral. This phenomenon is delimited in space (a few micrometers from the electrode, whereas the total gap is on the order of mm) in an area characterized by an intense electric field: what is called the ionization zone. Beyond the latter, the electric field is no longer strong enough for electrons to acquire sufficient kinety energy to cause impact ionization. They will then associate with the air molecules and form negatively charged ions. These ions come

into contact with the particles, and their lifetimes are long enough for the separation of materials. The particles, subjected to the ionic flow, will become negatively charged [33 -36]. When using corona effect as an electrical charging mechanism for electrostatic separation of powdery material mixtures, the particles are acquiring positive or negative charges depending on the polarity of the active electrode (Figure 1.6).

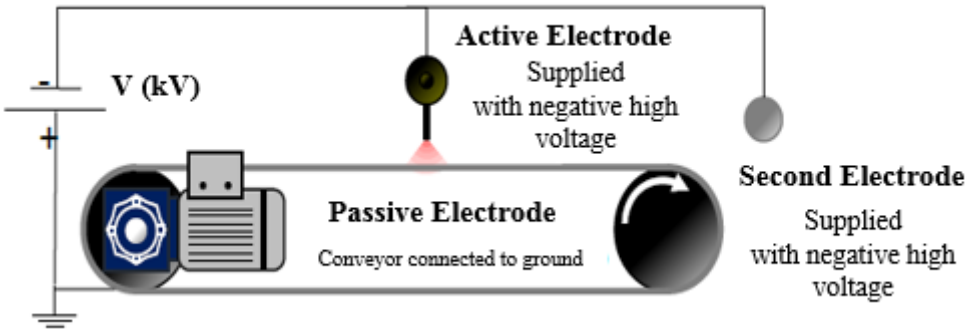

Figure 1.6. Principle of corona effect in electrostatic separation

The particles that pass through this cloud acquire an ionic charge; however, the conductive particles lose this charge immediately due to their contact with the earth and become neutral again, while the insulating particles keep it longer. This phenomenon therefore allows the separation of the mixture of powdered materials, confirms the effectiveness of the corona effect as a particle charging mechanism, and justifies its use in several electrostatic installations [37-39].

However, corona discharges also create an ionic wind due to the acceleration of ions, which, during their movement in an electric field, collide with gas molecules, transmitting to them not only energy in the form of heat but also kinetic energy, which has an impact on many applications, such as the control of aerodynamic flows on aircraft wing profiles, but remains a harmful effect on separation process, because it can disturb the path of the finest particles (under 1 mm typically micrometric) and be the cause of dispersion or even loss of material.

I.5.2.2 Charging devices

Over time, many devices have been implemented to generate corona discharges. The most used are wire and needle electrodes (Figure 1.7), and to a lesser extent, blade electrodes. Corona electrodes based on fine wire are characterized by ease of production, as well as their low cost, and are the most appreciated in industry. These corona electrodes, however, struggle to meet practical criteria during the process of separating a mixture of powdery materials, even if they meet important economic criteria [40].

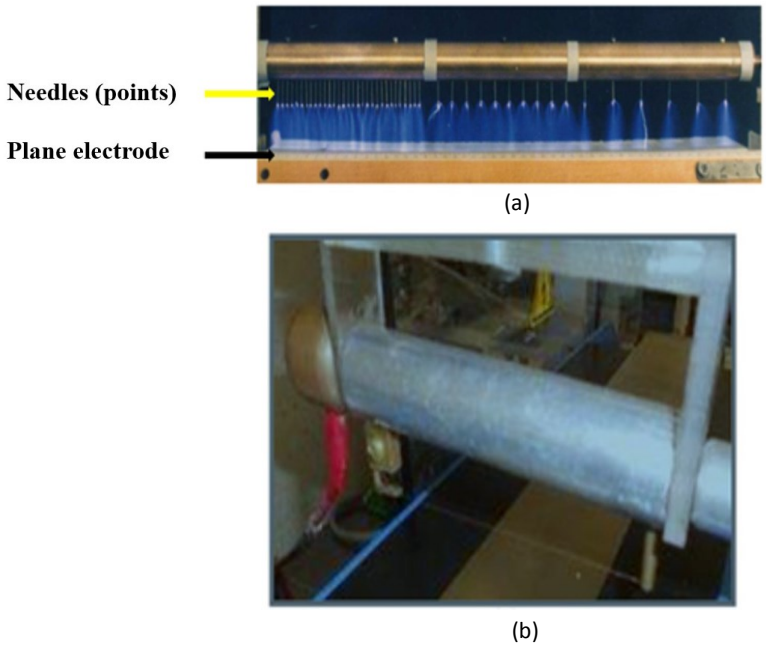

Figure 1.7. Different types of corona electrodes: (a): needle electrode; (b): wire electrode

It should be noted that the appropriate electrode is the one that allows for the efficient charging of particles at reasonably high voltages. Therefore, needle electrodes are more efficient than conventional wire electrodes.

I.5.3 Electrostatic induction

Electrostatic induction is one of the physical mechanisms of electrical charging used in the separation of a mixture of powdered materials.

I.5.3.1 Description

Electrostatic induction can be defined as a method by which an electrically charged object is used to create a movement of electric charges in a second neutral object without being in contact with it. The charged object generates an electric field, causing the polarization of the neutral object.

If the neutral object is conductive and temporarily in contact with a grounded electrode, the polar charges located near the point of contact will flow towards the ground. Therefore, when the object is disconnected from the ground, it carries a non-zero net charge. Since charges do not flow in an insulating body [41], it is never charged by electrostatic induction.

This mechanism explains, for example, a conductive charge placed between two electrodes of different polarities. Figure (1.8) represents a conductive particle, initially neutral, deposited on

the surface of a passive electrode, polarized in an electric field created by another active electrode.

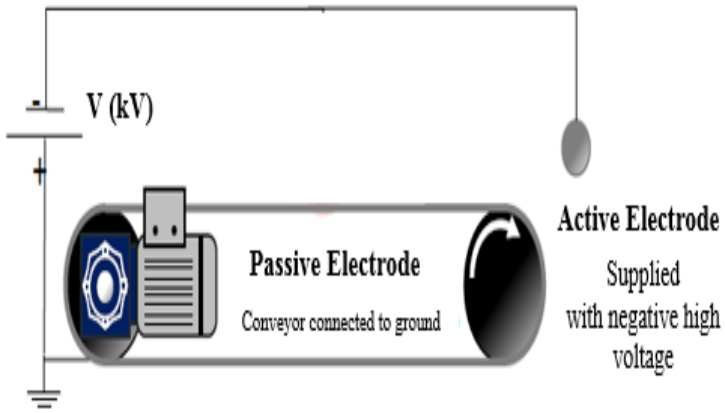

Figure 1.8. Principle of electrostatic induction in electrostatic separation

In electrostatic separation of insulator/conductor mixtures, performance can be improved by combining electrostatic induction and corona effect by adding a second electrode producing an intense and quasi-uniform electric field. Which increases the electrical force of detachment of conductive particles deposited on a grounded metal surface [42].

I.5.3.2 Charging devices

Figure 1.9 represents a static electrode of elliptical shape used in the CARPCO separator for conductor/insulator mixtures (copper, PVC).



Figure 1.9. Electrostatic separator with elliptical electrode [43]

Figure 1.10 represents a rotating electrode of cylindrical shape used in the separator of INRA of Montpellier in the laboratory for plant mixtures. The electrodes used to generate this electric

field are often tubular or elliptical in shape, this shape is used to extend and standardize the generated field whether the electrode is rotating or static.



Figure 1.10. Electrostatic separator with rotating electrode [43]

I.5.4 Triboelectric effect

The triboelectric effect is one of the physical mechanisms of electrical charging used for separation of materials, due to the ability of these materials to retain the acquired charge as long as possible. It is based on the transfer of the charge.

Triboelectricity or triboelectrization is a Greek word "tribein" which means to rub, that is to say an electrostatic phenomenon by which the transfer of electric charges is created when two materials of different natures are brought into contact (Figure 1.11).

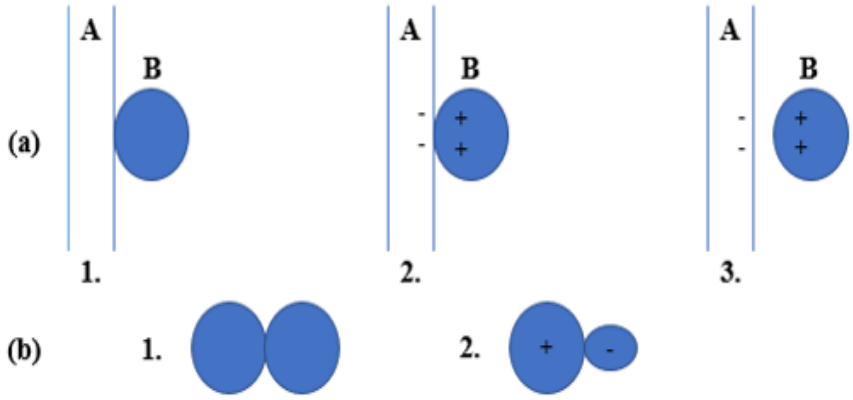

Figure 1.11. Triboelectric effect and the exchange of electric charge between two surfaces

After separation, surface A tends to be charged negatively, and particle B positively. If neutral particles of the same size in contact, the large particles tend to be charged positively and small ones negatively.

If two electrically neutral materials rub against each other, electrical charges are transferred at the surface level from one to the other, in the same direction, resulting in two differently charged materials. The static charge thus acquired occurs in a system where generally the conductivity of the material is low; it therefore persists even after the contact is broken, and new contacts will have the effect of producing other transfers [44-49], which makes it possible to produce charges at high levels (Figure 1.12). This is the most widley used physical mechanism for charging granular or micronized plastic materials for their separation in an intense electric field [50-54].

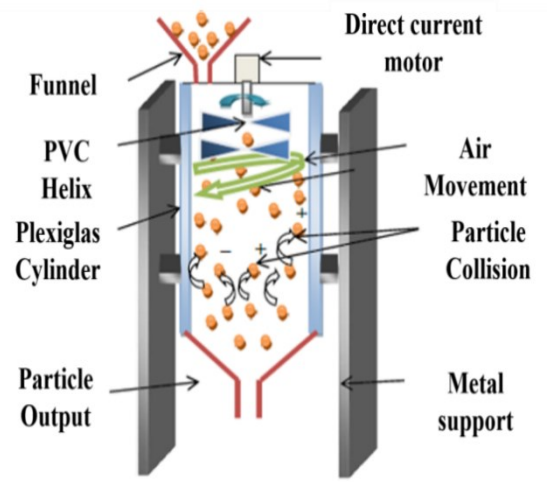

Figure 1.12. Continuously operating multi-helix triboelectric [55]

The device consists of an insulating cylinder (Figure 1.13). The powdery materials to be charged are introduced in a horizontal direction.

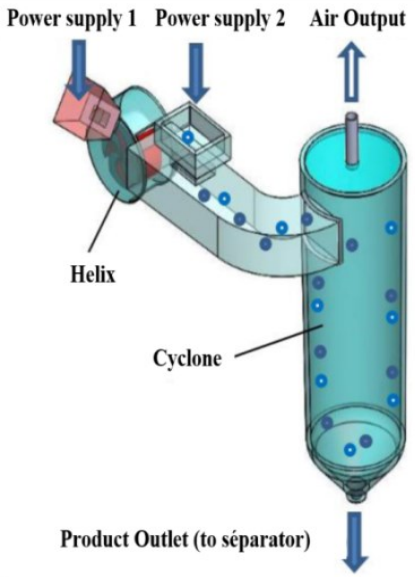

Figure 1.13: Cyclone charging device [56]

I.5.5 Electrostatic separation installations for powdered materials

For industrial recycling, multiple research studies have been carried out by American, Japanese, European, Canadian and Algerian laboratories on electrostatic separation [57]. This technique has proven effective in the selective sorting of granular or powdery materials according to their physical characteristics, by using the forces exerted.

The majority of installations treating powdery particles use the triboelectric effect as a charging mechanism, which prevents the appearance of agglomerates. The common point between these devices is the need to have two successive parts, the first for triboelectric charging of the particles, and the other for their separation.

I.5.5.1 Conveyor belt tribo-electrostatic separator

The diagram in Figure 1.14 explains the operation of a tribocharged Belt Separator.

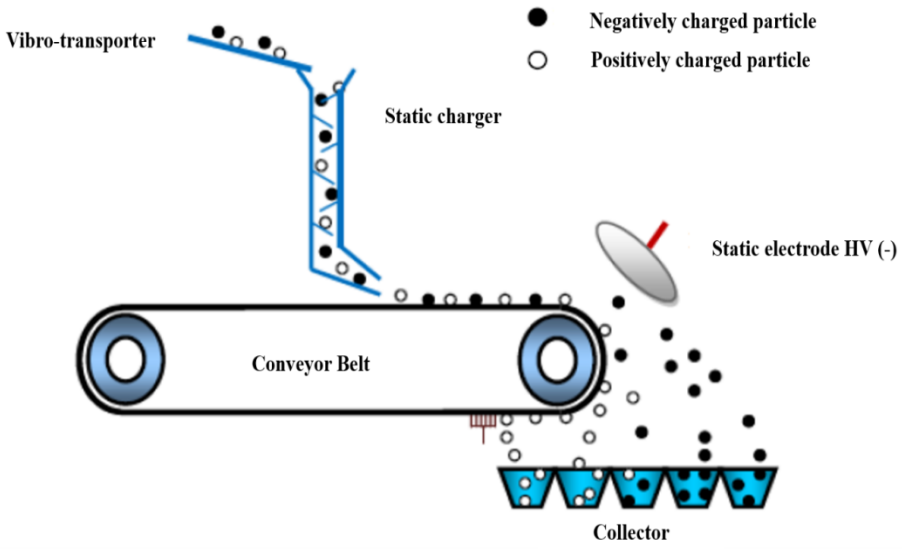

Figure 1.14. Tribocharged Belt Separator

The particles are tribocharged by a static charging device, then they fall onto a conveyor belt and are transported to the separation zone. The particles separate under the action of the forces generated and attracted by an electrode of one polarity and repelled by an electrode of the opposite polarity, thanks to the Coulomb forces, thus enabling separation [58,59].

I.5.5.2 Multifunction electrostatic conveyor belt separator

The second installation is a multifunction separator capable of sorting granular or micronized materials through the use of three different physical mechanisms for particle charging (Figure 1.15).

This device is intended for feasibility studies on the electrostatic separation of powdery materials. Mixtures consisting of fine particles are deposited in a single layer on the surface of a 700 mm long and 70 mm wide metal conveyor belt, which also acts as a grounded electrode. The conveyor is driven by a 120 W three-phase electric motor equipped with a variable frequency drive. Particle deposition is carried out using an oscillating chute (model APB 4/30, VIBRA France) with a dedicated control unit and is equipped with a particle dispersion device of unique design.

For each option, a device will be attached to the separator. Thus, it could be equipped with one or more of the following: (1) a triboelectric charging device (fluidized bed, compressed air gun, or oscillating chute), (2) a single corona electrode made of fine metal wire (diameter: 0.2 mm), 130 mm long, (3) a rotating cylindrical steel electrode with a diameter of 30 mm and a width of 70 mm, driven by an electric motor equipped with an electronic speed controller. A few of them bounce back after contact with the rotating electrode and are then collected in the compartments of collectors 1 and 2 as product A. The other non-conductive particles are collected in collector 3 as product B.

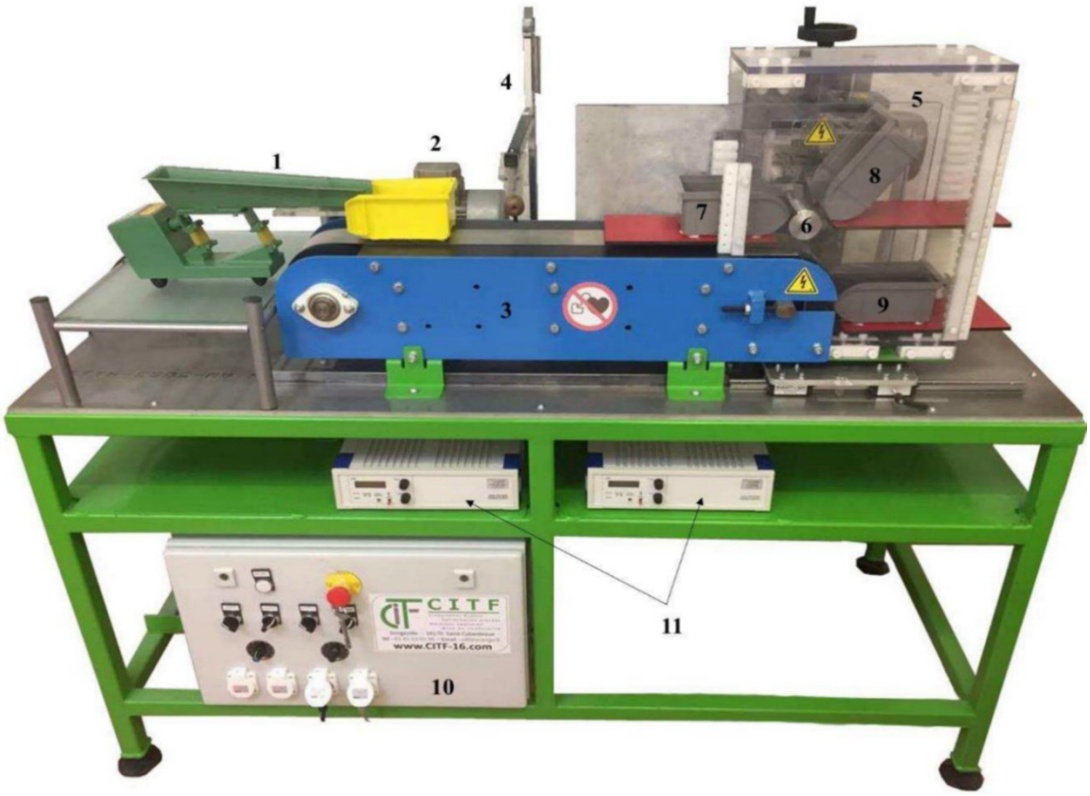

1. Oscillating chute; 2. Electric motor driving the metal conveyor, 3. Metal conveyor, 4. Corona electrode, 5. Electric motor driving the cylindrical electrode, 6. Rotating cylindrical electrode, 7. Box 1, 8. Box 2, 9. Box 3, 10. Electrical cabinet, 11. High voltage DC power supplies

Figure 1.15. Multifunctional electrostatic separator [60]

This electrostatic separator is available in several configurations from 0° to 90°. The cylindrical electrode can change its direction of rotation [60].

I.5.5.3 Tribo-aero-electrostatic separator with two metal disks

This electrostatic separation installation shown in figure (1.16) is primarily intended for the treatment of mixtures of insulating materials of millimetric and sub-millimetric sizes.

A quantity of 750 g of powdered material is introduced into a fluidized bed generated in a separation chamber of dimensions 160 × 160 × 240 × mm^3, the walls of which are made of transparent PMMA. Air injection is ensured by a 1.5 kW / 4000 rpm / 166 m^3/h blower controlled by a variable frequency imposing a rotation between 1000 rpm and 4000 rpm.

The fluidized bed is at a height of 10 cm from the porous plate or grid that distributes the air evenly. Electrostatic effects in the fluidized bed are due to collisions between the particles themselves and between the particles and the walls of the separation chamber. This results in the triboelectrification of the powdered materials.

The electric field is generated between two rotating stainless steel discs, D=220 mm in diameter and e=2 mm thick, immersed in the fluidized bed, each located at a variable distance between 40 mm and 120 mm. They are driven in rotation by two electric motors whose speed is controlled by an electronic speed variator. This speed can vary continuously from 25 rpm to 70 rpm. The rigidity of the shafts carrying the discs has been calculated to avoid bending at the shaft end that could modify the parallelism between the planes of the discs during operation.

The high-voltage power supply to the discs is provided by two SPELLMAN 30 kV / 15 W / 0.5 mA generators of opposite polarity. The applied voltages can vary from 0 V to 30 kV. The shaft guide bearings are used to supply the discs with high voltage. Note that one of the unique features of this device is the simultaneous triboelectric charging and separation.

The separated products are collected in two collection boxes placed outside the separation chamber. Particle collection on the electrodes is ensured by scrapers that lick the particles off the surfaces of the discs. The separated particles are collected in the boxes, the bottoms of which are made of Faraday cages. Thus, the electrical charges acquired by the particles are measured as separation progresses by KEITHLEY model 6514 electrometers connected to the Faraday cages. These boxes are supported by electronic balances with a resolution of 0.1 g that measure the masses of the separated particles.

This separator is equipped with a control panel that allows for the direct or instantaneous acquisition and reading of all operating data [61].

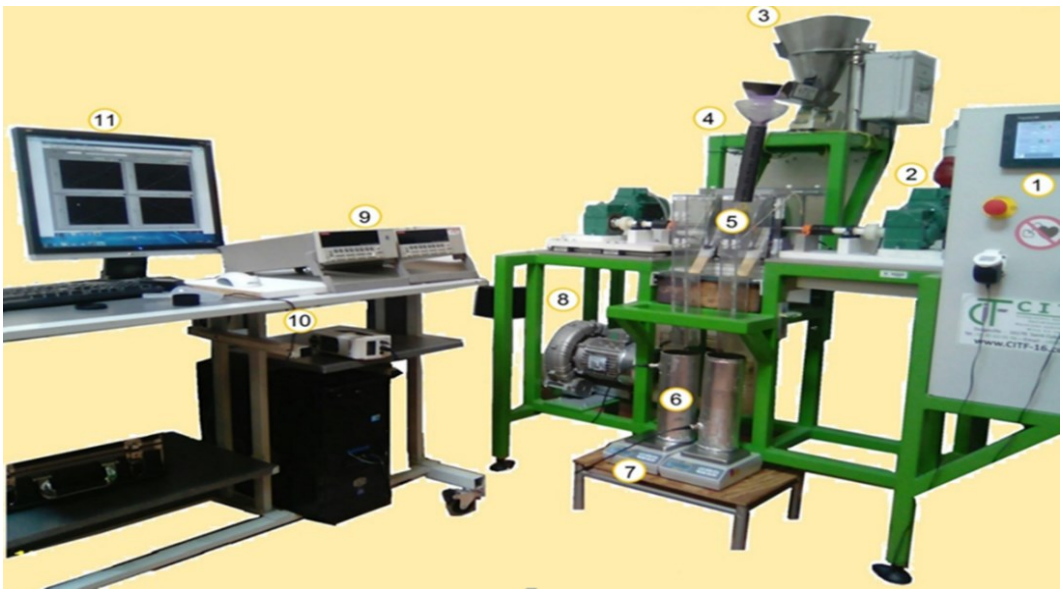

1. Control panel, 2. Variable-speed DC motors, 3. Vibratory feeder, 4. Cylindrical feeder, 5. Separation chamber with two rotating disk electrodes, 6. Faraday cages, 7. Scales, 8. Air blower, 9. Electrometers (Keithley 6514), 10. Portable colorimeter NH310, 11. Computer

Figure 1.16. Two-rotating disk-type tribo-aero-electrostatic separator [61]

I.5.5.4 Electrostatic separator with two vertical electrodes

The new tribo-aero-electrostatic separator is designed for the treatment of mixtures of fine insulating materials (average size: 10-100 µm). The device consists of two vertical plate electrodes of dimensions 200 mm × 300 mm, connected to two high-voltage DC power supplies of opposite polarities. The two electrodes perform reciprocating movements inside the fluidized bed containing the micronized materials to be separated. Fluidization is achieved by air injection using a variable-speed air blower (Figure 1.17).

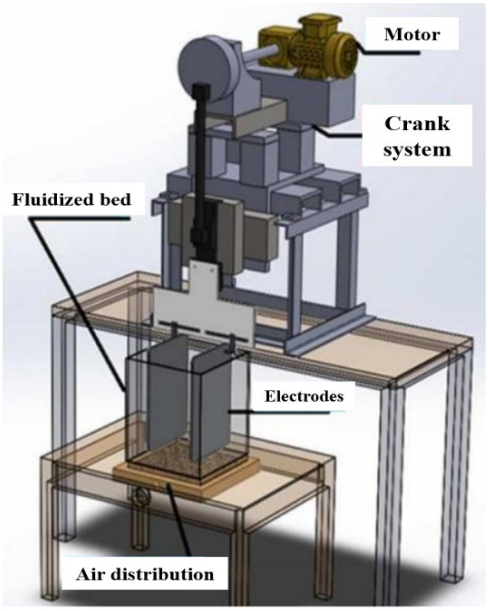

Figure 1.17. Electrostatic tribo-aero separator with two vertical electrodes [62, 63]

I.6 Conclusion

Academic studies on exposure and health effects have primarily been conducted on a small scale. Some of these studies have reported contamination of control groups, suggesting that pollutants are widespread. No large-scale longitudinal studies have been published.

Collecting statistics on the health effects of WEEE raises numerous challenges, particularly concerning the large number of potential health effects, the difficulties associated with studying chemical mixtures, the lack of a confirmed relationship between exposure and effects, and the long latency periods of some diseases. Internationally harmonized indicators can help measure the number of people exposed to health risks from WEEE and track trends over time.

Electrostatic separation of powdered materials can be achieved by combining one or two different charging mechanisms. Three physical mechanisms allow particle charging: corona effect, electrostatic induction, and triboelectric charging.

The triboelectric effect provides irreplaceable advantages for the separation of mixtures of non-conductive materials. For materials mixtures, electrostatic separation requires the use of electrostatic induction and/or a corona discharge.

There are a multitude of electrostatic installations that process different types of powdered material mixtures whose effectiveness has already been proven for particulate applications.

CHAPTER II

Study the corona discharge parameters

II.1 Introduction

The introduction of simulation has a profound impact on the approach to complex systems in the world of engineering and technology. This numerical solver plays a particularly important role in a number of electrostatic applications, including electrostatic precipitators and electrostatic separators, which implement the phenomenon of corona discharge in gases from electrodes with a strong curvature. These electrodes inject charges into the gas and the resulting space charge modifies the electric field distribution. Complex models and algorithms combine to provide a new perspective on the behavior of corona discharges in electrostatic separators. The most complex phenomena of real-world occurrences can be recreated and analyzed through simulations, which offer researchers a means to study the electric fields and potentials in the charging zone and the particle separation zone with unprecedented depth.

In this chapter, we present the study of the behavior of dc corona discharge in point-to-plane electrostatic separator depending on the bias voltage. Physically, the corona discharge has been studied by solving partial differential equations represented by Poisson's equation. The various corona discharge parameters are obtained and analyzed by the finite element method (FEM) computation for this simulation model developed by COMSOL - Multiphysics Software.

II.2 Corona discharge physics

The physico-chemical mechanisms within corona discharges are quite complex and are currently being studied by plasma physicists, as they are not yet fully understood.

The corona effect encompasses all the phenomena occurring in a gas near a conductor with a small radius of curvature, subjected to a high enough voltage for the electric field to exceed the threshold for the onset of pre-disruptive discharges.

The corona discharge threshold depends on the availability of a free electron, called a seed electron, in the region of intense electric field (near the active electrode). As electrons move towards the anode, they ionize the neutral gas by impact, creating an electron avalanche. Radiation is also generated, leading to the photoionization of gas further from the anode. The photoelectrons create new avalanches, and a self-sustaining discharge is thus established [64, 65].

Electrons in the weak electric field region lack sufficient energy to ionize molecules, so they bind to neutral gas molecules. The inter-electrode space is thus divided into two zones (Figure 2.1): an ionization zone with a strong field where electrons trigger the ionization of neutral molecules and new positive electron-ion pairs are created. This active zone, extremely localized near the electrode, remains visible to the naked eye. The second zone is the ion drift zone where the geometric electric field is insufficient for ionization of the medium.

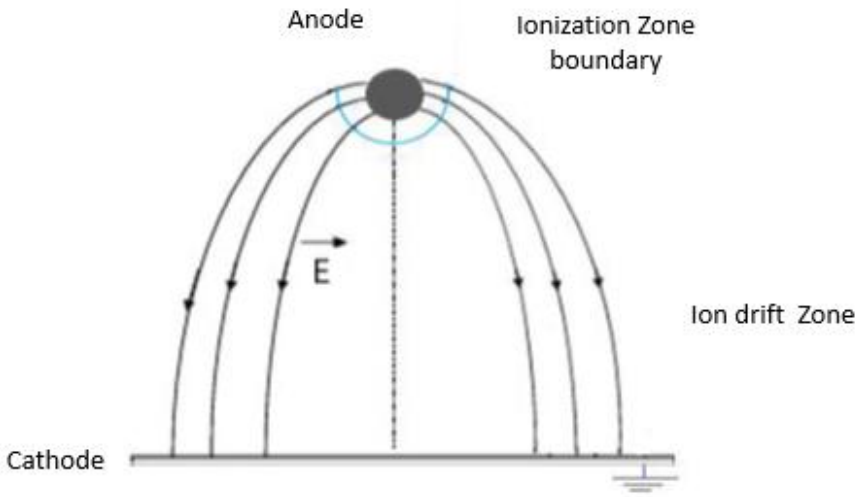

Figure 2.1 Topology of the corona discharge [64]

Mass spectrometry studies of ionic species formed in positive and negative corona discharges in air have been conducted by several authors. The results have shown that the species generated by the corona discharge are strongly influenced by the type of gas near the active electrode, humidity, pressure, inter-electrode distance, and discharge current intensity [66, 67].

In dry air, the dominant ion for a negative corona discharge is OH^-. In the presence of humidity, this is converted to form hydrated $(H_2O)_nOH^-$) ions, where n is an integer that increases with relative humidity. If sufficient quantities of ozone and nitrogen oxides are produced by the discharge, both simple and hydrated OH^- ions are produced. For short inter-electrode distances, hydrated $(H_2O)OH^-$ ions are produced in abundance. Other types of ions can be produced by the negative corona discharge, such as:

$O-$, O_2-, O_3-, CO_4-, $(H_2O)OH-$ and $(H_2O)nHCO_3-$.

For positive corona discharge, the dominant species are hydrated ions. $(H_2O)H+$ where n is an integer that increases with humidity. When the humidity level decreases, the hydrated ions $(H_2O)NO+$ and $(H_2O)nNO_2+$ begin to appear, and at very low levels, non-hydrated ions $NO+$ and $NO2+$ are produced in dominant quantities. The positive corona discharge can generate other types of ions such as:

$CO+$, $C+$, C_2O+, C_3O_2+,CO_2+,H_3O+,$CHO+$,CHO_2+.

II.3 Corona discharge mechanism

A corona discharge is established between an active electrode and a passive electrode. The active electrode is a tip (or a small-diameter wire) to which a high electrical potential is applied, while the passive electrode is a plate or a grid (Figure 2.2). This results in a volumetric corona discharge. The

asymmetry of the electrodes leads to an inhomogeneous electric field in the interelectrode space. In this tip-plate configuration, the electric field near the tip is intense, which allows for ionization. The passive electrode then serves to collect the charges. Furthermore, the corona discharge is the site of strong physicochemical activity. Depending on the polarity of the potential applied to the tip, we distinguish between a positive corona discharge and a negative corona discharge.

Due to the difference in radii of curvature between the electrodes, the electric field in the inter-electrode space is highly non-uniform, so that air ionization and the generation of charged particles occur only in a region close to the electrode with the smaller radius of curvature. The spatiotemporal evolution of the electric field within the inter-electrode space shows that this space can be divided into two distinct zones. Each of these zones is characterized by a predominant type of interaction between the charged and neutral particles of the ionized gas.

In the first zone, known as the "ionization zone," located near the tip and approximated as a sphere with a radius of a few tens of micrometers, the electric field has a high amplitude and gradient, which favors ionization processes. The particles formed, particularly the electrons, which are lighter and faster, heat up under the influence of the electric field and transfer heat to the air molecules during collisions. The neutral air particles then diffuse this heat due to their thermal agitation.

The second zone, known as the "drift zone," occupies the rest of the inter-electrode space, and the electric field there is weaker and relatively uniform. Some electrons produced by the ionization processes possess enough energy to be ejected from the ionization zone and cross the inter--electrode space. As for the other, less energetic electrons, the creation of negative ions results from their attachment to the neutral particles. The term "unipolar zone" can also be used because the charged particles circulating in this zone are exclusively negatively charged. These particles drift along the electric field lines toward the flat anode. Due to their inertia, it is primarily the negative ions that impart momentum to the neutral particles during the numerous collisions. This phenomenon is responsible for an overall flow of gas, described as an "electric wind," with a speed on the order of a few meters per second. The drift zone can be approximated by a truncated cone. This cone-like shape closely matches the shape of the electric field lines along which the charged particles responsible for the acoustic emission drift.

In the inter-electrode space, charged particles (primarily electrons and negative ions) interact with neutral air molecules, imparting a motion (ordered or disordered) through collisions. By electrically modulating these interactions, either with an alternating current flowing through the inter-electrode space or with an alternating voltage applied between the electrodes, it is possible to disturb the air and thus create an acoustic wave. For a tip-plane electrode configuration, the two distinct inter-electrode space regions defined earlier are respectively associated with the two different types of interactions between charged and neutral particles responsible for acoustic emission (heat transfer

and momentum transfer, respectively). It is then possible to consider a transduction mechanism specific to each of the two regions: an acoustic heat source associated with the ionization region, and an acoustic force source associated with the drift region.

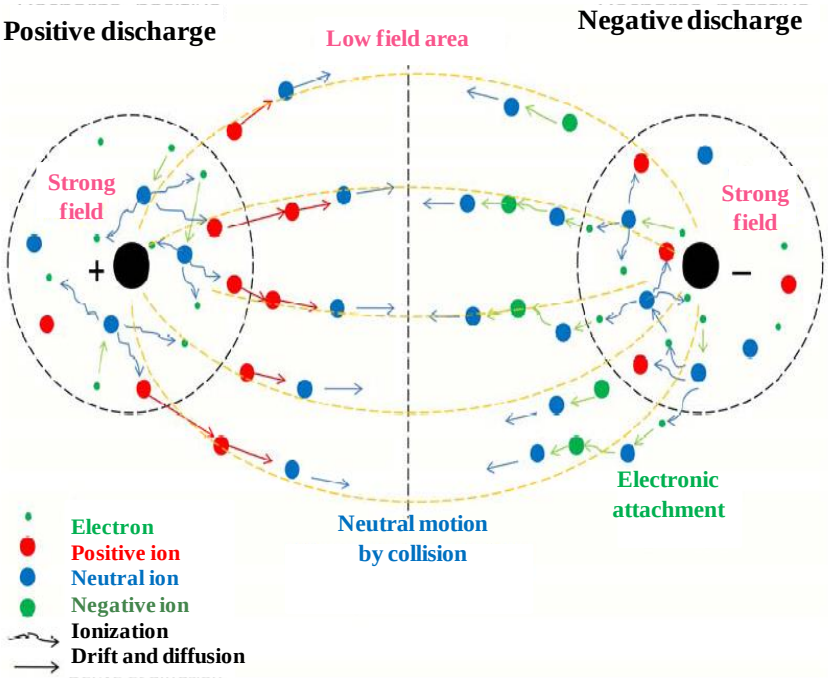

Figure 2.2. Mechanism of bipolar corona [68]

II.4 Different types of corona discharge

Numerous electrode systems are used to generate corona discharges, the most common being tip/plane, multi-tip/plane, knife/cylinder, wire/plane, wire/cylinder, or cylinder/cylinder, as illustrated in figure (2.3). The electrode with the smallest radius of curvature is designated as the active electrode. Generally, wire-cylinder or cylinder-cylinder configurations are most commonly used in gas treatment reactors, multi-tip or wire array configurations for electrostatic precipitation, and dual configurations for electrostatic separation.

Depending on the intended application, the high voltage, which is generally applied to the active electrode, can be pulsed, alternating, or direct current with positive or negative polarity. It is crucial to emphasize that the voltage range applied during corona discharge must exceed the critical corona ignition level (which is determined by the curvature of the corona electrode, the roughness of its surface, the length of the air gap separating the two electrodes, temperature, pressure, and humidity) and remain below the breakdown voltage.

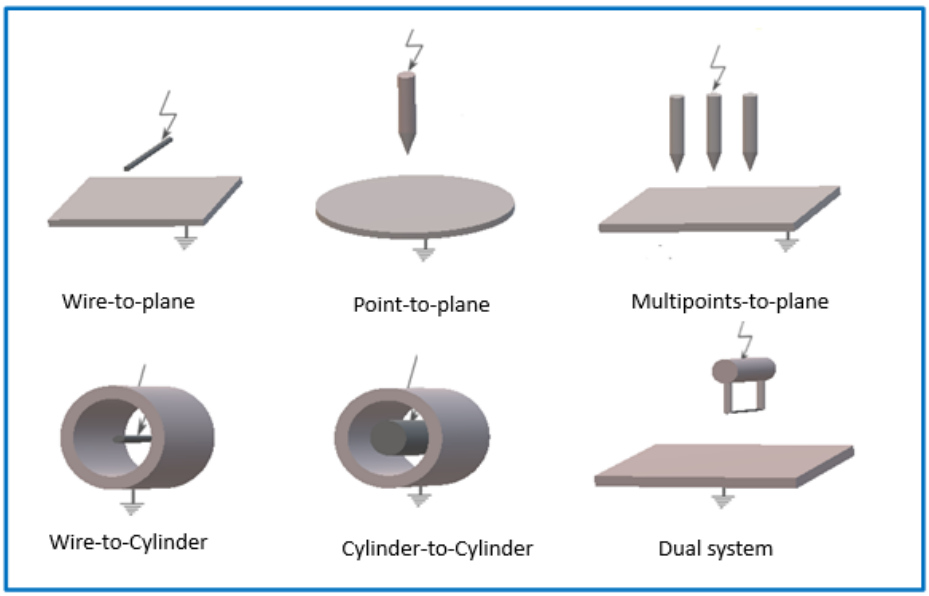

Figure 2.3. Different configurations producing corona discharge [64]

II.4.1 Positive corona

A positive corona discharge occurs when the tip is held at a positive potential and the plate is grounded. In this case, in the intense field region around the tip, electrons are produced by photoionization and accelerated towards the anode. A region of strong ionization then develops around the anode: the dotted line in figure (2.4). The positive ions thus created are repelled by the anode, under the effect of Coulomb forces, to a distance from the tip (less than one millimeter) beyond which the electric field is too weak (< 30 kV/cm in air at atmospheric pressure) to allow the creation of further positive ions.

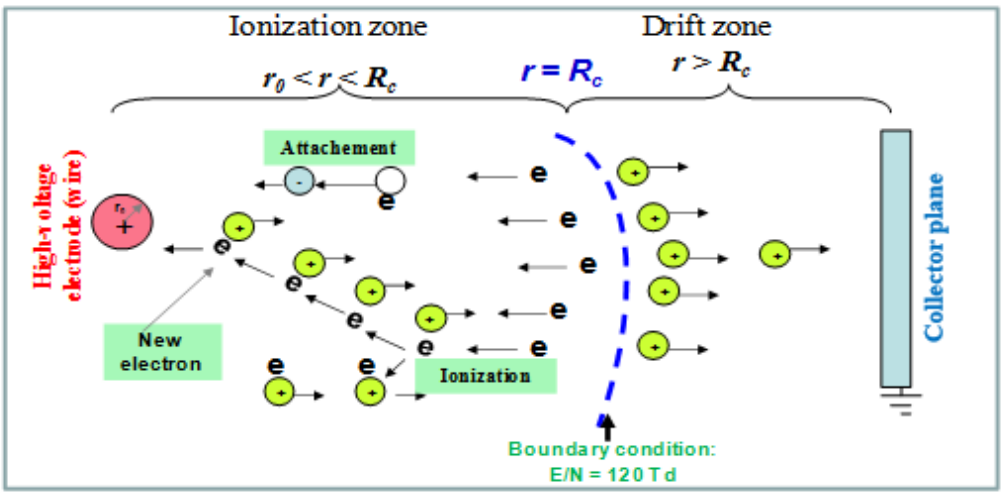

Figure 2.4. Description of the positive corona discharge [69, 70]

The positive ions therefore migrate towards the cathode (the plate). This unipolar region, since it contains only positive ions, is called the "drift" region. During this discharge, there is an advance of

streamers, which propagate somewhat like an extension of the anode. According to the models of Loiseau et al. [71], the discharge consists of a streamer propagation phase (propagation duration of 50 ns at a speed of 210 m/s) and a recovery phase during which the ions drift. These two phases form a 10 kHz frequency cycle. The discharge current is therefore not continuous, but corresponds to a succession of transient phenomena (Figures 2.5 – 2.6).

Goldman et al. in 1985 [72] indicate that a positive current of 50 µA would decompose into a continuous unipolar current of 20 µA, distributed uniformly over the surface of the cathode, and streamers contributing 30 µA striking the cathode at a frequency of 10 kHz.



Figure 2.5. Bright aspect of the positive corona discharge [73]

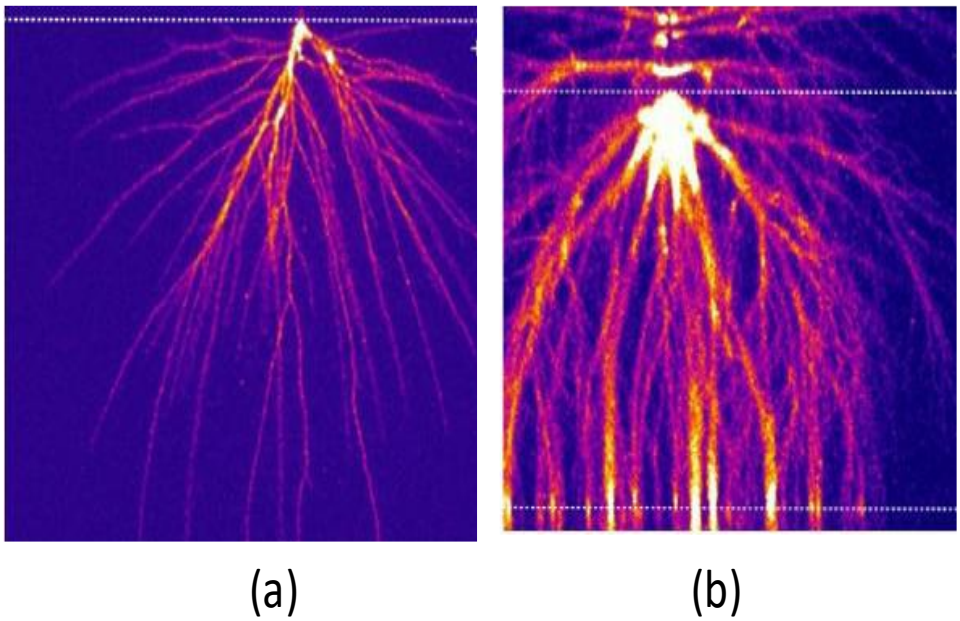

Figure 2.6. Photograph of a positive streamer [74] :

(a) U = 20 kV, (a) U = 46 kV

II.4.2 Negative corona

When the tip is brought to a negative potential, electrons are always created by photoionization, and an ionization zone appears around the tip.

Goldman and Sigmond in 1982 [75] explain that the positive ions created then quickly return to the cathode (Figure 2.7).

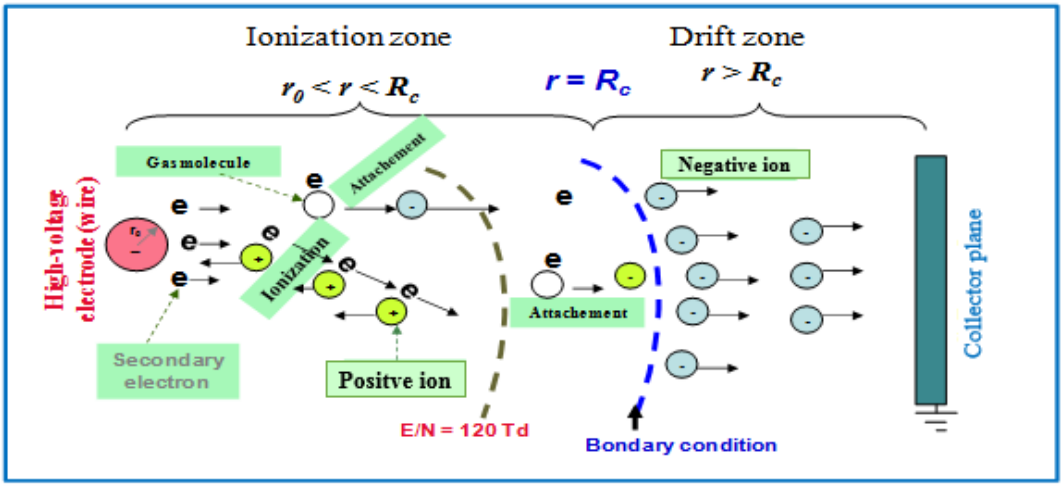

Figure 2.7. Description of negative corona discharge [69, 70]

Only negative ions created by attachment in an area of weaker field can migrate towards the plate. Furthermore, when the high voltage exceeds a certain threshold, arcing occurs. The current from this discharge is due to Trichel pulses, the frequency of which depends on the applied voltage.

These pulses are regular and are caused by the weakening electric field near the cathode. The negative ions effectively prevent the multiplication of electron avalanches. Once these ions migrate towards the anode, new avalanches appear. The interval between two current peaks, or Trichel pulses, therefore depends on the time it takes for the negative ions to reach the anode.

Generally, the threshold field and the onset voltage of corona discharge are lower in negative polarity than in positive polarity (Figures 2.8–2.9).

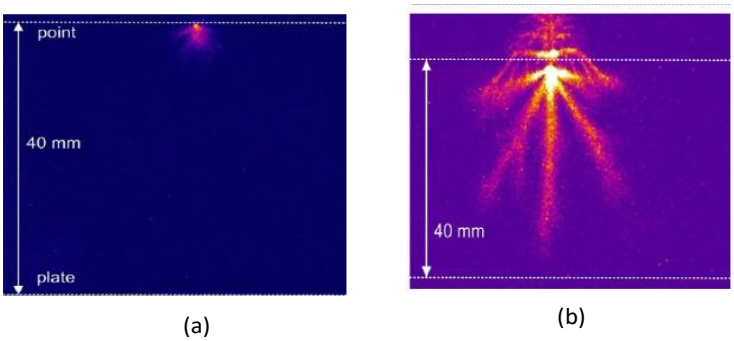

(a) (b)

Figure 2.8. Photographer of a negative streamer [74]:

(a) U = 20 kV, (a) U = 46 kV

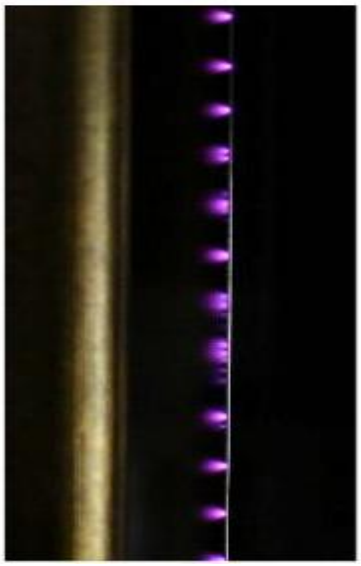

Figure 2.9. Bright appearance of the negative corona discharge [73]

II.5 Numerical simulation of corona discharge in the point-plane configuration

The development of numerical methods has opened up very diverse fields of application, particularly that of determining the characteristics of heterogeneous materials. The performance of these numerical methods has been demonstrated by several researchers [76]. The finite element method (FEM) is one of the most widely used methods today for solving partial differential equations, including Maxwell's equations that govern electromagnetic phenomena. It was first used to solve equations of elasticity and structural mechanics and later adapted to electromagnetism. It appeared in the 1970s, after the FDM. However, its history dates back to 1943 [77, 78]. The FEM is a general method that applies to the majority of problems encountered in practice: stationary or non-stationary, linear or non-linear problems, defined in any geometric domain in one, two or three dimensions.

II.5.1 Geometric description

This configuration is used to analyze various parameters of corona discharge. The geometric model consists of a point-plane system. The various elements of this geometric model are described in Figure 2.10.

As for the physical dimensions, it is a point with length L = 30 cm and a base plane length L = 20 cm. The ion mobility was set at $\mu = 2.10^{-4}$ m^2. V^{-1}. s^{-1}.

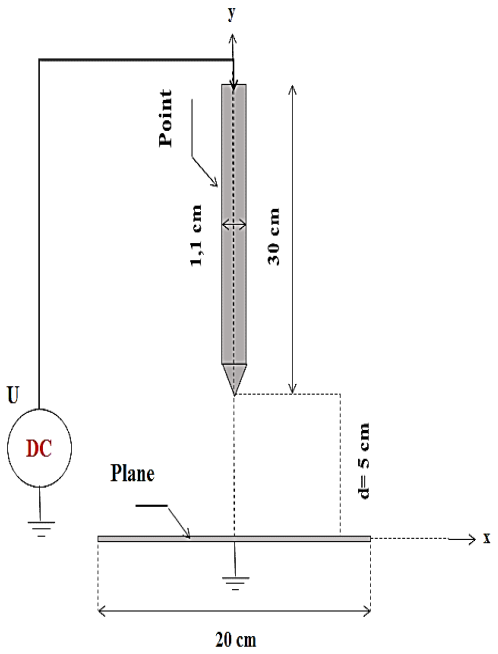

Figure 2.10. Geometry of the discharge point - plane

II.5.2 Solution method flow chart

Figure 2.11 shows the method of analysis used in this work.

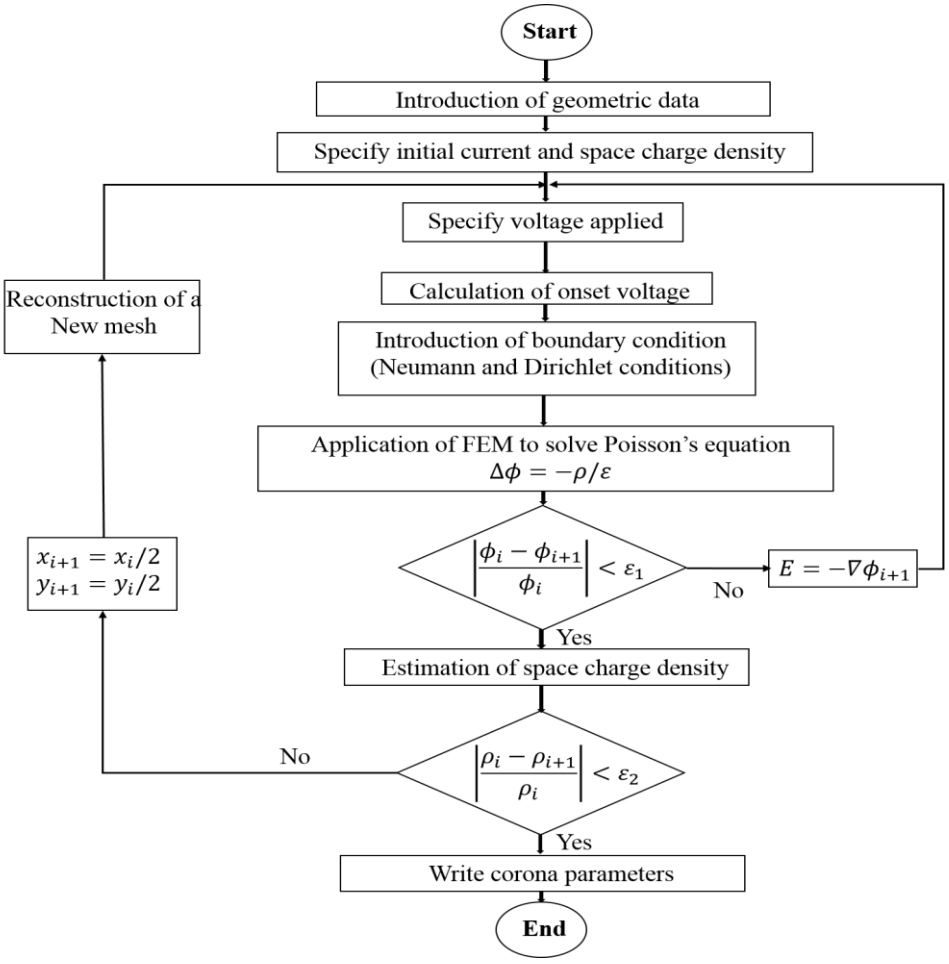

Figure 2.11. Flow chart used in simulation

A solution to a boundary value problem is a solution to the differential equation which additionally satisfies the boundary conditions. To find the solution, we need to know the conditions associated with the field limits of electric potential and space charge density. These conditions are:

- ✓ The potential on the active electrode is equal to the applied voltage.
- ✓ The voltage at the ground is zero.
- ✓ The electric field on the point is equal to the field E_s threshold.
- ✓ Potential values for points on the artificial boundary are determined and used later in finite element formulation.

II.5.3 Results and discussion

In the present work, we used the finite element method found on the COMSOL Multiphysics software, and this method is based on Maxwell's equations, as this program is used by many engineers and designers in the world and covers many areas of physics, including mechanics and electromagnetism. So it is the best program to simulate our problem and it is very convincing and gives reliable results.

II.5.3.1 Mesh grid

Figure 2.12 represents the generated grid for a point-plane electrostatic separator. This mesh grid obtained by the intersection of field lines with equipotential contours. This is called field mapping. it is in the form of a triangular mesh.

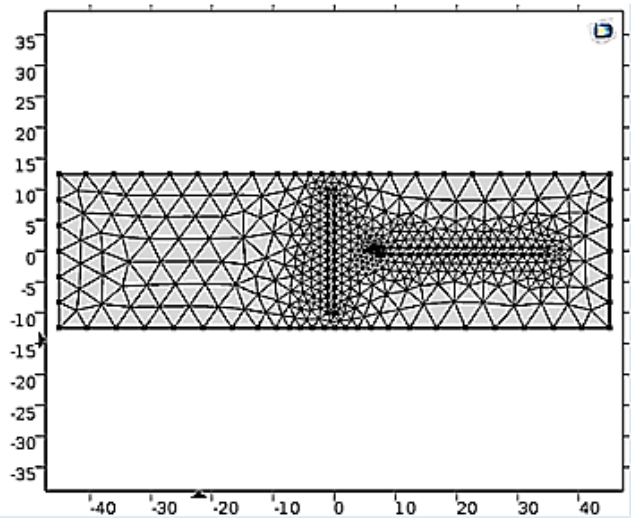

Figure 2.12: Generated grid for an electrostatic separator.

II.5.3.2 Electric potential

The potential distributions and the electrical potential variation are shown in Figures 2.13-2.14.

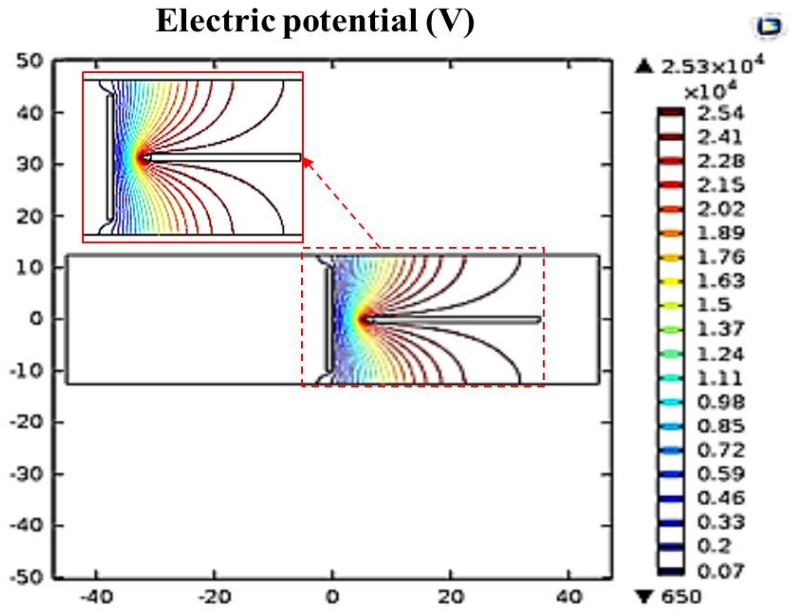

Figure 2.13. Electric potential distribution

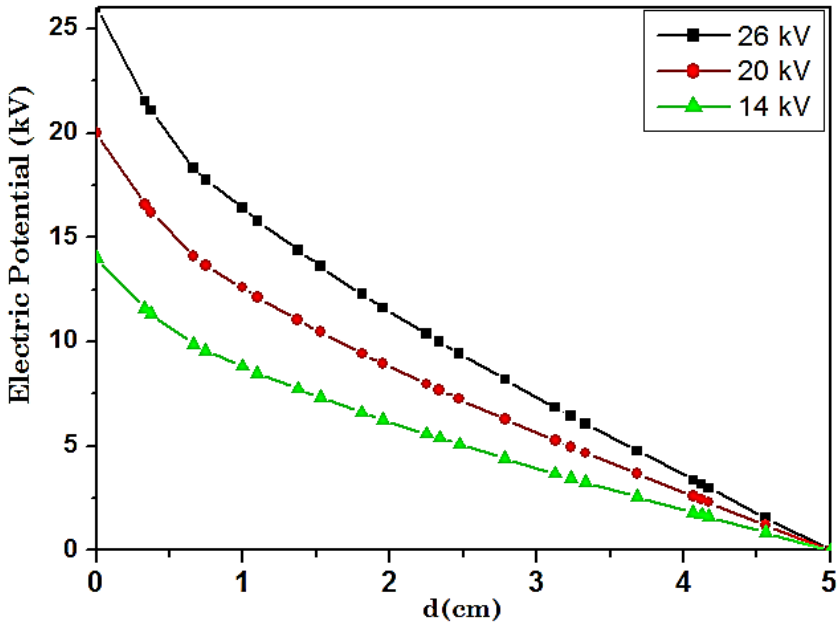

Figure 2.14. Electric potential at the ground plane for different voltages

We observe that the potential distribution has a maximum value around the point and decreases inversely to the distance. The electric potential is directly proportional to the voltage applied.

II.5.3.3 Electric field

Figures 2.15-2.16 present the electric field distribution and the electric field variation at the ground for various applied voltages. The curves show that the electric field is maximum (i.e., highly intense) and non-uniform, there is an ionization of gas produced near the pointed electrode. The

amplitude of the field is proportional to the voltage applied, decreases inversely to the distance and where the electric field is weak, there is constitution of a monopolar spatial charge.

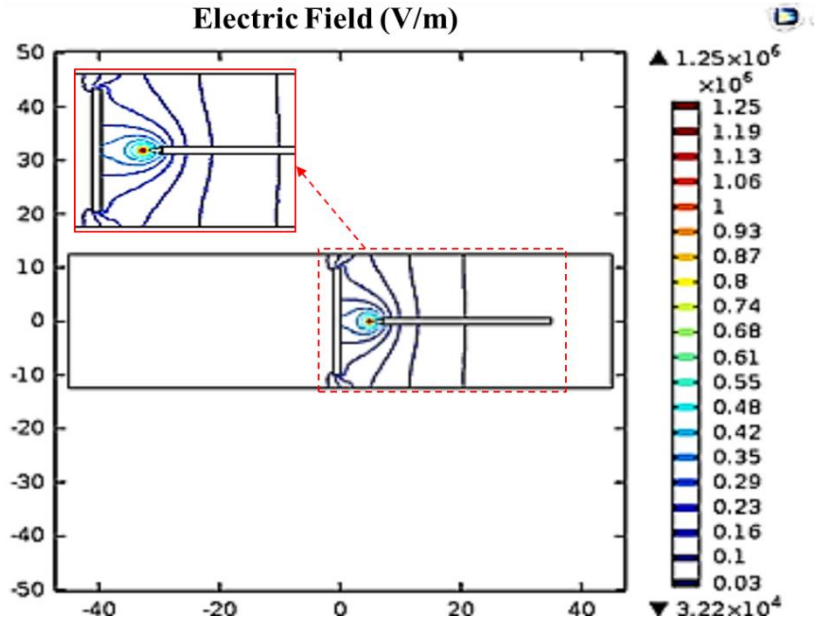

Figure 2.15. Electric field distribution

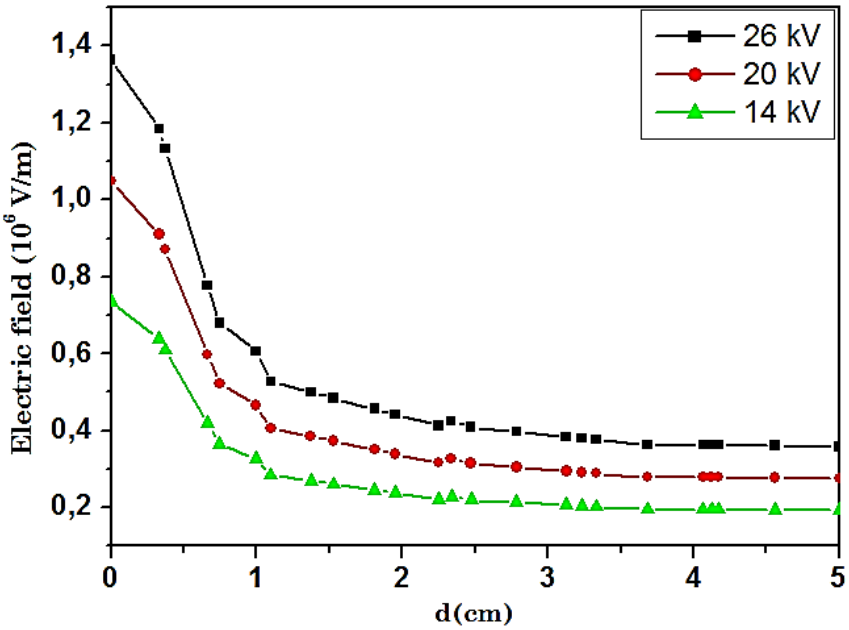

Figure 2.16. Electric field at the ground plane for different voltages

II.5.3.4 Electric displacement

The electric displacement is given by:

$$\vec{D} = \varepsilon_0 . \vec{E} \qquad (2.1)$$

The curves representing the electric displacement according to the different applied voltage are given in Figures 2.17-2.18.

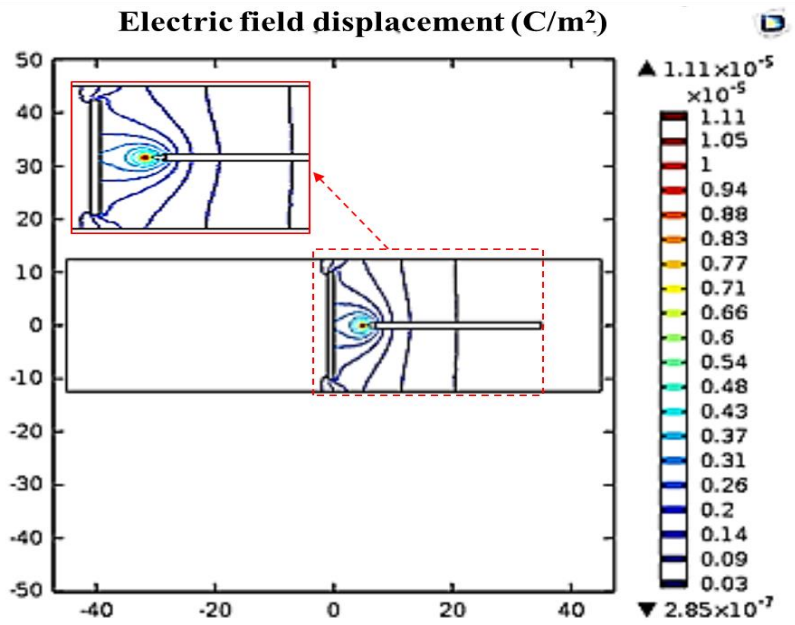

Figure 2.17. Electric field displacement distribution

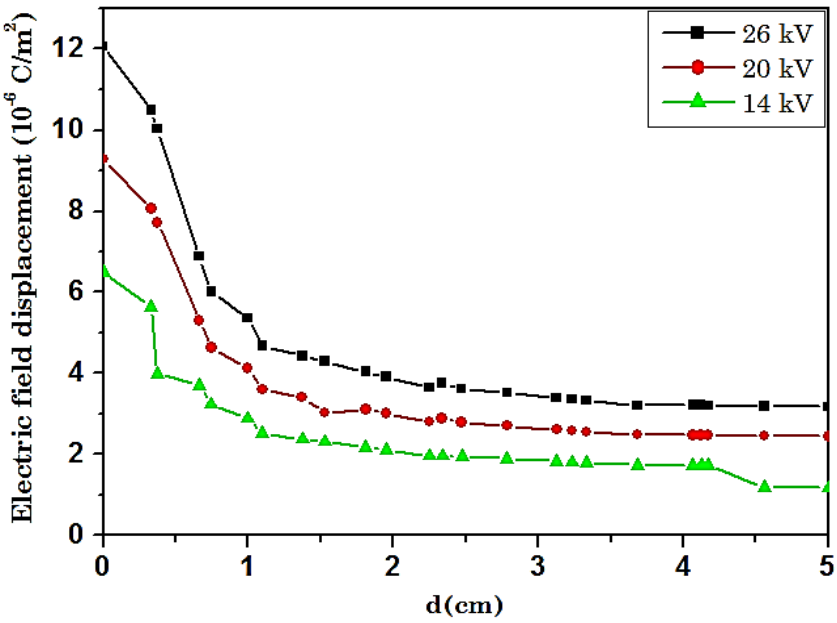

Figure 2.18. Electric field displacement at the ground plane for different voltages

We note that the displacement around the point is maximal and it is not uniform, there is ionization of gas occurs only near the electrode and does not occur near the plane electrode and decreases inversely to the distance.

The electric field displacement magnitude increases directly with the increase of voltage applied.

II.5.3.5 Current density

Figures 2.19-2.20 show the current density. It is maximum in the proximity of the point electrode and approaches zero near the plane electrode.

The current density increases proportionally with the increase of applied voltage.

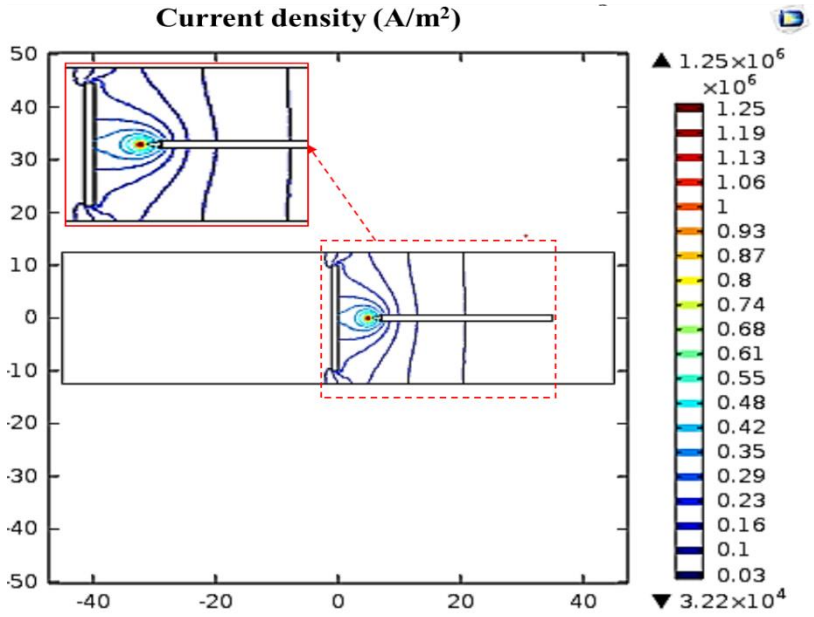

Figure 2.19. Current density distribution

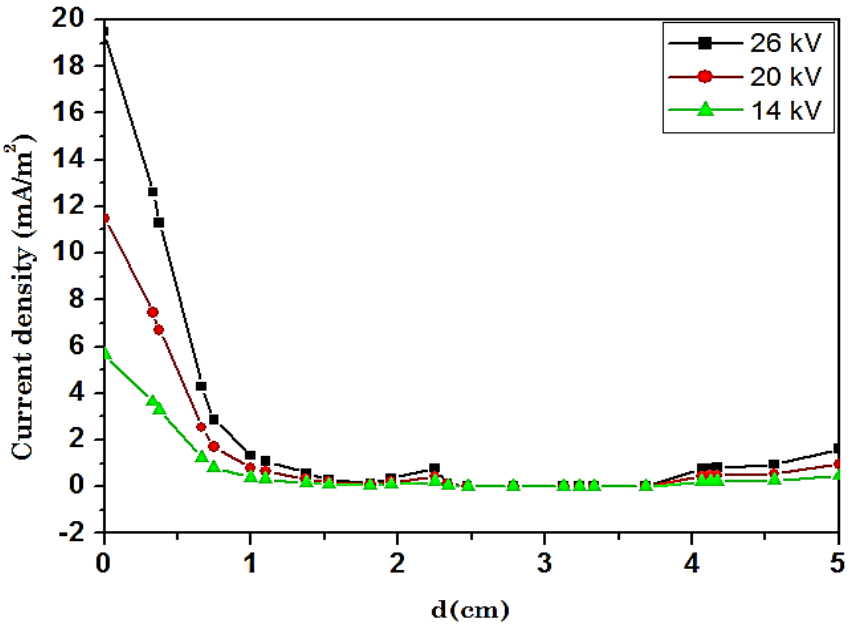

Figure 2.20. Current density at the ground plane for different voltages

Figure 2.21 shows the current-voltage curves in the case of positive high voltage polarity. The discharge current increases with the applied voltage when it exceeds the corona onset voltage (V_s) until gas breakdown occurs.

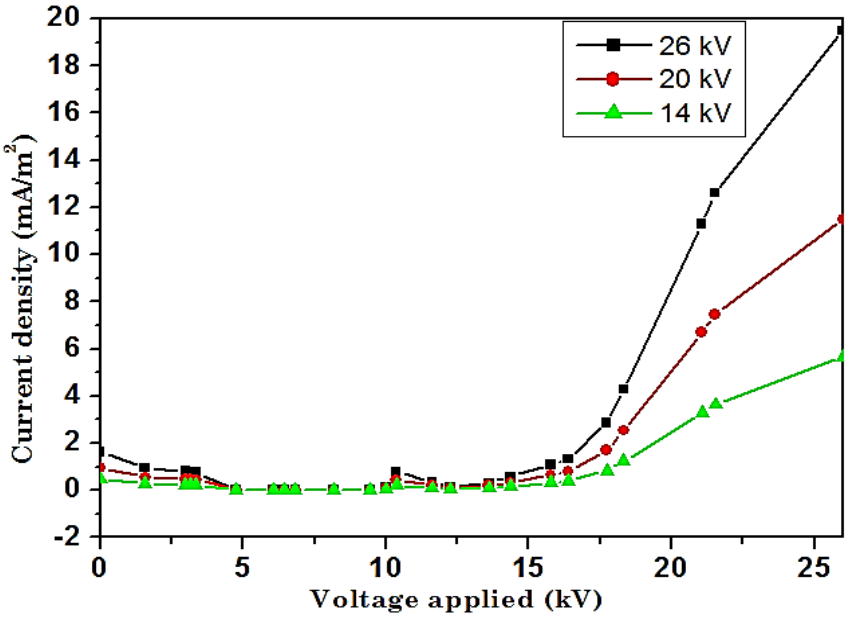

Figure 2.21. Corona discharge current-voltage characteristic

II.5.3.6 Space charge density

The space charge density at the ground plane is shown in Figures 2.22 - 2.24.

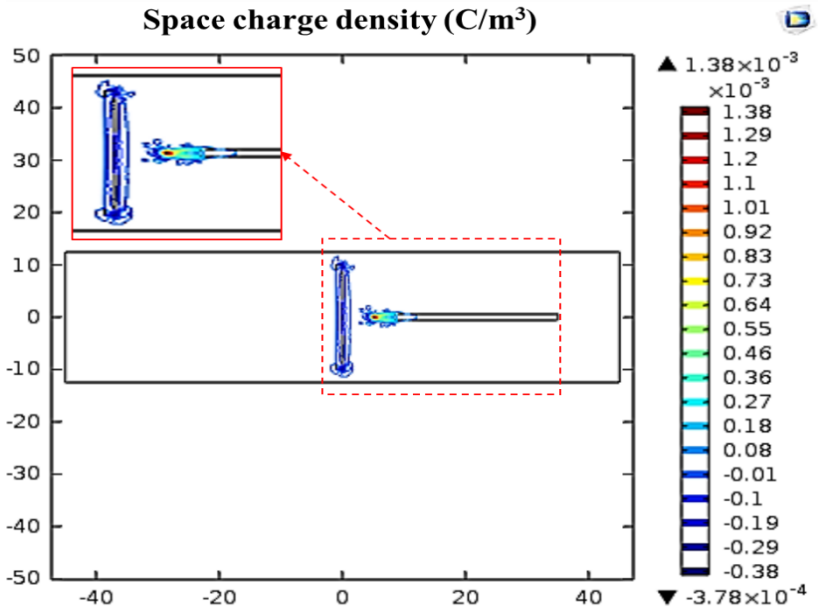

Figure 2.22. Space charge density distribution

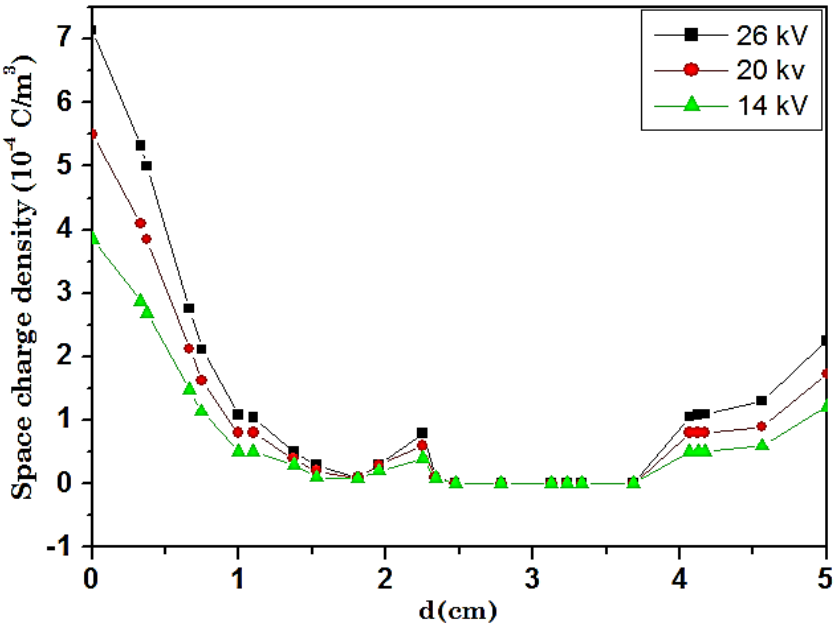

Figure 2.23. Space charge density at the ground plane for different voltages

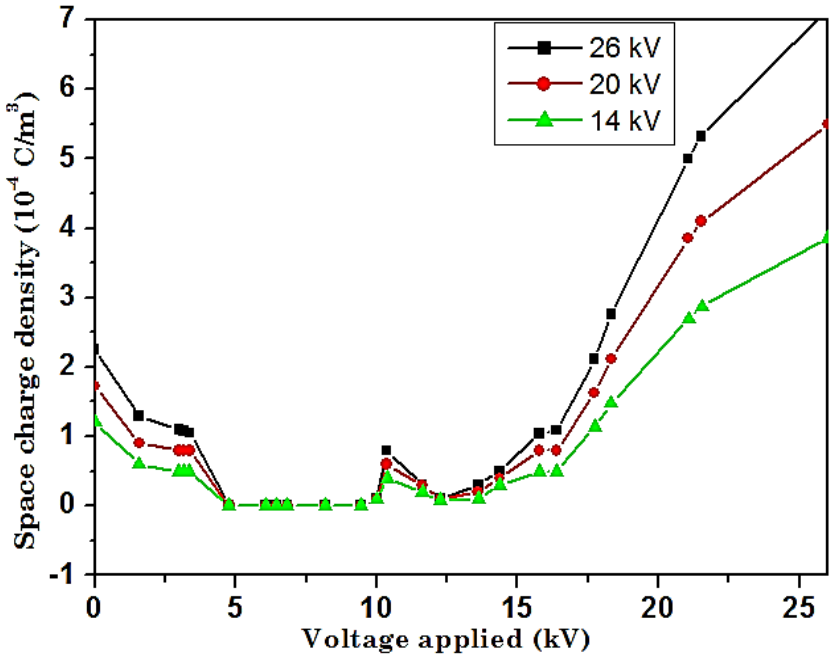

Figure 2.24. Space charge density variation at the ground plane.

We observe that the space charge density reaches its maximum value around the point and decreases inversely to the distance. The effect of the space charge is to weaken the electric field near the corona discharge electrodes, thereby removing some of the corona and its ion generation. The space charge density magnitude increases directly with the increase of voltage applied.

II.6 Conclusion

The numerical model we developed in this chapter was designed to calculate the various electrical parameters characterizing corona discharge. The calculation principle is the iterative and simultaneous solution of the Poisson and current continuity equations. The difficulty of analytically solving these partial differential equations necessitates the development of a strategy for solving the coupled space charge-electric field problem, based on numerical techniques. This solution strategy must be based on a discrete scheme that accounts for the complexity of the geometry and the boundary conditions.

For solving the partial differential equations, we used the COMSOL Multiphysics software. This software offers fully coupled multiphysics and monophysics modeling capabilities, simulation data management, and user-friendly tools for creating simulation applications. Additional modules provide specialized functionalities for electromagnetism.

CHAPTER III

Modeling the separation of fine particles by corona effect

III.1 Introduction

Environmental pollution is one of the most important problems in the world. This is very important because without a safe and healthy environment, humans will not be able to continue with their natural lives. Therefore, protecting and maintaining the environment is considered one of the most important basic needs for every human being. Environmental protection consists of taking measures to limit or eliminate the negative impact of human activities on the environment. Human health and comfort of inside buildings or enclosed spaces are associated today with indoor air quality. Indoor air quality is also governed by a suite of airborne contaminants such as particulate matter. Treating waste and particles suspended in the air are pollution control actions. They prevent pollution of water, air and soil which would be inevitable if the waste is fine particles. We can use particle capture devices that work thanks to electrostatic phenomena.

In this paper, a new method for solving the Maxwell's equations associated with electrostatic separator is presented. The boundary value problem is transformed into an optimization problem by using the finite element method.

Numerical simulations were carried out using Matlab software that performs equation-based multiphysics modeling for different physical processes by applying the finite element method and modified method of characteristics to a system of partial differential equations.

III.2 Principle of electrostatics applied to air filtration and material separation

Electrostatic precipitators are widely used in environment technology to collect suspended particles in gases using an electrostatic force and they are one of the ways to control air pollution caused by industrial plants [79-83]. Much research has been carried out during the last decades. The configuration mostly used in electrostatic precipitation system is the wires-to-plates. It consists of high-field parallel active wires located midway between the collecting electrodes where the air flows through. The ions produced by the corona discharge near the wires charge and the dust particles which are thus driven toward the collecting plates. The particle charges are neutralized and the particle is thus collected [84-86].

Generally, the efficiency collection of electrostatic precipitator is high, approaching 100%. Several installations have efficiencies of 98% and 99%. Some materials ionize more easily than others and are therefore more suitable for removal by electrostatic precipitation. For acid mists and catalytic recovery units, yields often exceed 99%; for black carbon, the normal collection efficiency is less than 35%, because of its tendency to agglomerate. However, by a suitable combination of an electrostatic precipitator with a cyclonic collector, high yields can be obtained for this material.

An electrostatic precipitator (ESP) is a particle control device that uses electrical forces to move the particles out of the flowing gas stream and onto collector electrodes. In the electrostatic

precipitation process, suspended particles in the flowing gas are first electrically charged and then driven to collecting electrodes under the force of the electrostatic field [87-89].

ESPs are configured in several ways. Some of these configurations have been developed for special control action, and others have evolved for economic reasons. The most common types are the tubular precipitator and the wire-plate precipitator [90]. There are also dry and wet types of precipitators depending on whether water is used to clean the collecting electrodes. ESP's are also classified as either single-stage or two-stage. In single-stage, the particle charging and the particle collection processes are all taken place in the same area. In the two-stage, the charging section is followed by a separate collection section. Most industrial ESPs are single-stage dry type, which can handle large volume of flue gas and are used extensively in many industries [91-93].

The corona effect is widely employed in various electrostatic processes, such as: precipitation of dust, xerography, or spraying of liquids. In electrostatic separators, corona discharge achieves the selective charging of insulating and conductive particles under the action of the electrostatic forces [94,95]. Corona is the name given to glow discharges at high pressure near points of high fields, usually caused by a small radius of curvature. Points are an obvious place for corona, and this is their intention in lightning rods. High voltage conductors are another good place, but here it is very undesirable. It is commonly stated that the breakdown field for air is 30kV/cm, but the phenomenon is far too complex for such a simple criterion. Nevertheless, this value is of use for engineering estimates. A negative wire becomes a cathode, and the glows contract to regular regions along the wire, like beads, each surrounded by a brush. A positive wire becomes an anode, with a uniform anode glow spread along it. Corona loss may exceed resistive loss in the conductors. It is less if the conductors are smooth and of large diameter.

Fine particles suspended in the air can collect electric charges thanks to several mechanisms which are: the natural charge by attachment of the ions existing in the atmosphere, the charge by space charge and triboélectrisation (the gaseous ions being produced in this case mainly using a radioactive source or electric discharge). The ion density can be unipolar (positive or negative used for particle charge) or bipolar (used for aerosol neutralization).

One of the areas of electrophysical technologies application is the beneficiation of rocks. In particular, dry separation of minerals based on the difference in electrical properties of different substances using electric corona separators [96].

This paper presents a numerical algorithm which can be used to simulate the essential parameters of the process including the electric field, the space charge density the current density and EPS efficiency. The objective was to develop a program that could perform all the computations of the model and the separation of materials in commercial use and being developed. This work is focused

to finding a solution for Poisson's equation. This allows introduction of current and electrode geometry as well as space charge and ionic [97-99].

III.3 Mathematical modelling

The solution of the space charge field for wire-duct precipitators is described in the following sections. The electric field is a function of two essential parameters: voltage and space charge density. To identify the values of this field at any point in the inter-electrode space, it is necessary to solve Maxwell's and the continuity of current flow equations.

III.3.1 Geometric description of the problem

To lead this study, the electrostatic precipitator configuration used as shown in Figure 3.1.

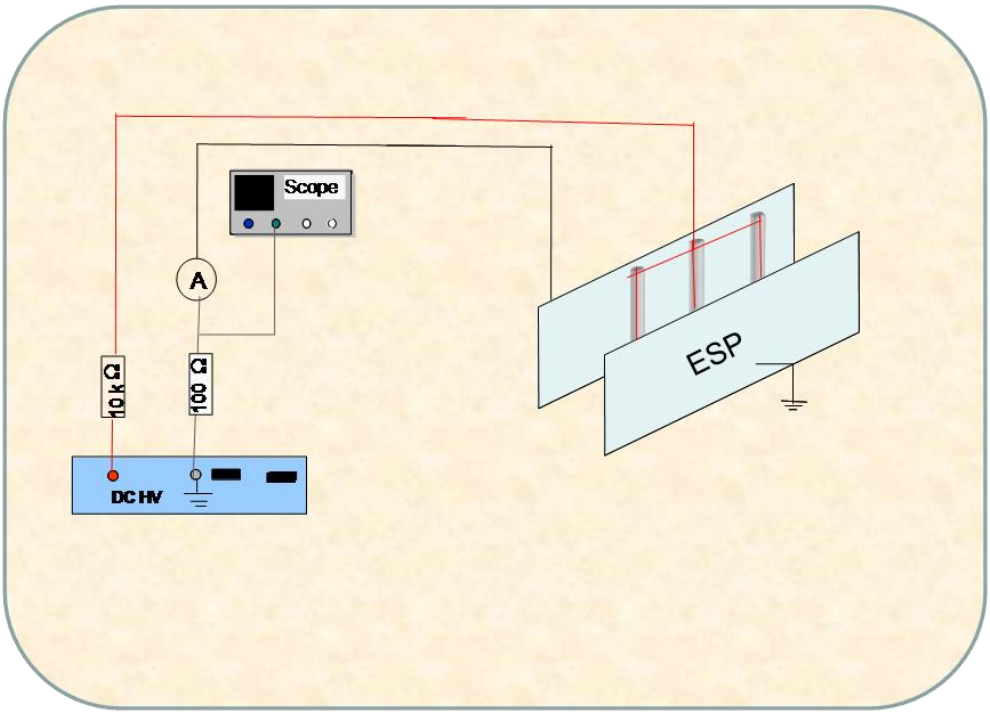

Figure 3.1. Assembly system of electrostatic precipitator

There investigated wires-two planes configuration has wires with radius R and height H above the ground plane (see Figure 3.1). Three parallel wires conductors are fixed with two insulating supports and located midway between two planes at H = 50 mm and the wire-to-wire spacing is fixed at a = 50 mm. Each wire is a radius R = 0.2 mm and supplied by a high voltage potential V_{app} = 20 kV. The ground plane has a length L=800 mm and width W=150 mm.

III.3.2 Governing equations

There system of equations that constitute the mathematical description of the corona phenomenon is obtained from the following relations [100 - 102]:

$$\nabla \cdot \vec{E} = \frac{\rho}{\varepsilon_0} \tag{3.1}$$

$$\nabla \cdot \vec{J} = 0 \tag{3.2}$$

$$\vec{J} = \rho \mu \vec{E} \tag{3.3}$$

$$\vec{E} = -\nabla \phi \tag{3.4}$$

$$\nabla^2 \phi = \mp \frac{\rho}{\varepsilon_0} \tag{3.5}$$

where E is the electric field intensity, ρ is the space charge density, J is the current density vector, ϕ is the electric potential, ε_0 is the permittivity of free space and μ is the ion mobility.

III.3.3 Boundary conditions

There in mathematics, a boundary value problem is a differential equation together with a set of additional constraints, called the boundary conditions. A solution to a boundary value problem is a solution to the differential equation which also satisfies the boundary conditions. To find the solution we need to know the conditions associated with the domain boundaries for the electric potential and space charge density. These conditions are [103, 104]:

- ✓ The potential on the coronating conductor is equal to the applied voltage.
- ✓ The potential on the grounded electrode is zero.
- ✓ The electric field on the conductor is equal to the onset field strength (Peek criterion) [105]:

$$E_{\text{peek}} = A_0 \cdot \delta + B_0 \sqrt{\frac{\delta}{r_0}} \tag{3.6}$$

where $A_0 = 32.3 \times 10^5$ V/m; $B_0 = 0.846 \times 10^5$ V/m$^{-1/2}$, δ: relative density of the air.

- ✓ The values of the potential to the points situated on the artificial boundaries are identified and subsequently used in the finite element formulation (Newman condition) [106]:

$$\frac{\partial E}{\partial n_i} = 0 \text{ [V/m]} \tag{3.7}$$

III.3.4 Proposed method of analysis

In the present work, the finite element method is shown to be uniformly applicable to all the equations describing the problem of electric field in corona devices.

The finite elements used to discredit the domain are generally grouped into topological families: segments, triangles, quadrilaterals, tetrahedral, parallelepipeds, prisms. Each element is represented by points called geometric nodes. Interpolation nodes are associated with each element where the unknown will be calculated. Thus, for each element resulting from the subdivision, the function modeling the phenomenon is defined by a polynomial interpolation.

Figure 3.2 shows the computational flow of this method. The procedures of this calculation are as follows: An iterative finite-element technique is used to solve Poisson equation. Two algorithms are proposed for satisfying the current continuity condition and updating the space-charge density. The first algorithm is a modified method of characteristics, which neglects ion diffusion. The second algorithm is based on application of Kirchhoff's current-balance law at each node of the finite-element grid and takes ion diffusion into account [107].

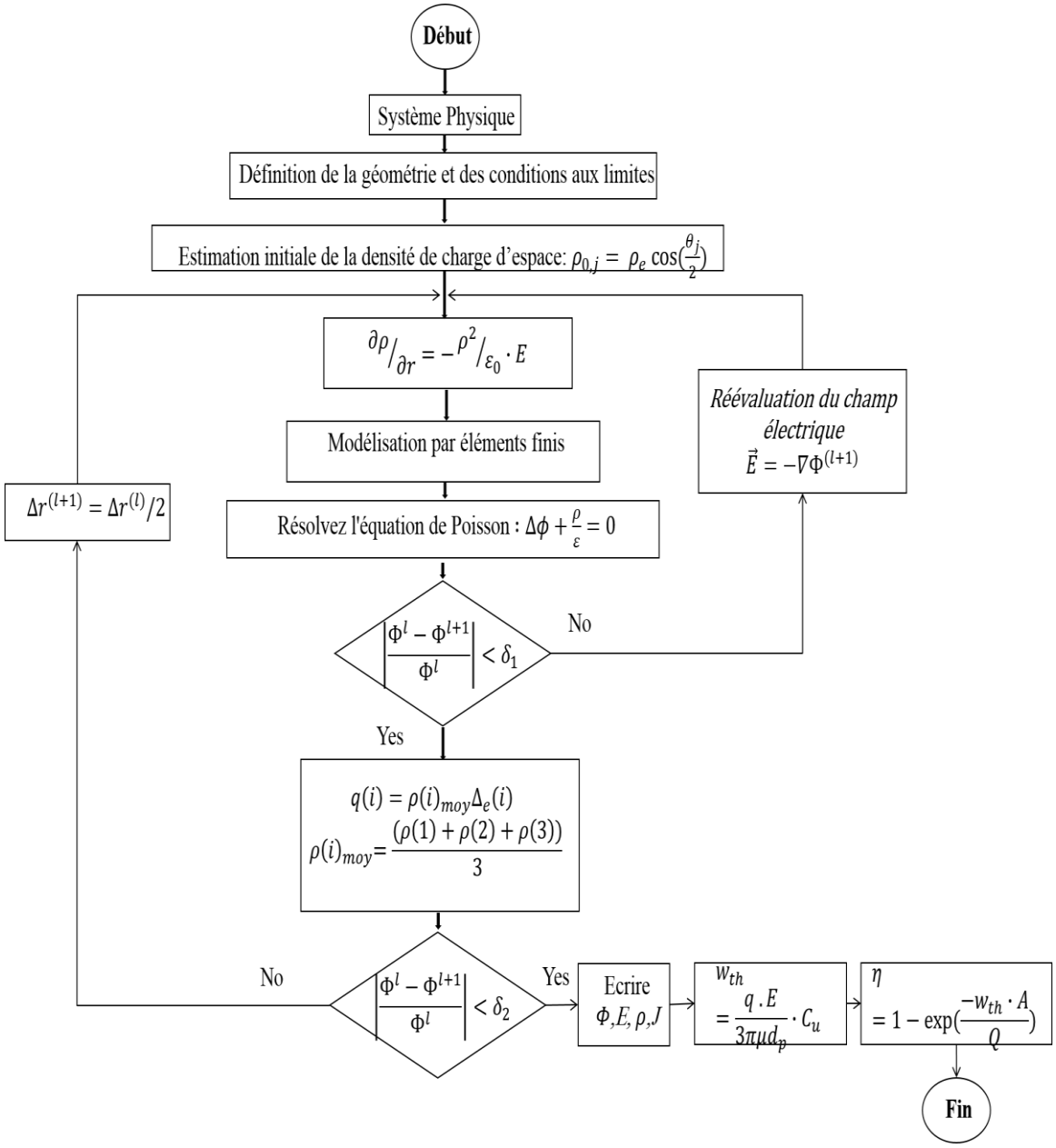

Figure 3.2. Flow chart of the solution method

III.3.5 Matrix formulations of the finite element method

When we use matrix techniques, we are successively led to consider two levels of formulation: elementary and global. The Poisson equation for two dimensions is given in the form:

$$\frac{\partial^2\Phi}{\partial x^2}+\frac{\partial^2\Phi}{\partial y^2}+g=0 \tag{3.8}$$

According to Euler's theorem, solving this differential equation is equivalent to minimizing the energy functional W which is written as:

$$W=\iint_{\Omega}[\frac{1}{2}[\frac{\partial^2\Phi}{\partial x^2}+\frac{\partial^2\Phi}{\partial y^2}]-g]dxdy \tag{3.9}$$

The integral is extended to a set of the computational domain, which is subdivided into small elements by triangular mesh where each triangle is identified by its three vertices (nodes). The interpolation polynomials of the potential at the vertices of the triangle are given by the following system of equations:

$$\begin{cases}\phi_1=\alpha_1+\alpha_2x_1+\alpha_3y_1\\ \phi_2=\alpha_1+\alpha_2x_2+\alpha_3y_2\\ \phi_3=\alpha_1+\alpha_2x_3+\alpha_3y_3\end{cases} \tag{3.10}$$

Solving the system (3.10) gives us the coefficients α_i:

$$\begin{cases}\alpha_1=\frac{1}{2\Delta_e}[a_1\cdot\phi_1+a_2\cdot\phi_2+a_3\cdot\phi_3]\\ \alpha_2=\frac{1}{2\Delta_e}[b_1\cdot\phi_1+b_2\cdot\phi_2+b_3\cdot\phi_3]\\ \alpha_3=\frac{1}{2\Delta_e}[c_1\cdot\phi_1+c_2\cdot\phi_2+c_3\cdot\phi_3]\end{cases} \tag{3.11}$$

With:
$$\begin{cases}a_1=x_2\cdot y_3-x_3\cdot y_2 & b_1=y_2-y_3 & c_1=x_3-x_2\\ a_2=x_3\cdot y_1-x_1\cdot y_3 \;; & b_2=y_3-y_1 \;; & c_2=x_1-x_3\\ a_3=x_1\cdot y_2-x_2\cdot y_1 & b_3=y_1-y_2 & c_3=x_2-x_1\end{cases} \tag{3.12}$$

$$2.\Delta_e=\begin{vmatrix}1 & x_1 & y_1\\ 1 & x_2 & y_2\\ 1 & x_3 & y_3\end{vmatrix}=b_1c_2-b_2c_1 \text{ : The area of the triangular element.} \tag{3.13}$$

The Φ at any point of an element) is expressed by the relation:

$$\Phi(x,y)=\sum_{i=1}^{3}\phi_i\cdot N_i(x,y)=[N_1N_2N_3]\begin{bmatrix}\phi_1\\ \phi_2\\ \phi_3\end{bmatrix} \tag{3.14}$$

With: $N_i(x,y)=\frac{1}{2.\Delta_e}(a_i+b_ix+c_iy)$; i=1, 2, 3 . (3.15)

The functions N_i are called shape functions. They must verify the following condition:

$$N_i(x_j, y_j) = \delta_{ij} = \begin{cases} 1 \ si \ \ i \approx j \\ 0 \ si \ \ i \neq j \end{cases} \quad (3.16)$$

The minimization of the functional W is achieved when the partial derivatives with respect to all the potentials of the nodes are zero, that is: $\frac{\partial W}{\partial \{\phi\}} = 0$. With $\{\phi\}$ is the potential vector for all nodes in the system.

Equation (3.9) shows that we can restrict the double integral to the domain formed by the n elements $(e_i)_n$ including vertex i. We deduce:

$$\frac{\partial W}{\partial \phi_i} = \sum_n \iint_{(e_i)_n} \left[\left(\frac{\partial \phi_{(e)}}{\partial x} \frac{\partial}{\partial \phi_i} \left(\frac{\partial \phi_{(e)}}{\partial x} \right) + \frac{\partial \phi_{(e)}}{\partial y} \frac{\partial}{\partial \phi_i} \left(\frac{\partial \phi_{(e)}}{\partial y} \right) \right) - g \cdot \frac{\partial \phi_{(e)}}{\partial \phi_i} \right] dx.dy \quad (3.17)$$

Which becomes, taking into account (3.9) to (3.17):

$$\frac{\partial W}{\partial \phi_i} = \sum_n \iint_{(e_i)_n} \left[\left(\frac{b_i}{2\Delta} \sum_j \frac{b_j \phi_j}{2\Delta} + \frac{c_i}{2\Delta} \sum_j \frac{c_j \phi_j}{2\Delta} \right) - g.N_i \right] dx.dy \quad (3.18)$$

We arrive at a linear system of matrix form:

$$K \cdot \Phi = F \quad (3.19)$$

With: K: Stiffness matrix; Φ: Matrix of unknowns at the nodes and F: Second member of the system.

III.4 Results and discussion

The permittivity of the various materials used in this work is listed in Table 3.1. These values are approximate and may vary markedly as a function of frequency, temperature, hygrometry or even atmospheric pressure. Permittivity is also called dielectric constant.

The relative permittivity is the permittivity of a material expressed as a ratio with the electric permittivity of a vacuum. A dielectric is an insulating material, and the dielectric constant of an insulator measures the ability of the insulator to store electric energy in an electrical field. Permittivity is a physical property that describes the response of a given medium to an applied electric field. It is a macroscopic property, essential to electrostatics, as well as to the electrodynamics of continuous media.

The dielectric constant or relative permittivity is one of the basic properties of semiconductor and insulating materials. The data reported in literature shows minor discrepancies about the values of this parameter. In this paper, a new method is proposed to calculate the collection efficiency and the charging mechanisms of particles in electrostatic precipitators where the electric field and permittivity are associated. The applied voltages are +20 kV. For this study, the air parameters are

constant, where the temperature, Pressure and relative humidity were maintained respectively at 20°C, 1bar and 50% (Table 3.1).

Table 3.1: Permittivity and rigidity of materials used in simulation.

Material	Relative permittivity	Resistivity (Ω.m) at 20 °C	Conductivity (S/m) at 20 °C
Air	1	1.3×10^{16} to 3.3×10^{16}	3×10^{-15} to 8×10^{-15}
Teflon	2.1	10×10^{22} to 10×10^{24}	10^{-25} to 10^{-23}
Hard rubber	4	1×10^{13}	10^{-14}
Dust particle	4.5	10^{2} to 5×10^{8}	10^{-2} to 2×10^{-7}
PVC	5	10^{14}	10^{-14}
Glass	6	10×10^{10} to 10×10^{14}	10^{-11} to 10^{-15}
Silicon	11.68	6.40×10^{2}	1.56×10^{-3}
Gallium arsenide	13.1	5×10^{-7} to 10×10^{-3}	5×10^{-8} to 10^{3}
Germanium	16.0	4.6×10^{-1}	2.17

III.4.1 Numerical determination of the mesh grid

Figure 3.3 shows an example of the triangular mesh to three nodes finite element for configurations to be studied. The node is obtained by the intersection of the line with the equipotential contours, these triangles around the wire section is reduced but increases if one goes to the plate.

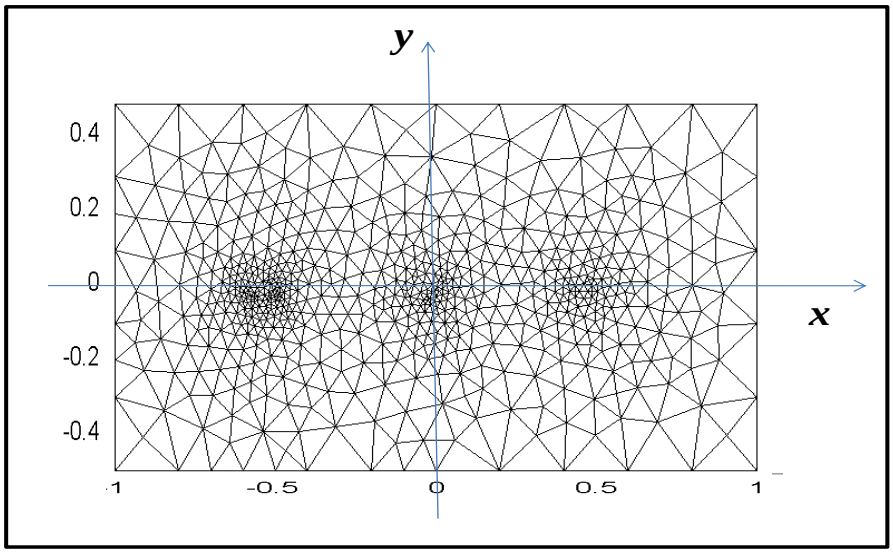

Figure 3.3. Generated mesh grid

An equipotential surface is the locus of points in space where the potential has a given value. Two equipotential surfaces never intersect. An equipotential surface is orthogonal to the field line

passing through a point in each of its points. The algorithm plot of the equipotential lines is quite similar to that of field lines.

III.4.2 Electric potential

The potential distribution is shown in Figure 3.4. The potential distribution has a maximum value around the wire and decreases inversely to the distance. If an electric field is defined as the force per unit charge, then by analogy an electric potential can be thought of as the potential energy per unit charge. Therefore, the work done in moving a unit charge from one point to another. The electric potential is just such a scalar function. Electric potential is related to the work done by an external force when it transports a charge slowly from one position to another in an environment containing other charges at rest.

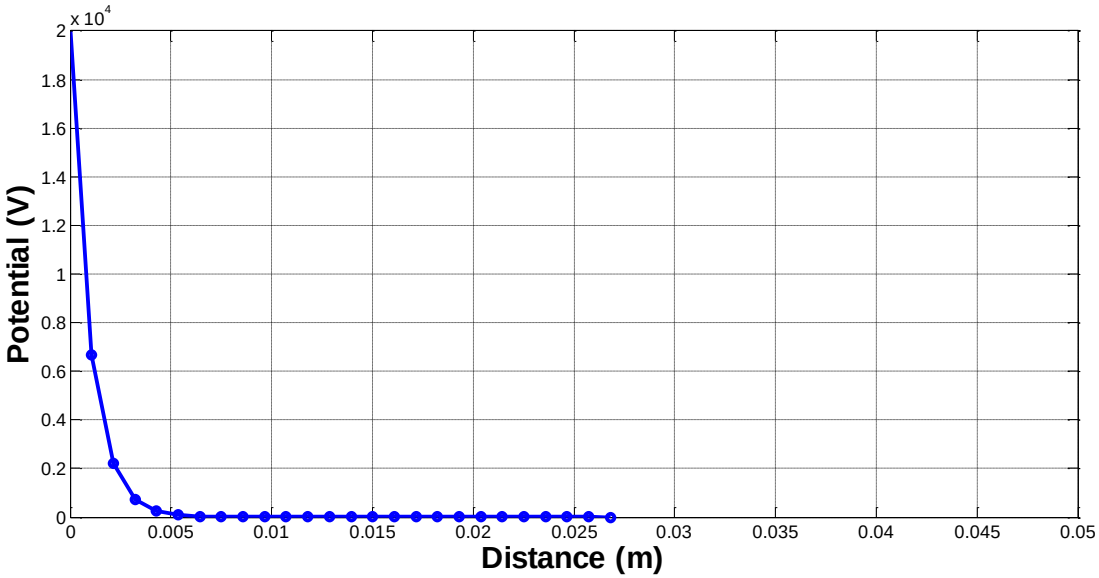

Figure 3.4. Electric Potential distribution

III.4.3 Electric field

This investigation describes the process of an electric field production in an electrostatic precipitator. The electric field, like charge and voltage, is a fundamental quantity of interest in electromagnetic compatibility, electrostatics, and many other disciplines. Electrostatics is based primarily on the observation that like charges repels and unlike charges attract. The electrostatic force and the electric field on the ith charge can be written more simply as:

$$E_i = \sum_{i=1}^{n} \frac{q_j}{4\pi\varepsilon_0 r_{ij}^2} a_{ij} \tag{3.20}$$

$$\vec{F} = q \cdot \vec{E} \tag{3.21}$$

The electric field variations are shown in Figure 3.5. We find that the electric field around the wire is maximal and decreases rapidly approaching the plane

It can be concluded that the wire diameter is inversely proportional to the discharge electric. This is quite normal because the electric field on the wire is inversely proportional to the radius wire r_0. In addition, we note that the variation of the electric field to the plane is not linear.

On the wire, the field is intense (ionization zone) and it decreases rapidly to a minimum value in the vicinity of the plane (drift zone). We also notice that the electric field in wire-cylinder is more intense than in wire - 2 plans and then wire-1paln geometries.

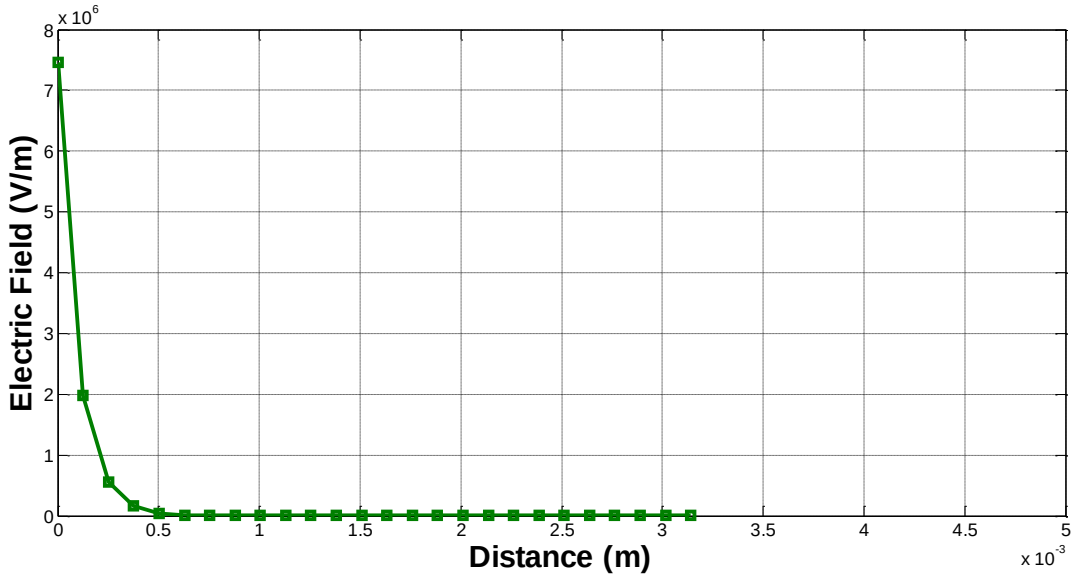

Figure 3.5. Variation of electric field

The electric field vector is the sum of the field due to the voltage applied at the electrode plus the field contribution of the continuous space charge distribution. It will be appreciated from this fundamental approach that the operation of an electrostatic discharge is dependent on having a voltage high enough to produce an electric field in order to precipitate the particles and have sufficient current capability to satisfy ion production for the initial charging of the particles.

III.4.4 Current density

Mathematically, the current and current density are linked by the following relation:

$$I = \iint_S J(x,y)dS \qquad (3.22)$$

I is the electric current in amperes A. $J(x,y)$ is the current density at the coordinates point (x,y) in A.m^{-2}. S is the area in m^2.

The calculated distributions of current density are shown in Figure 3.6. Current density is maximal under the coronating wire and then decreases gradually away from it.

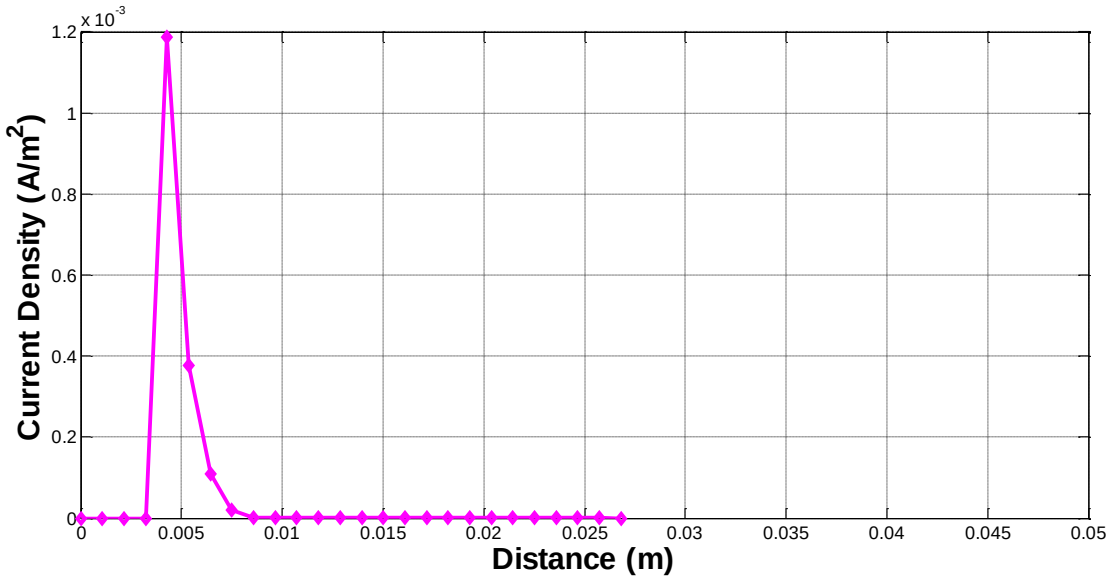

Figure 3.6. Variation of current density

The current density is the ratio of the electric current flowing at a particular point in a conductor to the cross-sectional area of the conductor taken perpendicular to the current flow at that point.

III.4.5 Space charge density

The space charge density variation is shown in Figure 3.7. The Space charge is the fundamental of the collective effects whose impact generally is proportional to the beam intensity. The charge and current of the beam create self-fields and image fields which alter its dynamic behaviour and influence the single particle motion as well as coherent oscillations of the beam as a whole.

The electric charge is the source of electric field, the electric field at any point in space can be mathematically related to the charges present.

From the current continuity equation:

$$\nabla J = 0 \Rightarrow \nabla[\rho(\mu E)] = 0 \Rightarrow (\nabla\rho)(\mu E) + \rho\mu\nabla E = 0 \tag{3.23}$$

$$\text{(3.1) and (3.23)} \quad \Rightarrow \nabla\rho = \frac{-\rho^2}{\varepsilon_0 E} \tag{3.24}$$

Along field lines, the equation1 becomes:

$$\frac{\partial\rho}{\partial r} = \frac{-\rho^2}{\varepsilon_0 E} \tag{3.25}$$

Integration of equation (3.25) gives values of the space charge density along field lines. The interelectrode space in electrostatic precipitator is subdivided in two distinct regions, the ionization and the drift regions: The ionization region is considered of circular form because its thickness layer is small. It is separated from the drift region. In this region, it is often assumed to the first order, that the electric field is described adequately by Laplace's equation. That is, within this region, the

space charge field is assumed to be dominated by the geometric electric field associated with the large curvature of the wire. The drift region is characterized mainly by the transport of positive ions to the grounded planes and within this region the electric field is significantly distorted by space charge. It is often assumed that, to the first order, the space charge is formed by positive ions. The space charge is a concept in which excess electric charge is treated as a continuum of charge distributed over a region of space rather than distinct point-like charges.

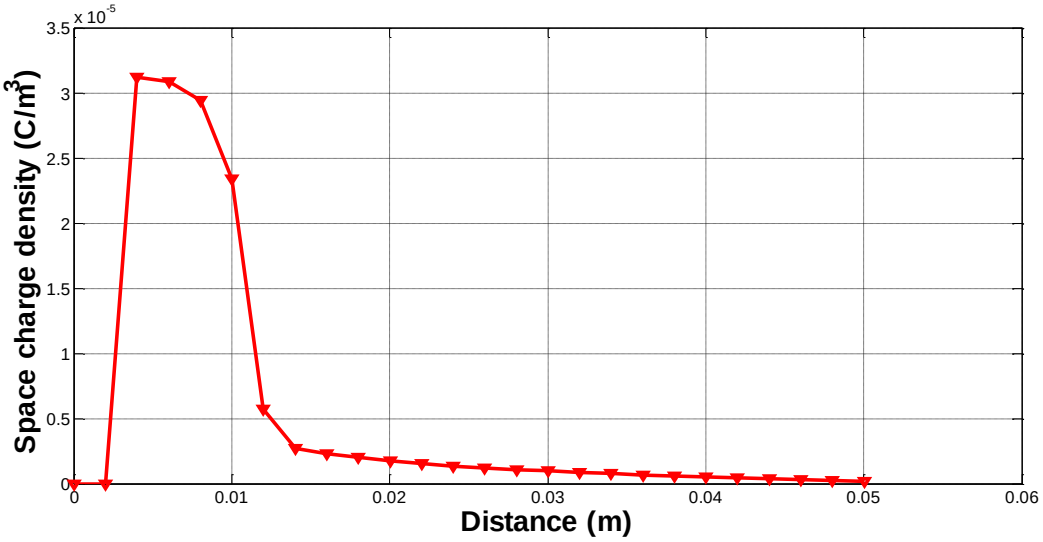

Figure 3.7. Variation of space charge density

III.4.6 Particle charging

The particles are charged by two principal charging mechanisms, diffusion charging and field charging (Figure 3.8).

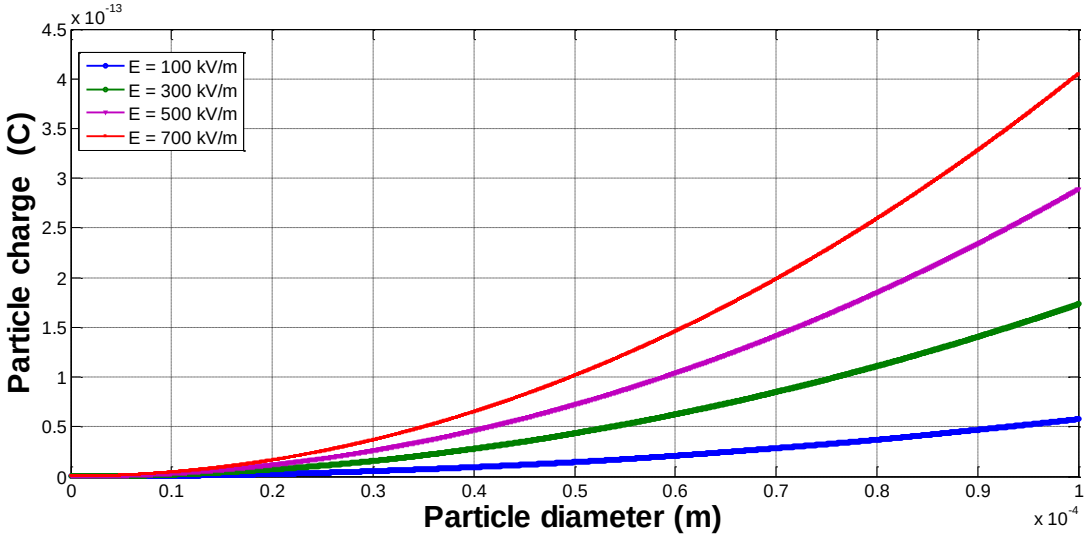

(a)

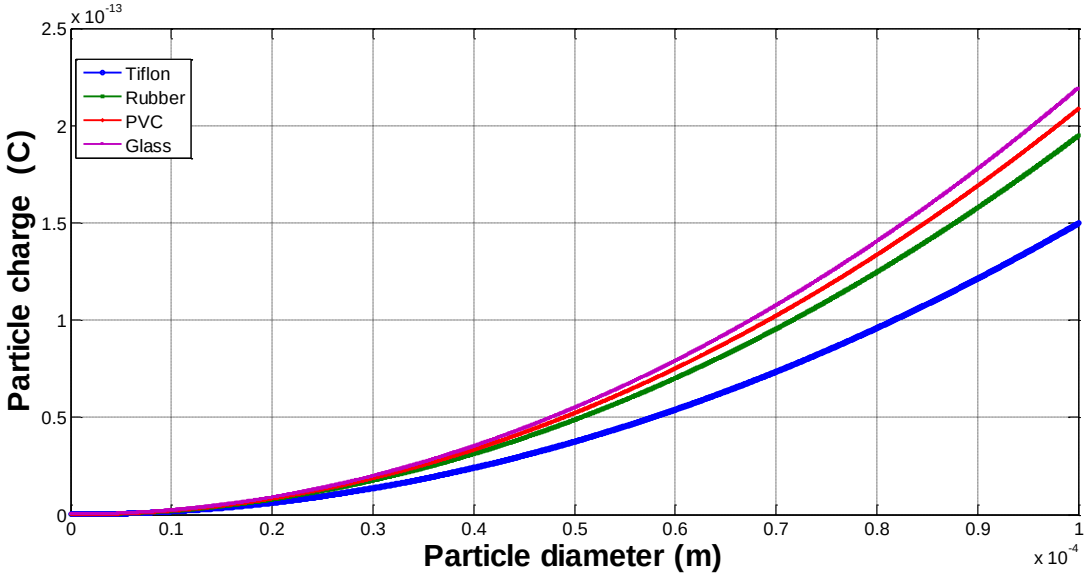

(b)

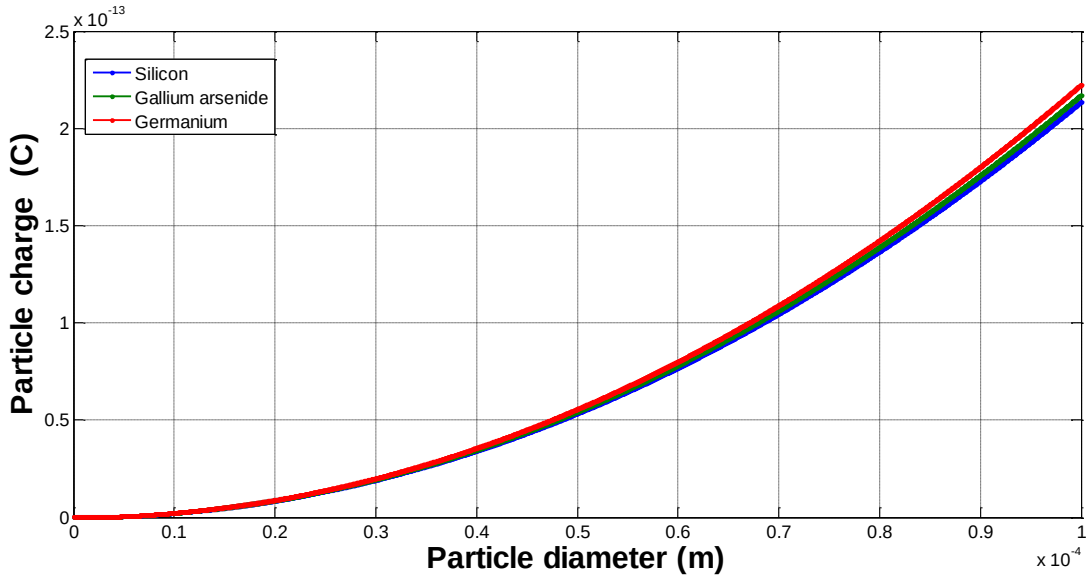

(c)

Figure 3.8. Variation of particle charging: (a) Dust, (b) Dielectric, (c) Semiconductor

Diffusion charging results from the Brownian motion of the ions and particles where the ions are attached to the particles by ion diffusion.

Field charging occurs when ions follow electric field lines in the inter-electrode space between the corona wires and the collecting electrodes until they terminate on a particle [92].

Charging calculation methods were rated as a function of the particle sizes, external discharge electric field strength, and ion density-time product [108]. The first combined charging model introduced by Cochet (1961) for predicting charge on each particle is shown in equation 3.26 [83, 109].

$$q_p^s = 3\pi\varepsilon_0 \frac{\varepsilon_r}{\varepsilon_r + 2} d_p^2 . E \tag{3.26}$$

where E is the electric field, d_p the particle diameter and ε_r is the specific permittivity.

The overall charging rate is given as [108]:

$$\frac{dQ_p}{dt} = \begin{cases} \frac{Q_s}{\tau_q}\left(1 - \frac{Q_p}{Q_s}\right)^2 + \frac{2\pi \cdot \alpha \cdot \rho \cdot k \cdot k_B \cdot T \cdot d_p}{e} & for \quad Q_p < Q_s \\ \frac{\alpha}{4 \cdot \tau_q}(Q_p - Q_s) \cdot \exp\left(\frac{e(Q_s - Q_p)}{2\pi \cdot \varepsilon_0 \cdot \rho \cdot k \cdot k_B \cdot T \cdot d_p}\right) & for \quad Q_p > Q_s \end{cases} \tag{3.27}$$

$$\alpha = \begin{cases} 1 & for \quad e_{norm} < 0.525 \\ \frac{1}{(e_{norm} + 0.457)^{0.575}} & for \quad e_{norm} > 0.525 \end{cases} \tag{3.28}$$

$$e_{norm} = \frac{e \cdot d_p}{2 \cdot K_B \cdot T} \left|\vec{E}\right| \tag{3.29}$$

$$\tau_q = \frac{4 \cdot \varepsilon_0}{k \cdot \rho} \tag{3.30}$$

where τ_q being the charging time constant, k_B is the Boltzmann coefficient and T is the temperature.

III.4.7 Migration velocity

The migration velocity variations are shown in Figure 3.9. For sub-micrometer particles, inertia is very small and can be neglected. The theoretical migration velocity is obtained by balancing the drag force with the Coulomb force or Electrostatic force acting on a particle.

Under a steady-state condition and in the Stokes regime, the theoretical migration velocity is expressed by [101, 102, 104]:

$$w_{th} = \frac{q.E}{3\pi.z.d_p} \cdot C_u \tag{3.31}$$

$$C_u = 1 + k_n[1{,}257 + 0{,}4\exp(-\frac{1.1}{k_n})] \tag{3.32}$$

$$k_n = \frac{2\lambda}{d_p} \tag{3.33}$$

where z is the gas dynamic viscosity, C_u is the Cunningham slip correction factor, k_n the Knudsen number and λ the gas mean free path.

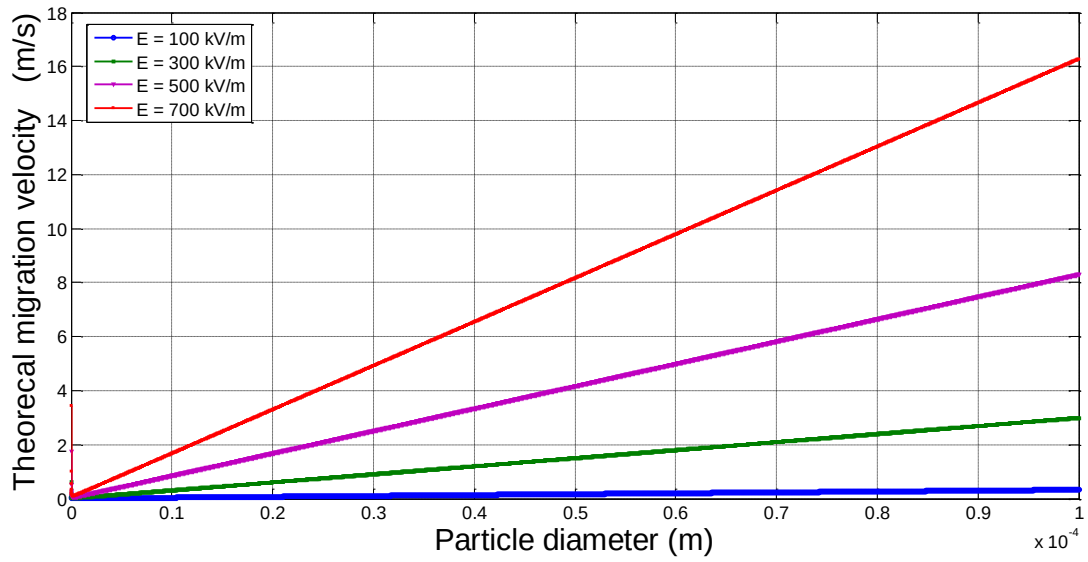

(a)

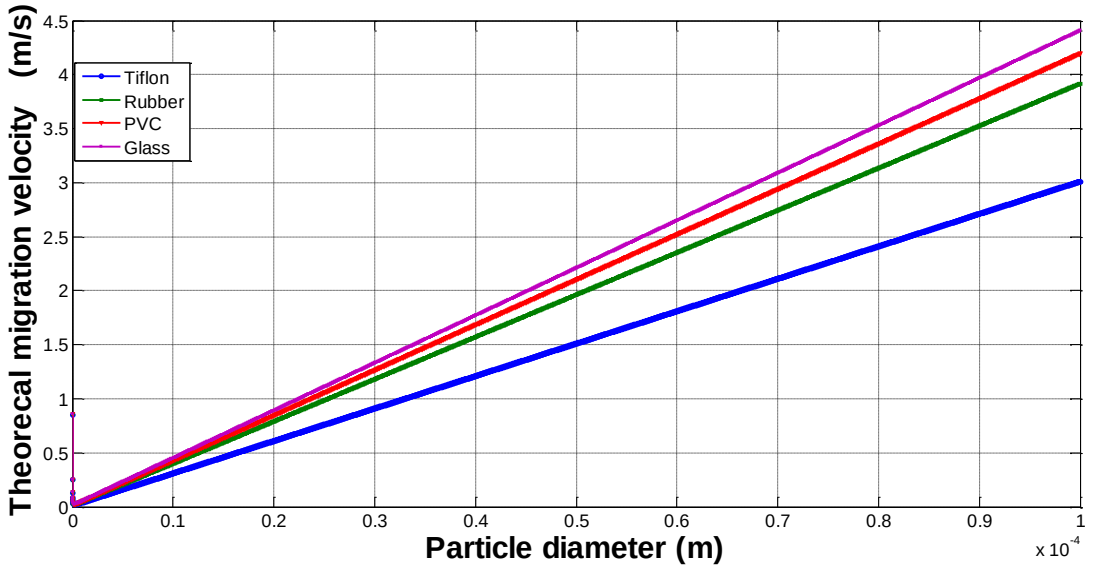

(b)

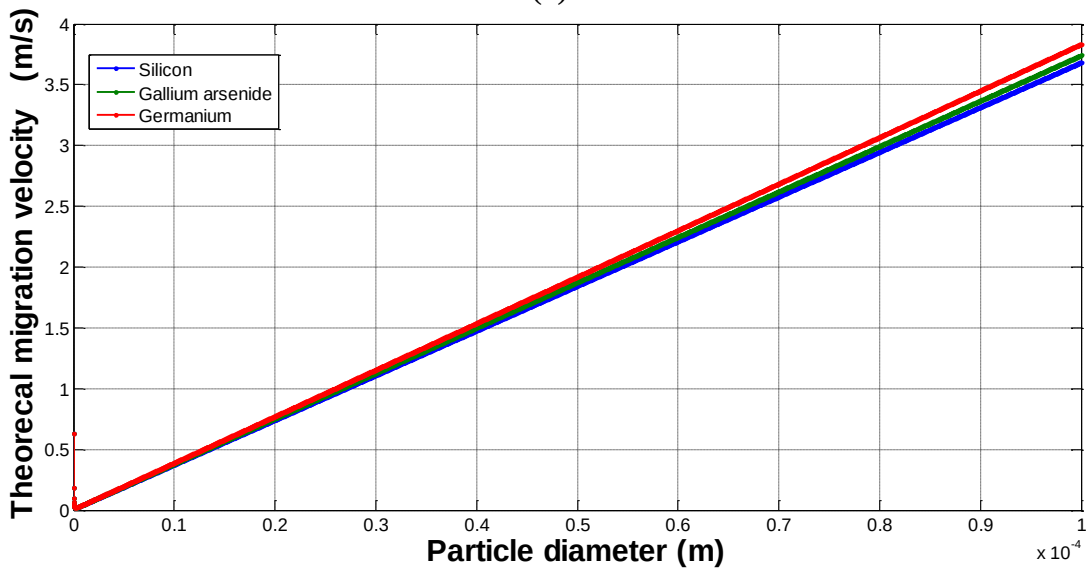

(c)

Figure 3.9. Variation of migration velocity: (a) Dust, (b) Dielectric, (c) Semiconductor

III.4.8 Collection efficiency

The collection efficiency variation of electrostatic precipitator is shown in figure (3.10). The model for collection efficiency, known as the Deutsch equation [104 - 110], Equation (3.34), is still frequently used to predict the performance of precipitators due to its simplicity.

$$\eta = 1 - \exp\left(-\frac{w_{th} \cdot A}{Q}\right) \tag{3.34}$$

where A the area of the collecting electrode, Q the gas flow rate and w_{th} is the migration velocity.

The magnitude and the time evolution of the corona field and particle charge are strongly affected by the system geometry and the nature of particles. It is find that Deutsch's formula does not take into account the gas leaks and particle re-entrainment that occur. When the formula is applied to metal plate precipitators, one of the main problems is the calculation of the electric field distribution and the charge distribution governed by the Poisson's equation, which must be solved with the current continuity equation subjected to boundary conditions involving a space charge, applied voltage and onset voltage.

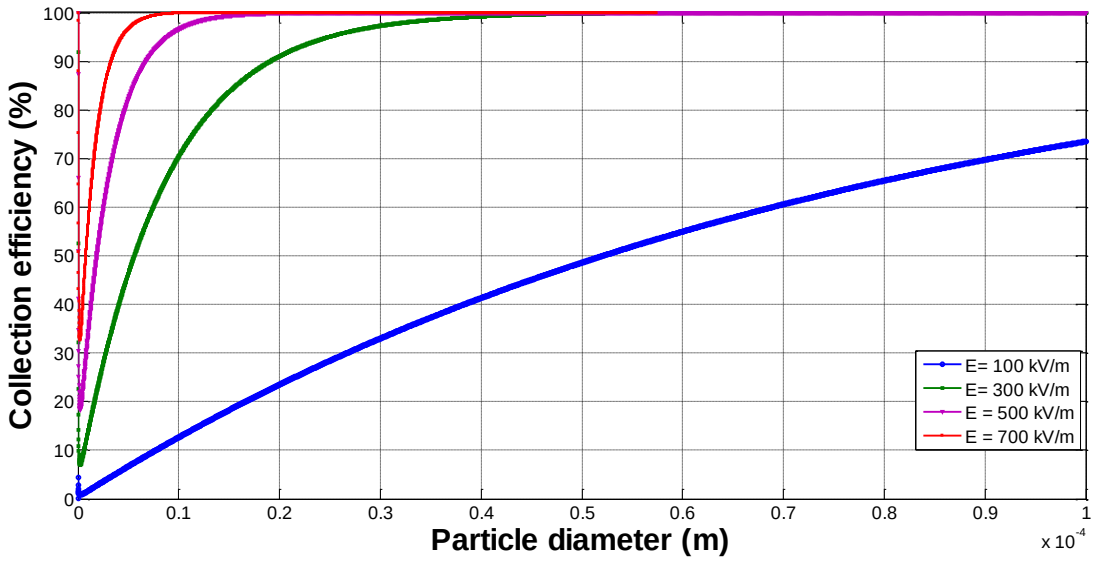

(a)

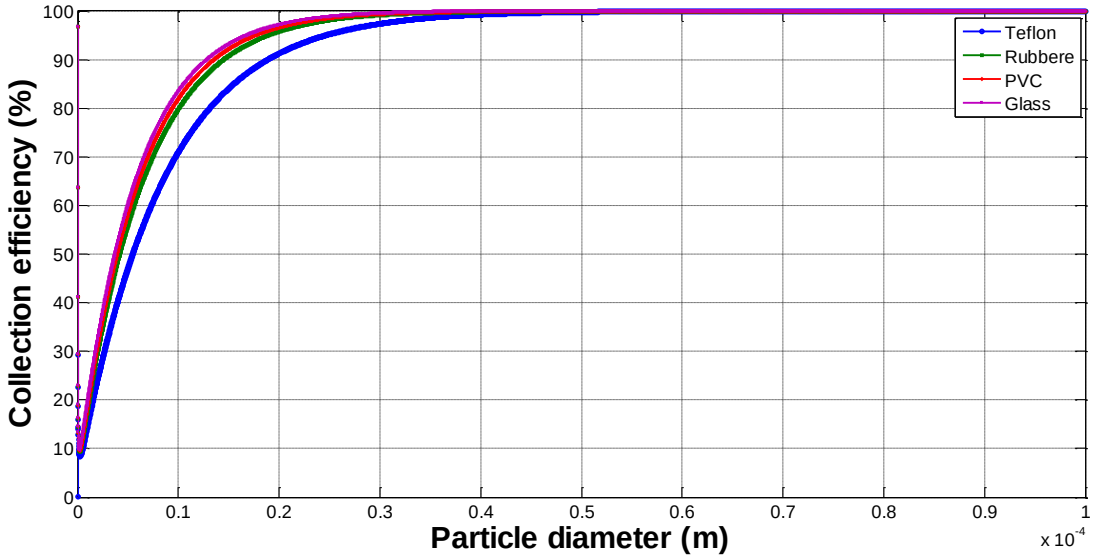

(b)

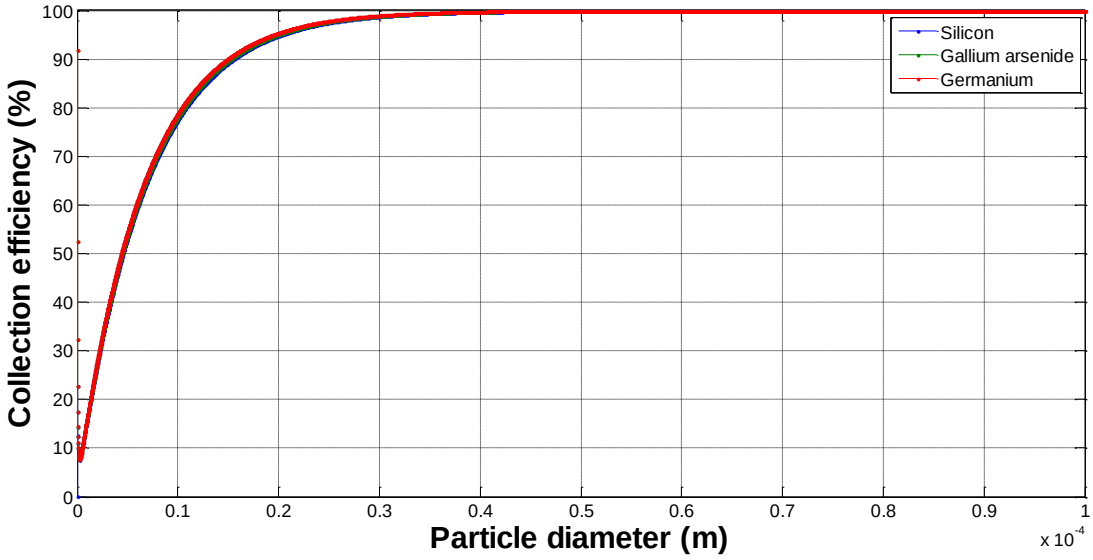

(c)

Figure 3.10: Collection efficiency variation: (a) Dust, (b) Dielectric, (c) Semiconductor.

The Deutsch-Anderson equation is used to determine the collection efficiency of the precipitator under ideal conditions. To make the equation more accurate in cases where all particles are not uniform in size, a parameter called the effective precipitation rate can be substituted for the migration velocity.

The overall operating performance of an electrostatic precipitator is quantified by a quantity called total collection efficiency η_t, defined by the following expression:

$$\eta_t = 1 - \frac{n_s}{n_e} \tag{3.35}$$

where η_s and η_e represent the concentrations at the outlet and inlet of the precipitator, respectively. η_t can be expressed in number of particles or in mass.

According to the Deutsch-Anderson equation (Figure 3.10), the ESP collection efficiency depends on:

- ✓ Volumetric flow rate,
- ✓ Electrostatic force
- ✓ Plate area,
- ✓ Particle charge
- ✓ Drift velocity.

The present finite element algorithm is applied and compared to the most recent previous work which adopted the FET by using the triangular elements. The FE grid is generated in a simple way with the characteristic lines following the FE grid pattern. This simplicity is due to the way by which the FE grid is generated.

The numerical model developed in this investigation, is based on the discretization of the calculation area with application of the fictive charges method to determine the distribution of the electric field and the potential. To estimate the space charge, the simplified method of characteristics is used.

This study confirms that the electrical potential varies with the variation of the geometry. This can be explained by the increase in the drift velocity of positive or negative ions in the direction of the electric field.

In this investigation, the introduction of a potential corresponding to the critical minimum ionization field directly in the finite element formulation as a Dirichlet conditions is proposed. the model which separates the corona in two distinct regions is used. The ionization region radius and the electric field at the ionization-region/drift-region interface, which corresponds to a zero net ionization coefficient of the ambient air.

III.5 Conclusion

Effects of the particle space charge density and the particle relative permittivity on the collection efficiency of a wires–plates electrostatic precipitator are studied.

In the present work, the corona parameters are analyzed by a combined iterative computational technique based on the finite element method. From the computed potential grid, the space charge grid was generated by solving the current continuity equation. Poisson's equation was then solved by applying the finite element method algorithm.

The current continuity equation and the Poisson's equations were solved simultaneously until the difference between two successive potential grids is less than or equal to one volt. The main advantage of this approach is that any shape of the corona electrodes can be modeled with ease and hence, helps in designing a precipitator with new innovative shapes of the corona and grounded electrodes.

It is observed that the inner electrical potential and electric field of the electrostatic precipitator is higher than the applied voltage when the particle space charge density is very high and are strongly modified with system geometry and particles permittivity. The collection efficiency increases for the high applied voltage but decreases with increasing the radius of wire and as the particle space charge density increases above the critical length of electrostatic precipitator.

In addition, we note that the electrostatic separation is very sensitive to the nature and size of the charged particles whatever the inter-electrode spacing and the voltage applied to the active electrode. These results extend previous work on electrostatic precipitators.

The study electrostatic phenomena is not simply to understand the applications of static charge, or the hazards they present, but because the ideas are applicable in other branches of electrical engineering, and the electrical aspects of other sciences.

CHAPTER IV

Investigation of particles trajectories in multifunctional electrostatic separator

IV.1 Introduction

Separation and sorting technologies are at the heart of modern recycling and waste management systems. By improving the recovery of valuable resources, reducing waste, and protecting the environment, these technologies contribute to a sustainable future. Thanks to the continuous emergence of innovations, the potential for improving efficiency and impact is growing. Electrostatic separation is a growing technology in the recycling industry. It is an effective technology for processing plastics and metallic materials in the form of granular mixtures or fine powders from waste electrical and electronic equipment. Understanding the various physical phenomena occurring in the separation zone is crucial for improving the efficiency of electrostatic
separation devices. This has led to the adoption of efficient and reliable numerical models for simulating particle trajectories.

The goal of the work is to represent graphically the trajectories of two insulating charged polypropylene particles of different sizes (2 mm and 4 mm) in the multifunctional electrostatic separator powered by photovoltaic (PV) system use a multipoint electrode as charging device employing numerical simulation and demonstrate its effectiveness and reliability for the study of particles trajectories by integrating PV panels as a power source for electrostatic separators according to the recommendations of the new energy system. Using the Euler-Cromer method as a numerical model to solve the equation of motion of the particles. This method was based on the calculation of the electric field intensity, which is done by the COMSOL Multiphysics software, which uses the finite element method (FEM). The numerical simulation was carried out using MATLAB software by varying the voltage applied to the active electrodes of the multifunctional electrostatic separator suggested, and the distance between them, taking into account the influence of electrostatic and mechanical forces on the charged insulating particles as they pass through the separation zone. The results showed that the numerical model used is an effective and reliable tool for the study of particles trajectories. Scientific novelty of this work is to integrate PV panels as the main low-voltage energy source at the input of the high-voltage generator supplying the electrostatic separator with an optimal voltage of 30 kV. In addition, this numerical study has used electrostatic forces, gravitational forces, and dynamic forces simultaneously. The numerical simulation was contributed to a thorough understanding of various physical phenomena occurring in the separation zone and was considered a tool to validate experimental results.

IV.2 Multifunctional electrostatic separator description

The use of photovoltaic panels ensures the required voltage to power the suggested electrostatic separator. During the separation process, 2 mm and 4 mm insulating particles are charged as they pass through the charge zone by coronal discharge generated by the multipoint configuration with the

same charge as the electrode. They then reach the separation zone, where they are separated in the presence of an intense electric field. This work aims to represent graphically the charged particles trajectories using mathematical modeling and simulation.

Figure 4.1 shows a design of a multifunctional electrostatic separator with two flexible vertical electrodes, powered by a photovoltaic system.

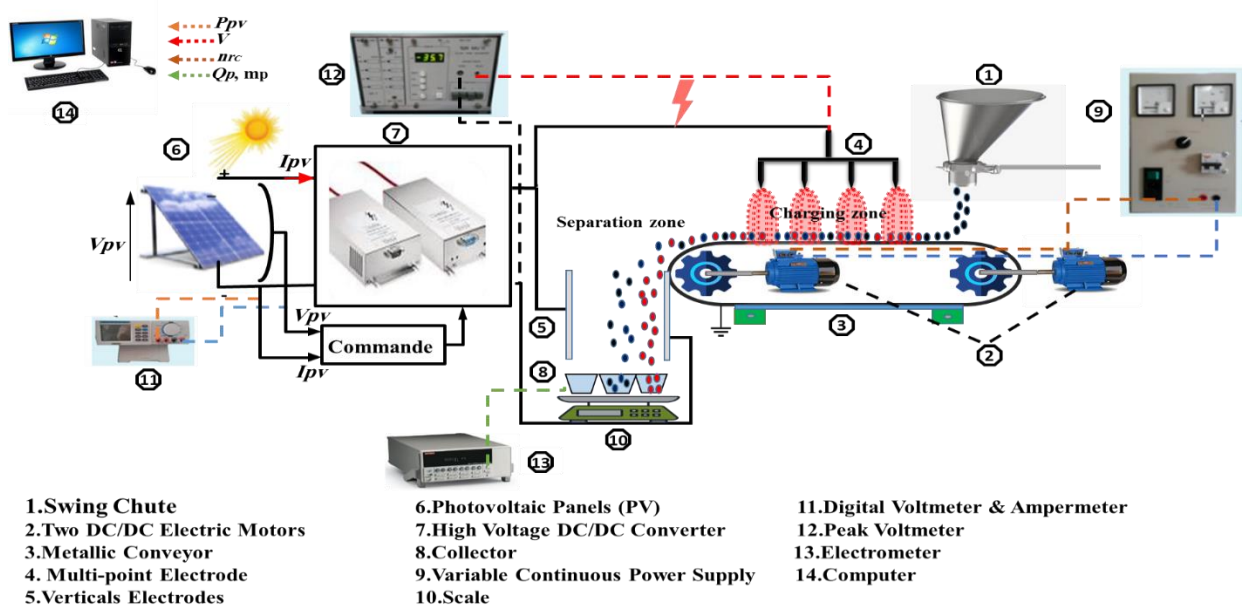

Figure 4.1. Global system of multifunctional electrostatic separator used

This system powers the electrostatic separator. The design consists of a grounded metal belt conveyor, measuring 1000 mm in length and 100 mm in width. The conveyor belt is responsible for transporting the particles in the form of homogeneous spheres deposited on its surface to the electrical charging zone and the separation zone. This conveyor belt is driven by two DC or three-phase motors. These two motors are powered by an adjustable voltage source and rotated at an appropriate speed.

A multi-point corona electrode in the form of needles perpendicular to the metal belt of the conveyor to generate corona discharges used to charge insulating particles. It consists of four points set 20 mm higher than the surface of the belt. Each point is 130 mm long and 2 mm in diameter, spaced 20 mm apart.

An electrostatic separation zone consists of two flexible vertical electrodes in the form of plates measuring 200 mm wide and 300 mm long, separated by a distance of 80 mm. The two electrodes can move back and forth between them.

The corona electrode and one of the vertical electrodes are connected to a 30 kV via a 500 V/30 kV high voltage DC/DC converter supplied by fourteen photovoltaic panels (Figure 4.2).

High-voltage DC-DC converters are essential for applications requiring extreme voltage step-up ratios, such as electrostatic systems and HVDC transmission. When powered by photovoltaic (PV)

arrays of around 14 panels, the input voltage is typically ~500 V, while the required output can reach 30 kV. Conventional boost converters are limited, since the gain equation:

$$V_{DC} = \frac{V_{PV}}{1-D} \tag{4.1}$$

demands impractical duty cycles near unity. Instead, isolated transformer-based converters, expressed as:

$$V_{out} = V_{in} \frac{N_2}{N_1} \tag{4.2}$$

combined with voltage multipliers such as the Cockcroft–Walton ladder

$$V_{out} \approx 2n\, V_p \tag{4.3}$$

enable efficient high-voltage generation. Integrated Maximum Power Point Tracking (MPPT) ensures optimal PV operation, while careful insulation, soft-switching, and safety design are critical to achieve reliable conversion from 500 V to 30 kV.

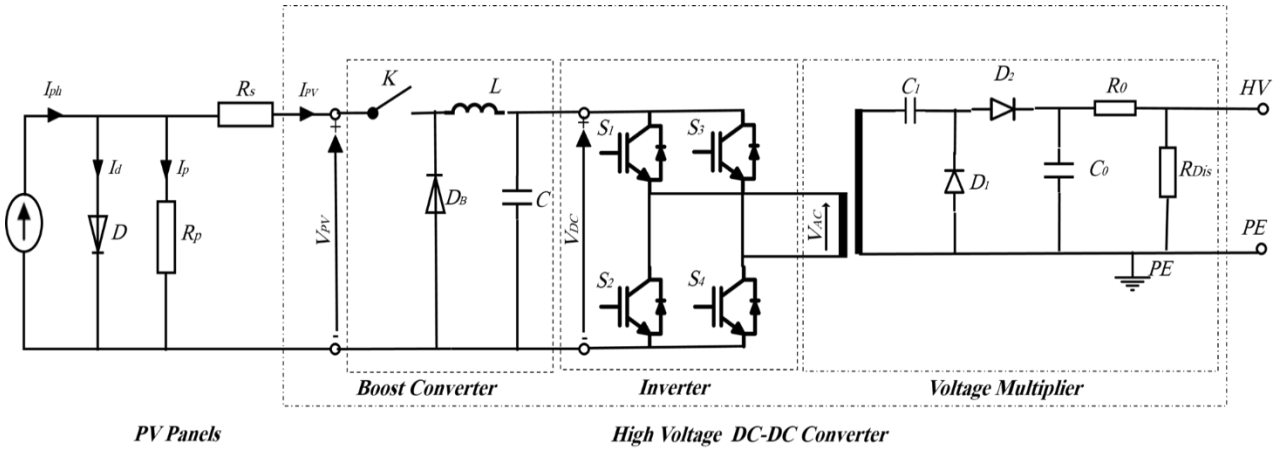

Figure 4.2. Simplified circuit for converting photovoltaic energy into high voltage

The voltages applied to the electrodes can vary from 20 kV to 30 kV for specific applications. The multi-point electrode generates corona discharges that expose the insulating particles. They acquire electrical charges of the similar sign as the applied voltage to the electrode and fall into electrostatic separation zone. When they freely fall into the separation zone, they are attracted to the electrode of opposite polarity and fall into the right part of the collector. However, the uncharged insulating particles, located in an intense electric field at the separation zone, fall into the middle part of the collector. The left part of the collector remains unchanged. Three collector boxes collect the separated insulating particles.

You can record real-time information about how this electrostatic separator is working on a computer. The computer can record the power produced by the photovoltaic panels (P_{pv}), the voltages applied (V), the speed of the metal (n_{rc}), the charges (Q_p), and the masses (m_p).

IV.3 Numerical modeling

This section involves the numerical modeling of three fundamental components of the proposed design. These include the PV panels that power the electrostatic separator suggested, the electric field, the motion of the charged particles and their trajectories in the separation zone.

IV.3.1 Photovoltaic panel modeling

A photovoltaic panel (PV), otherwise called a photovoltaic module, is generally made up of a set of elementary photovoltaic cells manufactured in the form of a thin layer of P-N junction semiconductor. These photovoltaic cells are connected in series and/or in parallel in order to obtain the required current, the required voltage, and the necessary power required to supply the load, due to the fact that each photovoltaic cell has a low nominal power. In this study, we are interested in using the single-diode model for its simplicity, accuracy, efficiency, and wide applicability compared to the two-diode model. Figure 4.3 presents the model of the equivalent electrical circuit of a photovoltaic cell. This model has a current generator that acts like light coming in or a photocurrent source, a diode that acts like a cell polarization phenomenon, and two resistors, *Rs*, which is in series, and *Rp*, which is in shunt to account for losses [111-115].

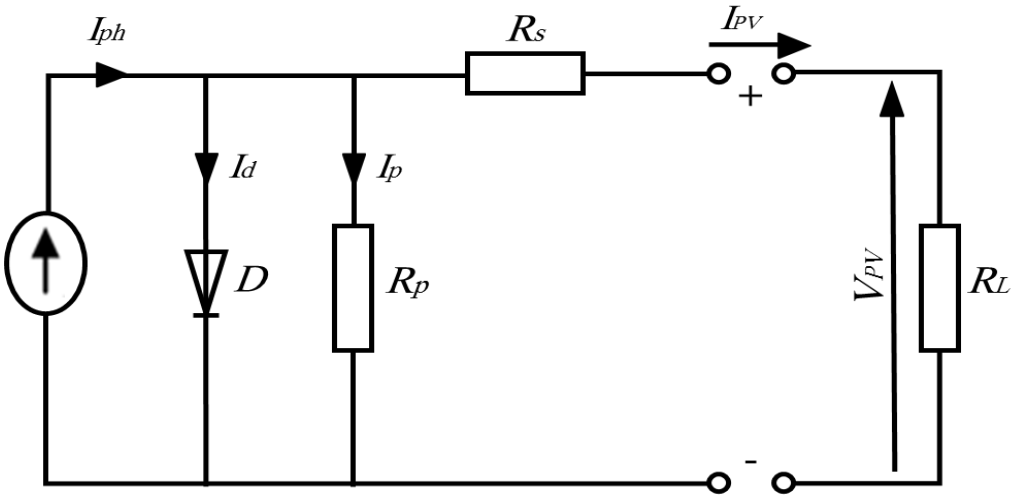

Figure 4.3: Single-diode model of photovoltaic cell.

The expression of the current generated by the single-diode photovoltaic cell is given as follows:

$$I_{ph} = I_d + I_p + I_{pv} \tag{4.4}$$

$$I_{pv} = I_{ph} - I_d - I_p = I_{ph} - I_0 \left[exp\left(\frac{q.(V_{pv}+R_S.I_{pv})}{n.k_B.T} \right) - 1 \right] - \frac{V_{pv}+R_S.I_{pv}}{R_p} \tag{4.5}$$

Where I_{ph} is the photocurrent, I_d is the current at the diode junction, I_p is the current in the resistor R_p, I_{pv} is the output current of the photovoltaic cll, I_0 is the saturation current of the diode, V_{pv} is the output voltage of the photovoltaic cell, R_s and R_p are the series and parallel resistances of the photovoltaic

cell, n is the ideality coefficient of the cell, k_B is the Boltzmann constant (k_B= $1.38\times10^{-23} J/K$), q is the electron charge (q=1.6×10^{-19} C), and T is the absolute nominal temperature of the photovoltaic cell.

The following equation provides the mathematical model for the photovoltaic (PV) panel, assuming that all the cells are identical:

$$I_{pv} = N_p.I_{ph} - N_p.I_0\left[exp\left(\frac{q.\left(N_S.V_{pv}+(\frac{N_S}{N_p}).R_S.I_{pv}\right)}{n.k_B.T}\right)-1\right]-\frac{N_S.V_{pv}+(\frac{N_S}{N_p}).R_S.I_{pv}}{\left(\frac{N_S}{N_p}\right).R_p} \quad (4.6)$$

Where N_s is the number of cells in series and N_p is the number of cells in parallel.

IV.3.2 Electrical field modeling

This study uses a numerical model of the electric field to study the motion and trajectory of charged particles in electrostatic separators. The electric field is an important and essential factor for the electrostatic separation process. It is generated by applying a high voltage to the active electrode and the grounded electrode. To obtain the electric field strength E, it must solve the Laplace equation or the Poisson equation, both of which are partial differential equations or use the COMSOL Multiphysics software that uses the finite element method [116,117]. It can be expressed as follows:

$$\vec{E} = -\nabla\Phi \quad (4.7)$$

Where $\vec{E}$ is the field intensity, and ϕ is the electric potential.

The boundary conditions are:

- ✓ The potential on the active electrode is equal to the high applied voltage.
- ✓ The potential on the grounded electrode is zero.
- ✓ The electric field on the active electrode is equal to the onset field strength.

IV.3.3 Modeling the particles trajectories

While moving, particles that have been charged by the corona discharge used in this study are affected by electrostatic force, gravitational force, and aerodynamic force. When they fall freely at the middle of the electrostatic separation zone, where there is a strong electric field, they are subject to all of these forces [118-120].

Gravitational force $\boldsymbol{F_g}$: Any charged particle with a mass m_p experiences a gravitational force during free fall. The following relationship determines its value:

$$\vec{F_g} = \begin{bmatrix} F_{gx} \\ F_{gy} \end{bmatrix} = \begin{bmatrix} 0 \\ -m_p \cdot g \end{bmatrix} \quad (4.8)$$

In equation 4.8, m_p represents the mass of the charged particle, and g stands for the gravitational constant.

Electrostatic force $\boldsymbol{F_{el}}$: Any charged particle Q_p located in a region of intense electric field is subject to an electric force of attraction or repulsion. Coulomb's law expresses it this way:

$$\vec{F}_{el} = \begin{bmatrix} F_{el,x} \\ F_{el,y} \end{bmatrix} = Q_p \cdot \begin{bmatrix} E_x(x,y) \\ E_y(x,y) \end{bmatrix} \tag{4.9}$$

Where Q_p represents the charge of the charged particle, E represents the electric field of the electrostatic separation region, and E_x and E_y are the horizontal and vertical components of the electric field vector, respectively.

Aerodynamic force $\boldsymbol{F_{aero}}$: Any charged particle in the form of a homogeneous sphere of radius r_p experiences an aerodynamic force when it rubs against the air. The following formula gives the aerodynamic force:

$$\vec{F}_{aero} = \begin{bmatrix} F_{aero,x} \\ F_{aero,y} \end{bmatrix} = \frac{1}{2} \cdot C_f \cdot \rho_a \cdot \pi \cdot {r_p}^2 \cdot v \cdot \begin{bmatrix} v_x \\ v_y \end{bmatrix} \tag{4.10}$$

as C_f= 0.5 is the drag coefficient, ρ_a is the density of air (ρ_a=1.204 kg/m^3), r_p is the radius of the charged particle, and v_x and v_y are the components of the vector of the relative velocity of the particle.

Gravitational, electrostatic, and aerodynamic forces act on the motion of charged particles, according to Newton's second law. It is defined by the following relationship [121,122]:

$$m_p \cdot \vec{a} = \sum \vec{F} = \vec{F}_g + \vec{F}_{el} + \vec{F}_{aero} \tag{4.11}$$

Where $\vec{a} = \frac{\overrightarrow{dv}}{dt}$ is the particle acceleration.

For represent graphically the trajectory of charged particles, we based on the Euler-Cromer method to solve the equation of motion numerically. Several researchers have employed this method. This method is given by the following relation [123]:

$$\vec{v}_{n+1} = \vec{v}_n + \vec{a}_n \cdot \Delta t \tag{4.12}$$

$$\vec{P}_{n+1} = \vec{P}_n + \vec{v}_{n+1} \cdot \Delta t \tag{4.13}$$

Where $\boldsymbol{v}$ is the velocity, P *is* the position and Δt is the time step.

IV.4 Results and discussion

In this paper, we will present the current-voltage (I-V) and power-voltage (P-V) characteristics of fourteen photovoltaic panels by varying the solar irradiation using the photovoltaic module

characteristics shown in Table 4.1, the evolution of the electric field in the electrical charging zone and the separation zone through the COMSOL Multiphysics program that uses the finite element method for the two configurations shown in table (4.2), and the graphical representation of the trajectories of two polypropylene insulating particles of 2 mm and 4 mm sizes in the separation zone through the Euler-Cromer method was programmed in MATLAB by varying the value of the voltage applied to the active electrodes and the inter-electrode distance and by injecting the intensity of the electric field previously obtained. The particle sizes for which the Euler-Cromer method is most effective range from 1 mm to 5 mm.

Table 4. 1. Photovoltaic parameters of an ET_{Solar} photovoltaic module

Reference	**ET-M572185**
Maximum Power (P_{max})	185 W
Open Circuit Voltage (V_{oc})	44.6 V
Short Circuit Current (I_{sc})	5.8 A
Rated Voltage (V_{mpp})	36.3 V
Rated Current (I_{mpp})	5.09 A
Cells per module	72
Maximum System Voltage	DC 1000 V
Series Fuse	15 A
Fire Rating	Class C
Maximum Field Wiring (Copper only)	14 AWG
Structural Load	112 lb/ft^2

Table 4. 2. Configuration dimensions

Configurations	***D1*[mm]**	***D2*[mm]**	***D3*[mm]**
Multipoint-Conveyor	60	40	20
Vertical Electrodes	80	95	110

IV.4.1 Photovoltaic characteristics

To determine the current-voltage (I-V) and power-voltage (P-V) characteristics of 14 ET-M572185 panels, representing the main power supply of a multifunctional electrostatic separator, we present a simulation model of a single photovoltaic panel under Matlab/Simulink. This model is based on the equivalent circuit of a single-diode monocrystalline cell, the most common and commercially available design.

Figures 4.4 and 4.5 show the simulation model created in Matlab/Simulink and its block, using the parameters of the photovoltaic module presented in Table 4.1.

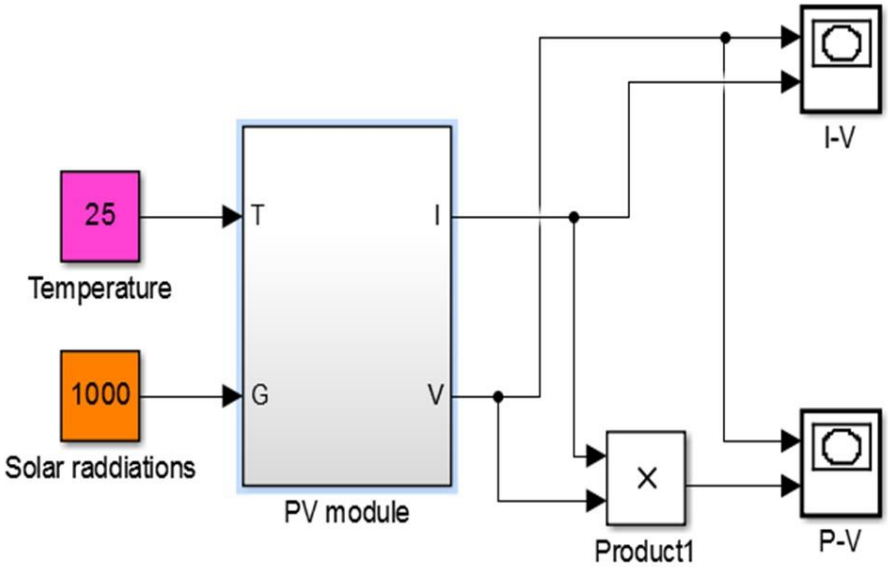

Figure 4.4. Simulation model of photovoltaic panel created in Matlab/Simulink

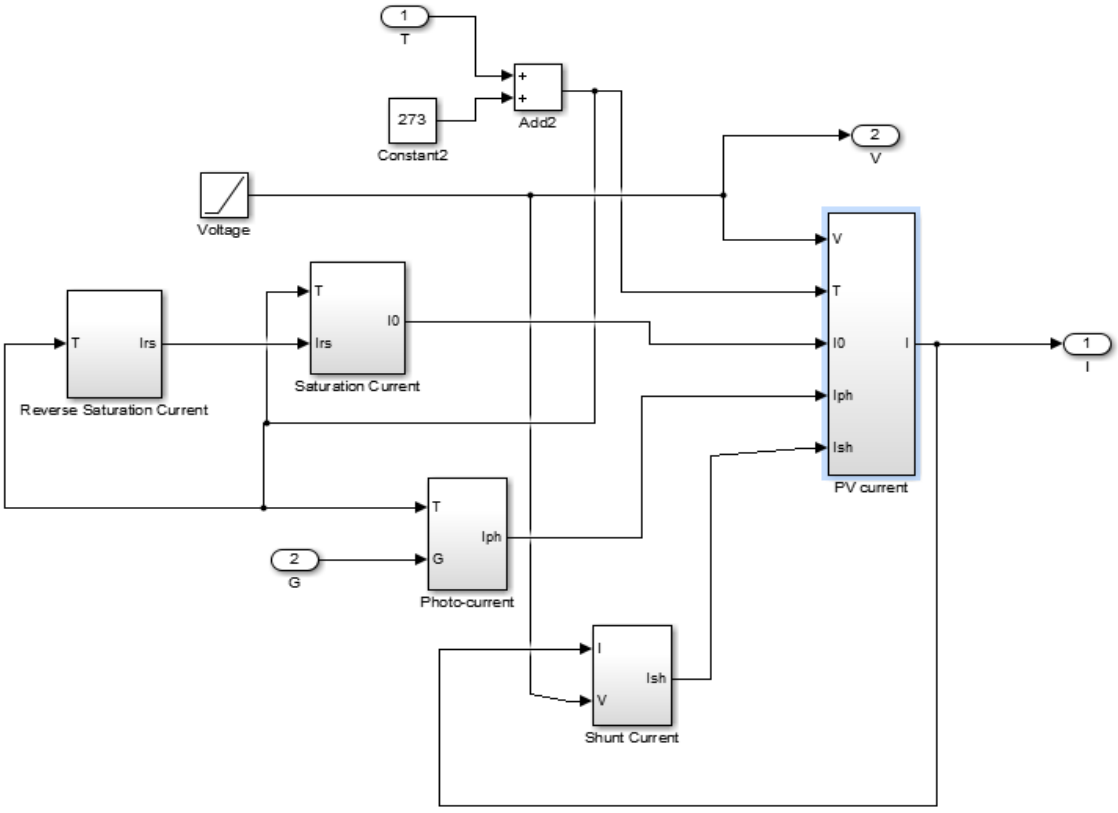

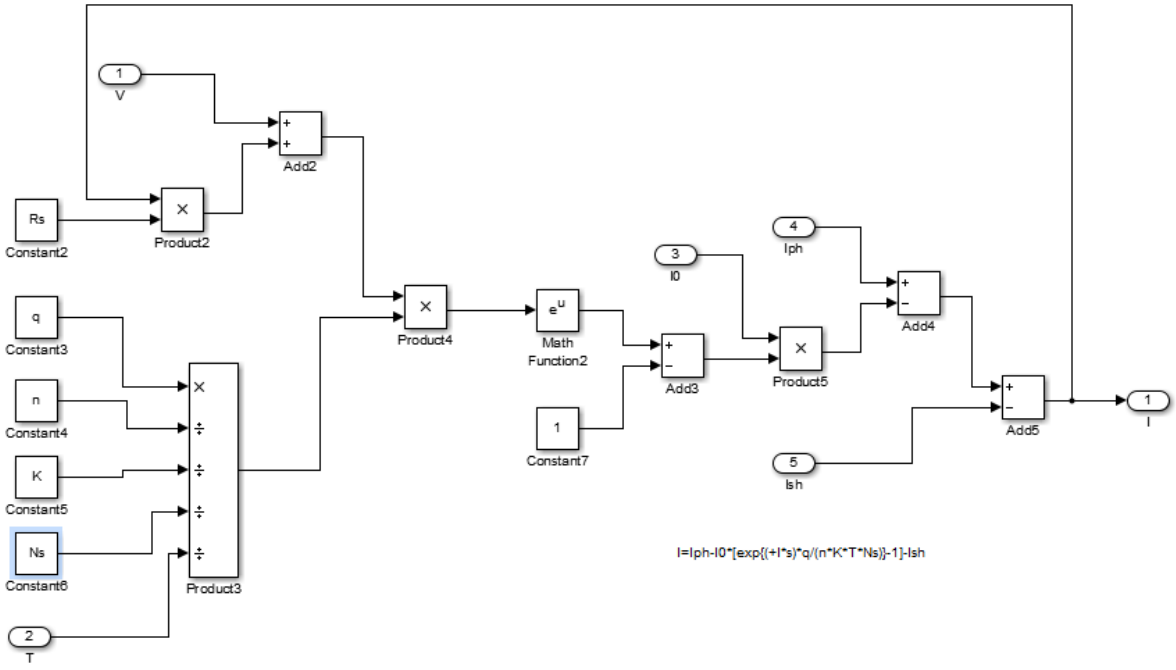

Figure 4.5. The photovoltaic panel block under Matlab/Simulink

Figures 4.6 and 4.7 display the (I-V) and (P-V) characteristics of fourteen ET-M572185 panels. These panels are linked in series to power the multifunctional electrostatic separator with two flexible vertical electrodes with a voltage of 30 kV via a high-voltage DC/DC converter of 500V/30kV. The study is conducted taking into account climatic conditions, such as the temperature of 25 °C and three different solar radiation values (800 W/m^2, 900 W/m^2 and 1000 W/m^2).

Each of these solar radiation values corresponds to a maximum electrical power that the fourteen panels could provide.

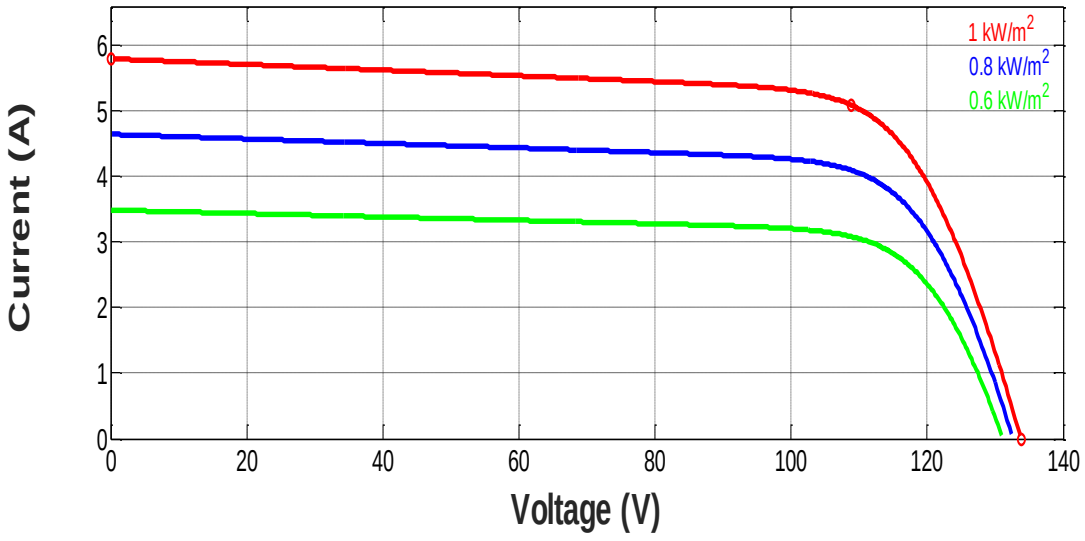

Figure 4.6. The (I-V) characteristics of fourteen ET-M572185 PV system for different solar radiation

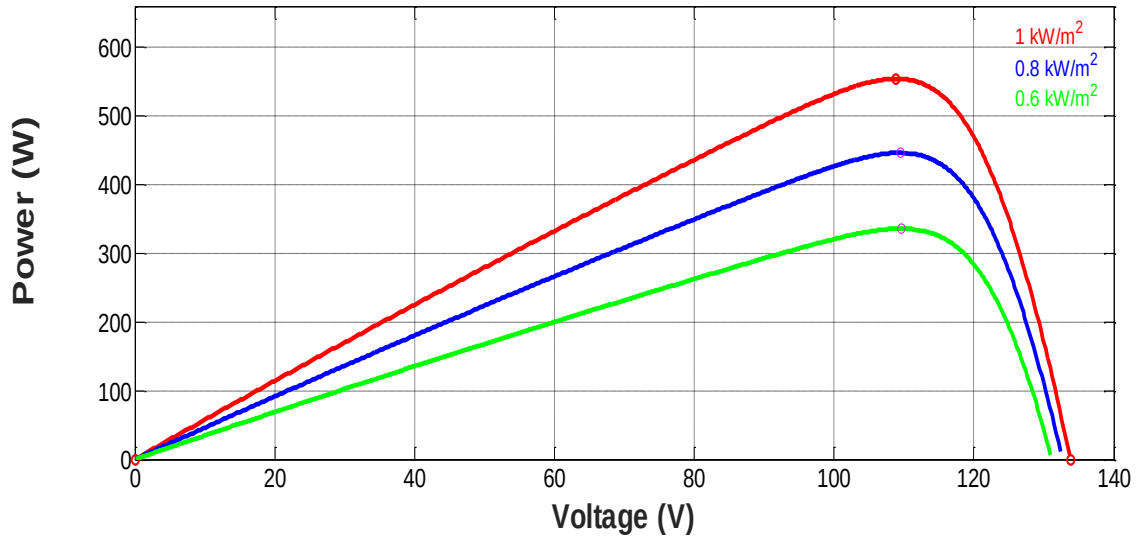

Figure 4.7. The (P-V) characteristics of fourteen ET-M572185 PV system for different solar radiation

IV.4.2 Electric field variation

COMSOL Multiphysics is a general-purpose numerical simulation software used in all fields of engineering, manufacturing, and scientific research. It is designed for engineers and researchers in electrostatics. The software offers modelling capabilities and solves complex physical phenomena by integrating several domains (electrical, thermal, mechanical, magnetic, ...).

COMSOL Multiphysics is widely used in electrostatics for modeling by simulating the distribution of electric fields in various configurations (capacitors, cables, insulators, etc.). It allows for the calculation of electric potentials, field lines, and charge density with high accuracy based on the finite element method (FEM). Among its practical applications in electrostatics are: the design of electrostatic devices (actuators, sensors, etc.), the study of insulation in electrical networks, and the optimization of high-voltage systems. It has a flexible and lightweight platform for understanding, predicting, and optimizing the behavior of electric fields in complex systems.

This software covers the following steps:

1. Define the physics type
    - Choose the appropriate module (e.g., Electrostatics in the AC/DC module).
    - This determines the partial differential equations (PDEs) that COMSOL will solve.
2. Create the geometry
    - Construct the geometry of the system (2D or 3D).
    - You can import CAD file or use the built-in editor.
3. Define the materials
    - Associate electrical properties (permittivity, conductivity).
    - COMSOL has a library of materials, but you can also enter custom values.

4. Apply boundary conditions
   - Set the electric potentials (one plate at 0 V, and the other at 30 kV).
   - Define free charges or insulators.
   - Specify symmetries or continuity conditions.
5. Mesh
   - Generate a mesh adapted to the geometry.
   - The finer the mesh, the more accurate the solution (but computationally expensive).
6. Solving
   - Launch the numerical solver based on the finite element method.
   - COMSOL offers different solvers (stationary, time-domain, iterative).
7. Post-processing
   - View the results: electric potential, electric field, current density, and space charge density.
   - Export data or create graphs for analysis.

The electric field is responsible for the charge and the motion of the particles through the electrostatic forces it generates (Figures 4.8 and 4.9).

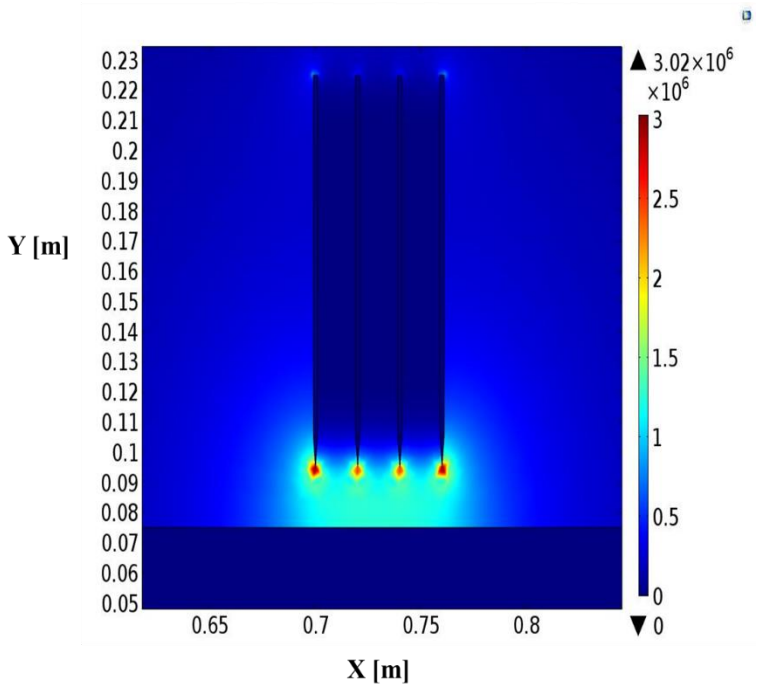

Figure 4.8. The distribution of electric field in the electric charging zone

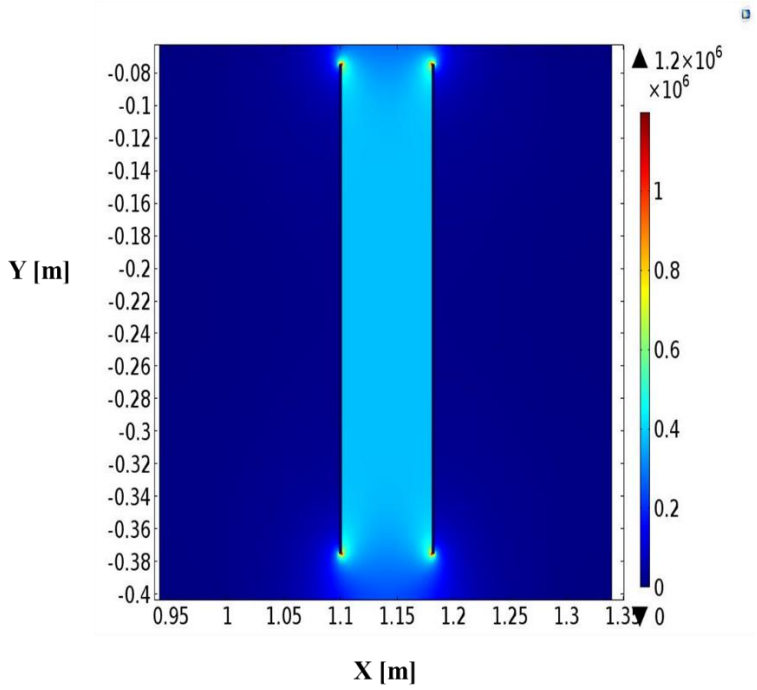

Figure 4.9. The distribution of electric field in the electrostatic separation zone

IV.4.2.1 Electrical charging zone

Figure 4.10 depicts the electric field variation at the conveyor generated by four points as a function of their positions, which represents the electrical charging zone of insulating particles for an applied voltage of 30 kV and an inter-electrode distance of 20 mm.

Figures 4.11 and 4.12 shown the electric field variation at the conveyor for three different applied voltages (20 kV, 25 kV, and 30 kV) and three different inter-electrode distances for a multipoint-conveyor configuration shown in Table 4.2.

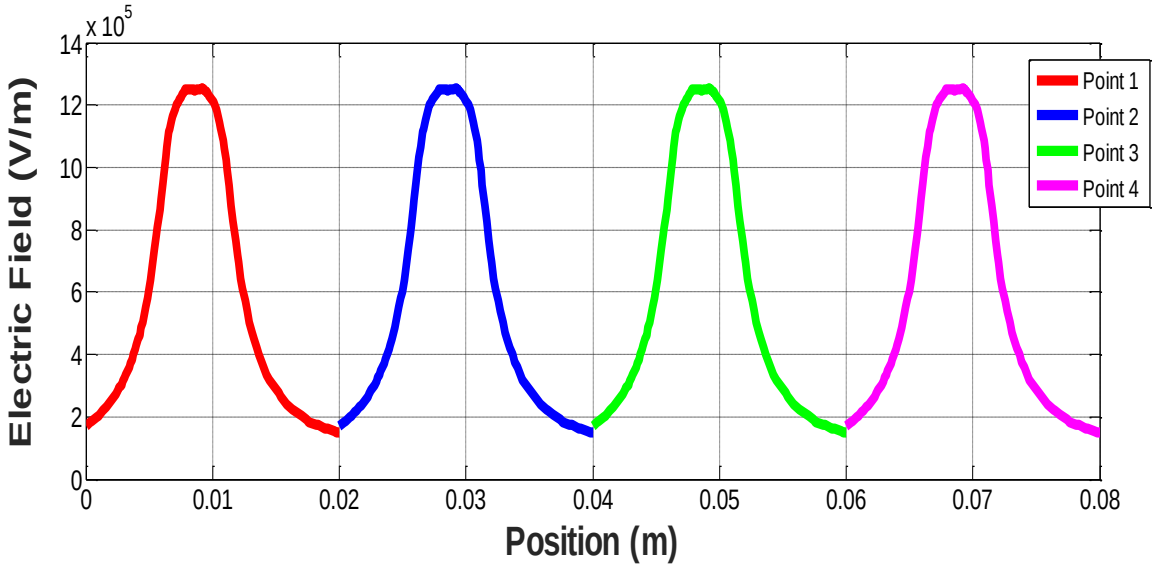

Figure 4.10. Electric field variation at the conveyor

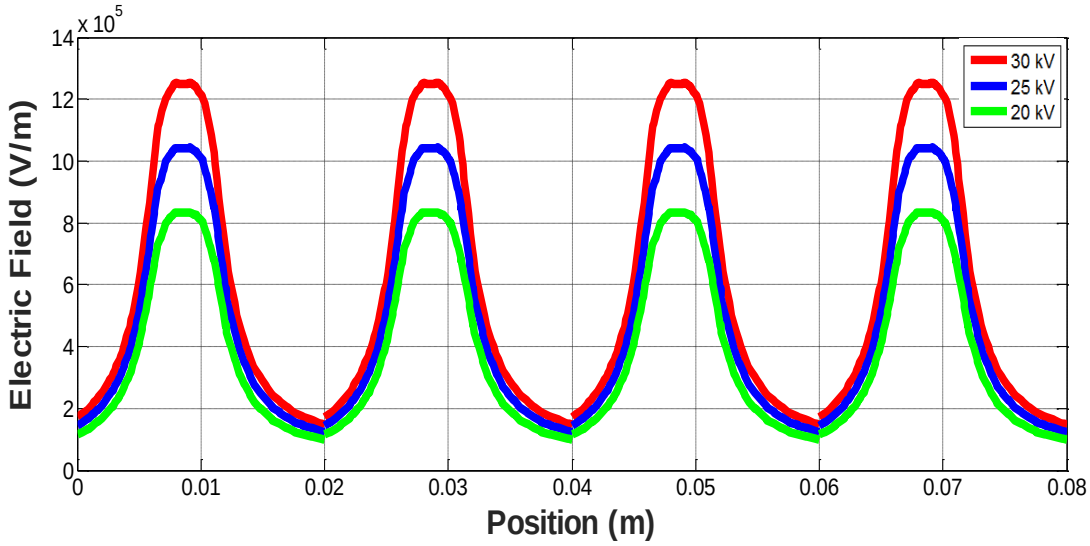

Figure 4.11. Electric field variation at the conveyor for different applied voltages

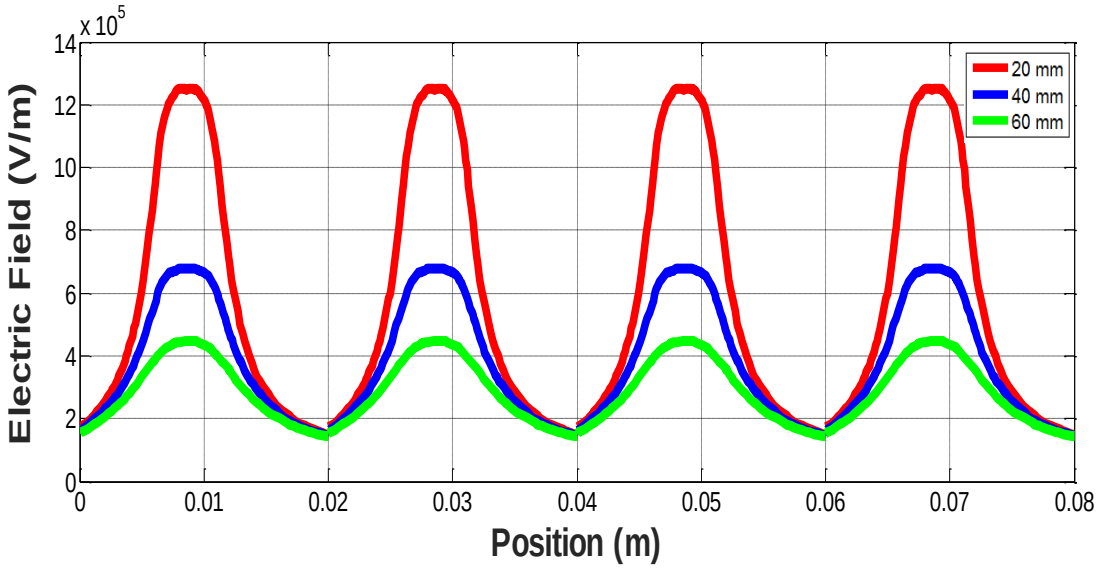

Figure 4.12. Electric field variation at the conveyor for different distances

The curves describe how a corona electrode creates a very strong, uneven electric field, especially near its sharp points. At 30 kV across a 20 mm gap, the field reaches about 1.2 kV/mm, strong enough to ionize air. The field strength increases with higher voltage and smaller electrode spacing, ensuring that particles moving through this region become electrically charged through collisions with ions and electrons, becoming charged entities that can subsequently be manipulated by electrostatic forces. This mechanism is fundamental to applications such as electrostatic precipitators, ozone generation, and electrostatic separators.

IV.4.2.2 Electrostatic separation zone

Figures 4.13 and 4.14 show the electric field variation generated in the separation zone represented by a configuration of two vertical electrodes. These results are for three values of the applied voltage

of 20 kV, 25 kV, and 30 kV and three values of the inter-electrode distance (80 mm, 95 mm and 110 mm).

The curves demonstrate that the electric field in the examined region is uniform, meaning its intensity remains constant across the inter-electrode gap. For an applied voltage of 30 kV and an electrode spacing of 80 mm, the field strength is calculated as E=V/d. This relationship highlights the direct proportionality of the electric field amplitude to the applied voltage and its inverse proportionality to the electrode distance. The investigation underscores the critical role of electric field intensity in electrostatic separation (ES). The value of 0.375 kV/mm is significant. The study therefore demonstrates that controlling voltage and electrode spacing is essential for achieving the intense electric fields necessary for reliable operation of electrostatic separators.

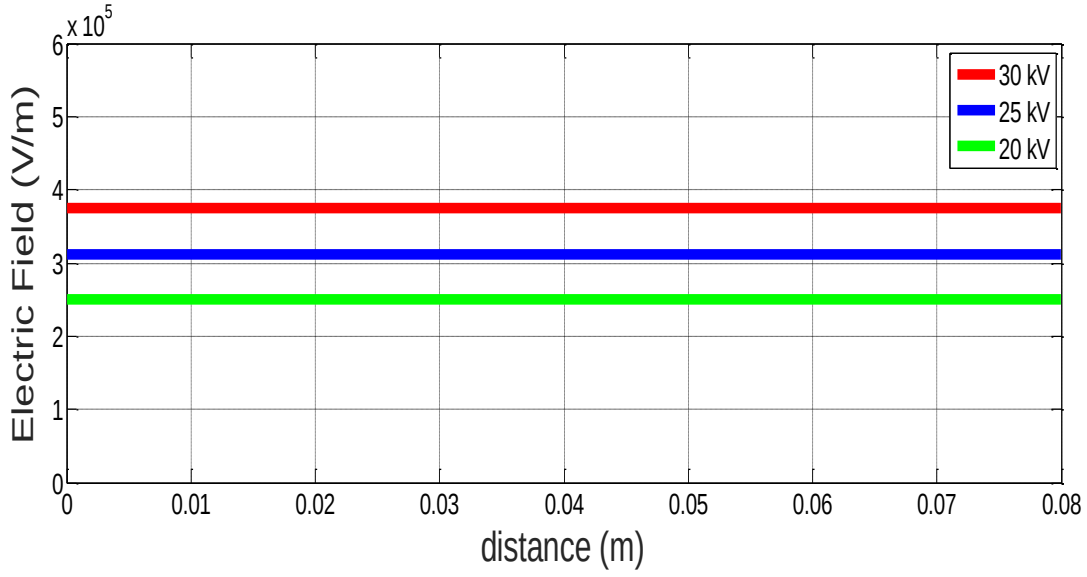

Figure 4.13. Electric field variation at the ground for different applied voltages

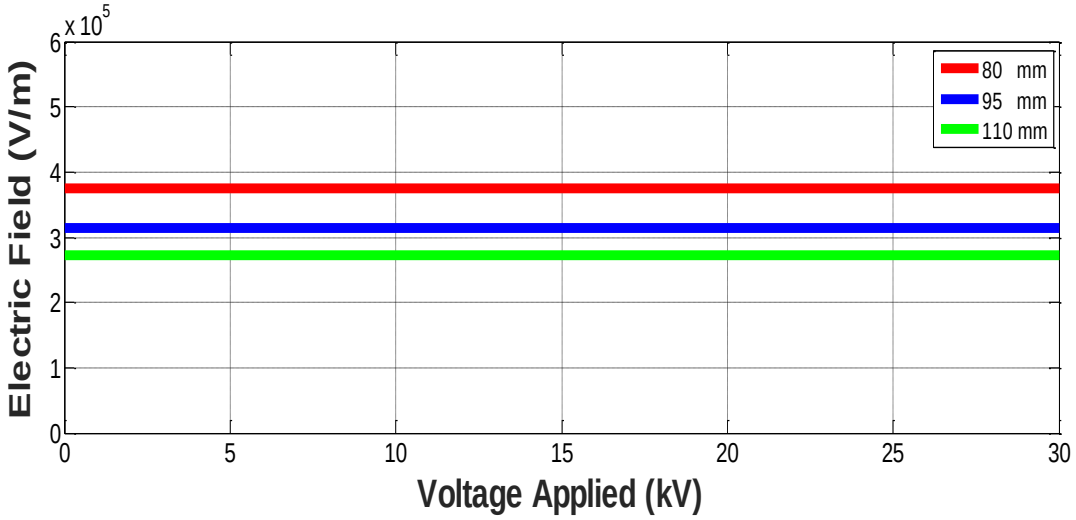

Figure 4.14. Electric field variation at the ground for different distances

IV.4.3 Trajectories of the charged particles in the separation zone

We illustrate in Figures 4.15-4.18, the trajectories of 2 mm and 4 mm polypropylene (PP) particles in the separation zone for three different values of the voltage applied to the active electrode (20 kV, 25 kV and 30 kV) and three different distances between the electrodes of 80 mm, 95 mm and 110 mm. These trajectories were obtained numerically.

The results demonstrate that charged particles of small size (2 mm) are strongly influenced by electrostatic forces, which dominate over the gravitational force due to their light mass. Under varying applied voltages and electrode distances, particles are accelerated toward the oppositely charged electrode and repelled when their charge matches the electrode polarity. As voltage increases, the electric field strength E=V/d rises, enhancing the electrostatic force F_e=qE and particle acceleration. The observed trajectories confirm that particles can be guided without direct collision, enabling efficient control of their motion. These findings are essential for optimizing the design of electrostatic separators, particularly in determining the placement of collector compartments, with particles ultimately gathering in the designated zone.

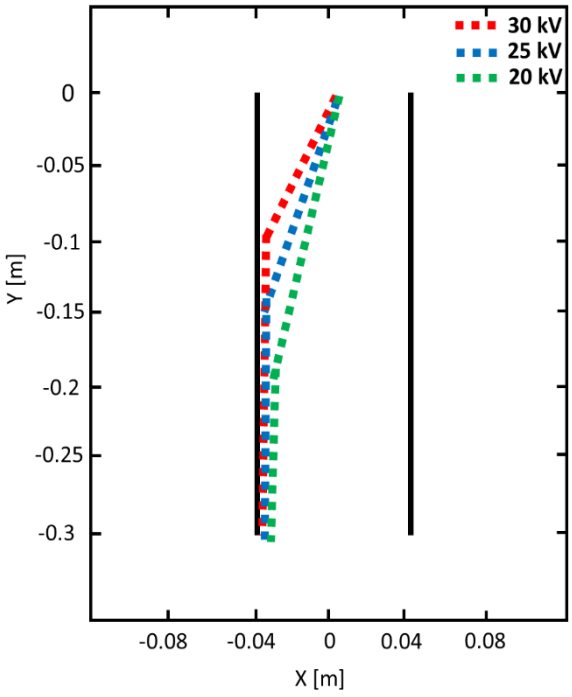

Figure 4.15. Trajectories variation with applied voltages for particle of size 2 mm

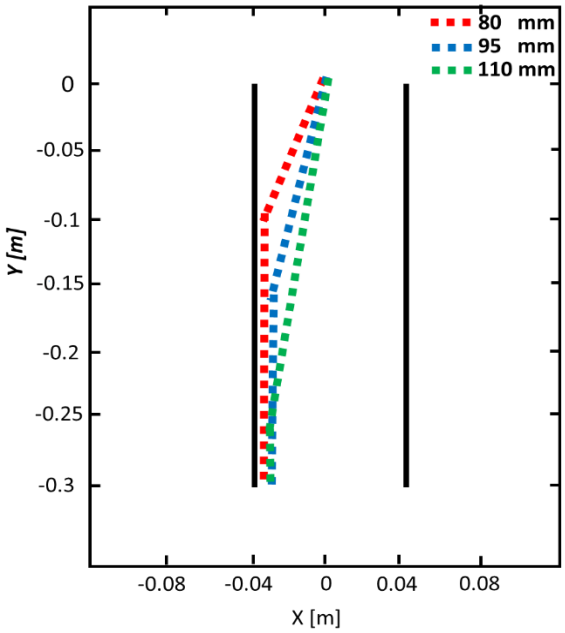

Figure 4.16. Trajectories variation with different distances for particle of size 2 mm

For the case of a charged particle of 4 mm diameter, the results reveal a clear ratio between gravitational and electrostatic forces, with gravity proving dominant. Due to its larger size and mass, the particle undergoes only slow acceleration, as the gravitational effect counteracts the influence of the electric field. Nevertheless, the particle's trajectory shows increasing deflection as the applied voltage rises, consistent with the proportionality of electrostatic force to field strength. Despite maintaining the same tangent path, the enhanced voltage ensures measurable deviation, guiding the particle toward the right compartment of the collector box. These findings highlight the critical interplay between particle size, applied voltage, and force balance in determining separation efficiency.

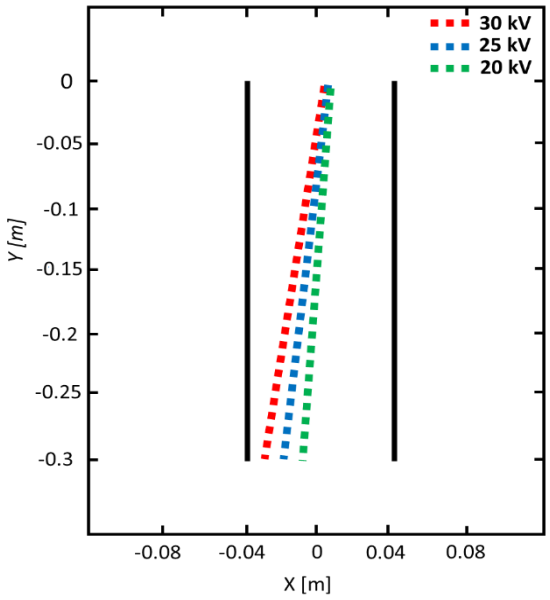

Figure 4.17. Trajectories variation with applied voltages for particle of size 4 mm

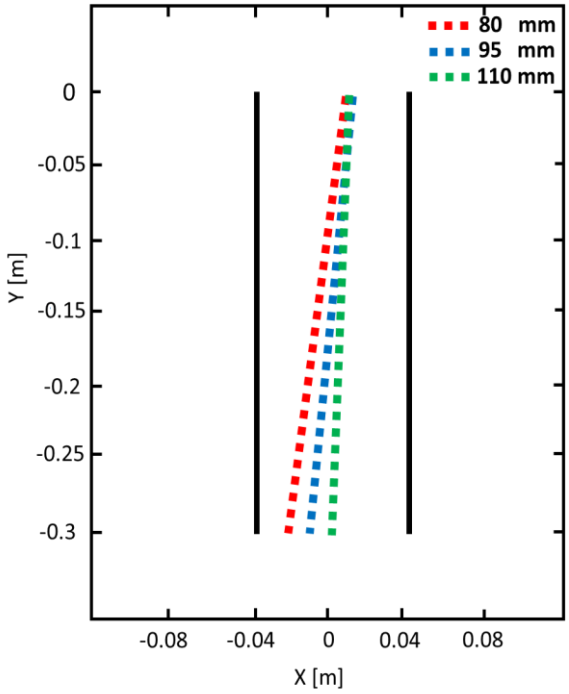

. **Figure 4.18. Trajectories variation with different distances for particle of size 4 mm**

Figure 4.19 shows the trajectories of two polypropylene (PP) particles of 2 mm and 4 mm sizes when a voltage of 30 kV is applied and there is an inter-electrode distance of 80 mm.

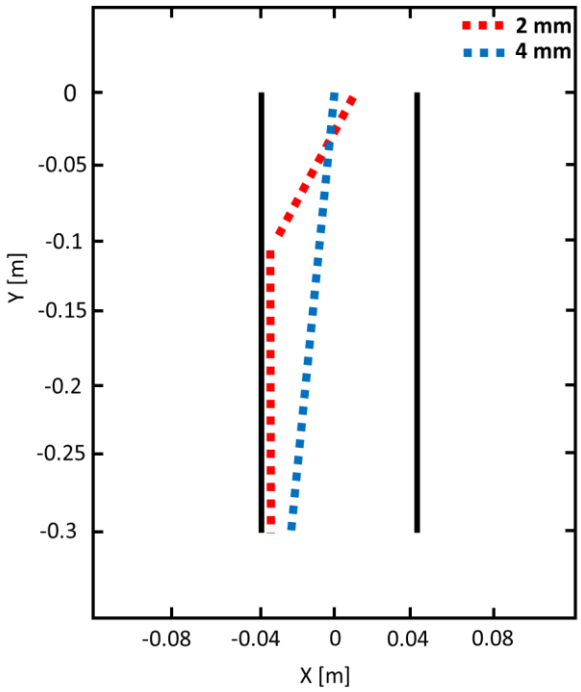

Figure 4.19. Trajectories variation particles of size 2 mm and 4 mm at 30 kV and 80 mm

IV.5 Conclusion

The results obtained through simulation allow us to formulate the following conclusions:

The integration of the photovoltaic system as a power source for electrostatic separators, and give it high priority according to the recommendation of the new energy system due to its numerous advantages and effective contribution to sustainable development.

The multi-point configuration used in this work has a exhibits high efficiency for charging the insulating particles.

To study the particles trajectories, a numerical model based on the Euler-Cromer method, which relies on the calculation of the electric field intensity, which is done by the COMSOL Multiphysics software, and programmed in MATLAB software, is an effective and validated tool for the study of the particles trajectories.

The numerical simulation has provided a profound comprehension of various phenomena that occur in the electrostatic separation zone. It is also considered a tool to validate experimental results.

GENERAL

CONCLUSION

Electrostatics plays a crucial role in emerging technologies by enabling the precise control of particles and surfaces. It is fundamental to touch screens, industrial painting, laser printers, nanotechnology, air purifiers, and particle separation. This technology improves productivity, reduces waste, and enables advancements in electronics and biophysics.

Electrostatics is a crucial branch of physics that studies the interactions between electric charges at rest. The basics of electrostatics are not only fundamental for physicists but also essential for anyone interested in electronics. Understanding the various forces at play and the concept of an electric field may seem complex, but this exploration demystifies these key elements.

In electrostatic separators, depending on the composition of the mixtures to be separated, three physical mechanisms of electrical charging are implemented: triboelectric charging, corona discharge, and electrostatic induction. Two of these mechanisms can be positioned in series along the particle trajectory and have reciprocal influences on the electric field.

Plastic waste shredding processes generate between 15% and 25% granular and powdered plastic materials, the recycling and recovery of which require research and development of new physical separation techniques based on a better understanding of these types of insulating particles. The electrical charging mechanism modeling, represented by a corona discharge with electrostatic field separation, is an efficient method for separating insulating granular and powdery materials, ensuring effective control of the forces acting on the fine particles and their trajectories within the separation zone. The charging device is a multi-point active electrode to increase the separation rate.

In this work, the charging device is a multi-point active electrode to increase the separation rate. We developed a mathematical model and performed a numerical analysis of the various characteristics of the electrostatic separation system. Essentially, we determined the electric field, the electric charge density and potential distribution, the system efficiency, and the particle trajectories as a function of the applied voltage and the dielectric permeability for conductor, semiconductor, and insulating materials.

We used a dynamic and autonomous model powered by photovoltaic energy, developing a computational code to solve the system of coupled equations, the current continuity equation, and the Poisson equation through successive approximations.

We conducted the study for a 2D configuration to simplify the work and to refine the structured mesh redefinition technique. We tested several numerical techniques to solve Maxwell's equations.

The significant contributions of this thesis are:

- Numerical simulation of particle trajectories makes a crucial contribution to particle separation by enabling:
  - Process optimization: it helps design more efficient systems and adjust parameters to improve yield.
  - Understanding the mechanisms: it allows for the analysis of forces and interactions influencing particle motion.
  - Reducing experimental testing: it limits costs and time by replacing certain physical tests with simulations.
  - Predicting behavior: it anticipates the efficiency based on the characteristics of the particles (size, density, shape).
- The impact of electrostatic separation on the socio-economic aspect:
  - Cost reduction: decreased raw material losses.
  - Process efficiency: improved recovery of useful materials.
  - Technological innovation: development of new equipment and methods.
  - Sustainability: reduction of waste and environmental impact.
  - Scientific advancement: exploration of complex physical phenomena.
  - Specialized training: development of engineering skills.
  - Interdisciplinary collaboration.

This thesis work opens up numerous perspectives for the technological applications of electrostatics. We can cite the following key research areas:

- Validation of the numerical simulation results through experimental work in specialized laboratories, by actually building the proposed autonomous electrostatic separator;
- Improvement of the study of the electrical separation process using new real-time simulation software;
- Performing measurements on the efficiency of electrostatic separators under different conditions through particle size analysis by introducing particles of varying diameters. To determine the influence of conveyor belt speed and the movement of fine particles.

Bibliographic References

Int.g

[1] A. Deprouw, M. Jover, S. Chouvenc, and E. Fangeat, 'Annual report of the register of waste electrical and electronic equipment. 2016 data', Deloitte développement durable, 2017.
www.ademe.fr/mediatheque

[2] X.N. Yang, L.S. Sun, J. Xiang, S. Hu, and S. Su, "pyrolysis and dehalogenation of plastics from waste electrical and electronic equipment (weee): A review," Waste Management, Vol. 33, pp. 462-473, Feb. 2013.
https://doi.org/10.1016/j.wasman.2012.07.025

[3] C. P. Baldé, R. Kuehr, O. Deubzer et al., 'Global Report on Waste Electrical and Electronic Equipment'. The Global Ewaste Monitor GEM, 2024.
www.globalewaste.org

[4] R. Taurino, P. Pozzi, and T. Zanasi, 'facile characterization of polymer fractions from waste electrical and electronic equipment (weee) for mechanical recycling', Waste Management, Vol. 30, pp. 2601-2607, Dec. 2010.
https://doi.org/10.1016/j.wasman.2010.07.014

[5] E. Williams, R. Kahhat, B. Allenby, E. Kavazanjian, J. Kim, and M. Xu, 'Environmental, social, and economic implications of global reuse and recycling of personal computers', Environmental Science & Technology, Vol. 42, no 17, pp. 6446-6454, 2008.
https://doi.org/10.1021/es702255z

[6] T. Huth-Fehre et al., 'NIR-Remote sensing and artificial neural networks for rapid identification of post-consumer plastics', Journal of Molecular Structure, Vol. 348, pp. 143-146, 1995.
https://doi.org/10.1016/0022-2860(95)08609

[7] D. M. Scott, 'A two-colour near-infrared sensor for sorting recycled plastic waste', Measurement Science and Technology, Vol. 6, no 2, pp. 156, 1995.
https://doi.org/10.1088/0957-0233/6/2/004

[8] M. R. Gent, M. Menendez, J. Toraño, D. Isidro, and S. Torno, 'Cylinder cyclone (LARCODEMS) density media separation of plastic wastes', Waste Management, Vol. 29, no 6, pp. 1819-1827, 2009.
https://doi.org/10.1016/j.wasman.2008.12.026

[9] G. Dodbiba, A. Shibayama, T. Miyazaki, and T. Fujita, 'Separation performance of PVC and PP plastic mixture using air table', Physical Separation in Science and Engineering, Vol. 12, no 2, pp. 71-86, 2003.
https://doi.org/10.1080/1478647031000139385

[10] F. Burat, A. Güney, and M. O. Kangal, 'Selective separation of virgin and post-consumer polymers (PET and PVC) by flotation method', Waste Management, Vol. 29, no 6, pp. 1807-1813, 2009.
https://doi.org/10.1016/j.wasman.2008.12.018

[11] H. Shent, R. J. Pugh, and E. Forssberg, 'A review of plastics waste recycling and the flotation of plastics', Resources, Conservation and Recycling, Vol. 25, no 2, pp. 85-109, 1999.
https://doi.org/10.1016/S0921-3449(98)00017-2

[12] S. Mouhoub, M. Kachi, and N. Zouzou, 'Influence of the initial charge on the triboelectrification of millimeter size set of particles in an inclined tube', Powder Technology, Vol. 428, pp. 118862, 2023.
https://doi: 10.1016/j.powtec.2023.118862

[13] A.M. Lopez-Paneque, V.H.G. García-Orta, J. M Gallardo, R. E. Sepúlveda-Ferrer, and E.Chicardi, 'The Influence of Electrostatic Separation Parameters on the Recovery of Metals from Pre-Crushed PCBs', Metals, Vol. 15, no 8, pp.826, 2025.
https://doi.org/10.3390/met15080826

[14] K. Enders, S. T. Alexander, and M. Labrenz, 'Evaluation of electrostatic separation of microplastics from mineral-rich environmental samples', Front. Environ. Sci., Vol. 8, pp.1-9, 2020.
https:// doi: 10.3389/fenvs.2020.00112

[15] J. Wang, M.D.Wit, R. M. Boom, and M.A.I. Schutyser, 'charging and separation behavior of gluten–starch mixtures assessed with a custom-built electrostatic separator", Separation and Purification Technology, Vol. 152, pp. 164-171, 2015.
https://doi.org/10.1016/j.seppur.2015.08.025

[16] S. D. Achilias, and E. V. Antonakou, 'chemical and thermochemical recycling of polymers from waste electrical and electronic equipment', In Recycling Materials Based on Environmentally Friendly Techniques, Publisher: In Tech, July 15, 2015.
https://doi.org/10.5772/59960

[17] I.I. Inculet, G.S.P. Castle, and J.D. Brown, 'Electrostatic separation of plastics for recycling', Part Sci. & Technol., Vol. 16, pp. 1691–100, 1998.
https://doi.org/10.1049/iet-smt.2018.5417

CH1

[18] J. B. Bahers, 'Dynamiques des filières de récupération-recyclage et écologie territoriale : l'exemple du traitement des déchets d'équipements électriques et électroniques (DEEE) en Midi-Pyrénées', Thèse de Doctorat, Université de Toulouse, France, 2012.

[19] V. Forti, C. P. Baldé, R. Kuehr, and G. Bel, 'Suivi des déchets d'équipements électriques et électroniques à l'échelle mondiale pour 2020 : quantités, flux et possibilités offertes par l'économie circulaire', Université des Nations Unies, Bonn/Genève/Rotterdam, UNU/UNITAR et ITU, 2020.
ISBN: 978-92-808-9124-9

[20] R. Gupta, D. Gidaspow, and D.T. Wasan, 'Electrostatic separation of powder mixtures based on the work functions of its constituents', Powder Technology, Vol. 75, no 1, pp. 79-87, 1993.
https://doi.org/10.1016/0032-5910(93)80027-8

[21] Y. Higashiyama, and K. Asano, 'Recent progress in electrostatic separation technology', Particulate Science and Technology, Vol.16, no 1, pp.77-90, 1998.
https://doi.org/10.1080/02726359808906786

[22] I. I. Inculet, 'Electrostatic minerals separation. John Wiley and Sons', Inc., New York, 1984.

[23] J. J. Spitzer, 'New electrostatic model for highly charged surfaces', Colloids and Surfaces, Vol. 12, 1984.

[24] C. Dragan, 'Modélisation du processus de charge et séparation tribo-aéro-électrostatique des matériaux plastiques granulaires', Thèse Doctorat, Université de Poitiers, France, 2010.

[25] S. D. Achilias, and E. V. Antonakou, 'chemical and thermochemical recycling of polymers from waste electrical and electronic equipment', In Recycling Materials Based on Environmentally Friendly Techniques, Publisher: In Tech, July 15, 2015.
https://doi.org/10.5772/59960

[26] L. Dascalescu, A. Samuila, A. Mihalcioiu, S. Bente, and A. Tilmatine, 'Robust design of electrostatic separation processes', IEEE Trans. Ind. Appl., Vol. 41, pp. 715-720, 2005.
https://doi.org/10.1109/TIA.2005.847308

[27] D.M Taylor, and P.E Secker, 'Industrial Electrostatics: Fundamentals and Measurements,' Baldock, UK: Research Studies Press, 1994.

[28] L. Dascalescu, A. Iuga, R. Morar, A. Samuila, V. Neamtu, and I. Suarasan, ''Corona charging of particulates in the corona field of roll-type electroseparators,' J. Phys. D: Appl. Phys., Vol. 27, pp. 1242-1251, 1994.

[29] J.M. Crowley, 'Fundamentals of Applied Electrostatics', Morgan Hill, California: Laplacian Press, 1999.

[30] C.H. Park, N. Subasinghe, and H.S. Jeon, 'Separation of covering plastics from particulate copper in cable wastes by induction electrostatic separation', Materials Trans. Vol. 56, pp. 1140-1143, 2015.

[31] H.J. White, 'Industrial Electrostatic Precipitation', London, U.K.: Addison-Wesley, 1963.

[32] J.A. Giacometti, S. Fedosov, and M.M. Costa, 'Corona charging of polymers: recent advances on constant current charging', Brazilian Journal of Physics, Vol. 29, pp. 269-279, 1999.
https://doi.org/10.1590/S0103-97331999000200009

[33] L. Dascalescu, A. Iuga, R. Morar, V. Neamtu, I. Saurasan, A. Samuila and D. Rafiroiu, 'Corona and electrostatic electrodes for high-tension separators', J. Electrostat., Vol. 29, no. 3, pp. 221-225, 1993.

[34] A. Abahazem, 'Etudes expérimentales des décharges couronne pour la dépollution des gaz', Thèse de Doctorat, Université de Toulouse III – Paul Sabatier, 2009.

[35] B. Tabti, R. Mekideche, M. Plopeanu, L. Dumitran and L. Dascalescu, 'Corona Charging and Charge Decay Characteristics of Non-woven Filter Media, IEEE Trans. Ind. Appl., Vol. 46, pp. 634-640, 2010.

[36] A. Antoniu, B. Tabti, M. Plopeanu and L. Dascalescu, 'Accelerated discharge of corona-charged non-woven fabrics', IEEE Trans. Ind. Appl., Vol. 46, pp. 1188-1193, 2010.

[37] L. Dascalescu, A. Mizuno, R. Tobazéon, et al,'Charges and forces on conductive particles in roll-type corona-electrostatic separators', IEEE Trans. Ind. Appl., Vol. 31, pp. 947–956, 1995.
https://doi.org/10.1109/28.464503

[38] L. Dascalescu, S. Vlad, A. Iuga, and P. L. Levin, 'Electrostatics of conductive particles in contact with a plate electrode affected by a nonuniform electric field', J. Phys. D: Appl. Phys., Vol. 34, pp. 60–67, 2000.
https://doi.org/10.1088/0022-3727/34/1/311

[39] M.C. Plopeanu, L. Dascalescu, B. Neagoe, A. Bendaoud, and P.V. Notingher, 'Characterization of two electrode systems for corona-charging of non-woven filter media', J. Electrostat, Vol. 71, pp. 517-523, 2013.

[40] A. Samuila, M. Blajan, R. Beleca, M. Huzau, R. Morar, L. Dascalescu, and A. Iuga, 'Modeling of wire corona electrode operation in electrostatic separation at small and large gaps', J. Electrostat., Vol. 63, pp. 955-960, 2005.

[41] Govi, 'Quelques expériences sur l'induction électrostatique',J. Phys. Theor. Appl., Vol. 4, pp.264-266, 1875.

[42] W. A. G. Richard, A.R. Salama, K. Medles, C. Lubat, S. Touhami, and L. Dascalescu, 'Electrostatic Separation of two Types of Copper Wires from Electric Cable Wastes', Proc. Electrostatics Joint Conference, West Lafayette, USA,13-17 June 2016.

[43] C. Mayer-Laigle, A. Cadin, S. Messal, L. Dascalescu, and X. Rouau, 'Dry fractionation of plant material powders using an electrostatic corona separator: a model study', 5th International Congress on Green Process Engineering, Canada, 2016.

[44] L.H. Lee, 'Dual mechanism for metal polymer contact electrification', J. Electrostat., Vol. 32, pp. 1-29, 1994.
https://doi.org/10.1016/0304-3886(94)90026-4

[45] W.R. Harper, 'Contact and Frictional Electrification', Morgan Hill, CA: Laplacian Press, 1998.
ISBN: 9781885540065, 188554006X

[46] A. Iuga, L. Calin, V. Neamtu, A. Mihalcioiu, and L. Dascalescu, 'Tribocharging of plastics granulates in a fluidized bed device', J. Electrostat, Vol. 63, pp. 937-942, 2005.
https://doi.org/10.1016/j.elstat.2005.03.064

[47] S. Nicoara, L. Calin, A. Iuga, and N. Serban, 'Considerations on triboelectrostatic separation of plastic material for recycling purpose', Environment and Progress, Vol. 6, pp.341- 346, 2006.

[48] M. Blajan, R. Beleca, A. Iuga, and L. Dascalescu, 'Triboelectrification of granular plastic wastes in vibrated zigzag-shaped square pipes in view of electrostatic separation', IEEE Trans. Ind. Appl., Vol 46, pp.1558 – 1563, 2010.
https://doi.org/10.1109/TIA.2010.2049552

[49] G. Buda, A. Samuila, S. Atroune, M. Bilici, and L. Dascalescu, 'Set point identification of a tribocharging process for mixed granular solids', J. Electrostat. Vol. 71, pp. 407-412, 2013.
https://doi.org/10.1016/j.elstat.2012.11.026

[50] E.G. Kelly and D.J. Spottiswood, 'The theory of electrostatic separations: a review, part 1, Fundamentals', Miner Eng, Vol 2, pp. 33-46, 1989.

[51] G.S.P. Castle, 'Contact charging between insulators', J. Electrostat, Vol. 40 and 41, pp. 13-18, 1997.
https://doi.org/10.1016/S0304-3886(97)00009-0

[52] W. Jing, and M.J. Realff, 'Design and optimization of free-fall electrostatic separators for plastics recycling', AIChE J, Vol. 49, pp. 3138-3149.2003.

[53] V. Gente, F.L. Marca, F. Lucci and P. Massacci, 'Electrical separation of plastics coming from special waste', Waste Manag, Vol. 23, pp. 951-958, 2003.

[54] R.D. Pascoe, and B.O. Connel, 'Development of a method for separation of PVC and PET using flame treatment and flotation', Miner Eng, Vol. 16, pp. 1205-1212, 2003.

[55] M. Sarki and A. Masumoto, 'Electrostatic separation of chopped waste electric cables', Journal of Environmental Engineering, Vol. 2, pp 227-236, 2007.

[56] Y. Higashiyama and K. Asano, 'recent progress in electrostatic separation technology', particulate science and technology, Vol. 16, pp.77-90, 1998.

[57] G. Wu, J. Li, and Z. Xu, Z. 'Triboelectrostatic separation for granular plastic waste recycling: A review', Waste Management, Vol. 33, pp. 585–597, 2013.

[58] E. Lévy, 'Dictionary of Physics', Paris, pp. 601,1988.

[59] Y. Matsushit, N. Mori and T. Sometani, 'Electrostatic separation of plastics by friction mixer with rotary drum blades', Electrical Engineering in Japan, Vol.127, pp. 33–40, 1999.

[60] S. Messal, T. Zeghloul, A. M. Benhafssa, and L. Dascalescu, 'Belt-Type Corona-Electrostatic Separator for the Recovery of Conductive and Nonconductive Products From Micronized Wastes', IEEE Trans. Ind. Appl., Vol. 53, pp. 1424- 1430, 2017. https://doi.org/ 10.1109/TIA.2016.2622684

[61] I. E. Achouri, T. Zeghloul, G. Richard, K. Medles, H. Nouri, and L. Dascalescu, 'Factors that Influence the Performance of a Two-Rotating Disks-Type Tribo-Aero Electrostatic Separator for Micronized WEEE', IEEE Trans. Ind. Appl,, Vol. 55, pp. 802-811, 2019.

[62] Z. Chen, F. Liu, L. Wang, Y. Li, R. Wang, and Z. Chen, 'Tribocharging properties of wheat bran fragments in air–solid pipe flow', Food Research International, Vol. 62, pp. 262–271, 2014.

[63] Z. Chen, L. Wang, R. Wang, Y. Li, and Z. Chen, 'Triboelectric separation of aleurone cell-cluster from wheat bran fragments in non-uniform electric field', Food Research International, Vol. 62, pp. 111–120, 2014.

CH2

[64] O. Chibane, 'Contribution à la caractérisation expérimentale des électrodes couronne multi-fils', Thèse de doctorat, Université de Bejaia, 2025.

[65] L. B. Loeb, 'Electrical coronas: Their basic physical mechanisms', Berkeley, University of California press, 1965.

[66] J. D. Skalny, T. Mikoviny, S. Matejcik and N. J. Mason, 'An analysis of mass spectrometric study of negative ions extracted from negative corona discharge in air', international journal of mass spectrometry, Vol. 233, pp. 317-324, 2004.

[67] B. Held and R. Peyrous, 'physical and chemical studies of corona discharges in air', CZECH. J. Phys., Vol. 49, no. 3, pp. 301-320, 1999.

[68] P. Bérard, 'Contrôle d'écoulement par décharge plasma à pression atmosphérique', Thèse de doctorat de l'école central de Paris, France, 2008.

[69] C. Junhong, 'Direct current corona-enhanced chemical reactions', Thèse de doctorat de l'université Minnesota, Etats-Unis, 2002.

[70] H. Nouri, 'Influence des paramètres physiques de l'air sur le précipitateur électrostatique d'aérosols', Thèse de doctorat, Université de Bejaia, 2010.

[71] J. F. Loiseau, J. Batina, F. Noël, and R. Peyrous, 'Hydrodynamical simulation of the electric wind generated by successive streamers in a point-to-plane reactor', J. Phys. D: Appl. Phys., Vol. 35, pp. 1020-1031, 2002.

[72] M. Goldman, A. Goldman, and Sigmond R.S, 'The corona discharge, its properties and specific uses', Pure and Appl. Chem. Vol. 57, no .9, pp. 1353-1362, 1985.

[73] P. Bérard, D. A. Lacoste, and O. Laux, 'Corona Discharges In Atmospheric Air Between A Wire And Two Plates''. Ieee Transaction On Plasma Science, Vol. 39, no. 11, pp. 2248-2249, 2011.

[74] T. M. P. Briels, J. Kos, G. J. J. Winands, E. M. van Veldhuizen, and Ute Ebert, 'Positive and negative streamers in ambient air: measuring diameter, velocity and dissipated energy', J. Phys. D: Appl. Phys., Vol. 41, p. 234004, 2008.
https://doi.org/10.1088/0022-3727/41/23/234004

[75] M. Goldman, R. S. Sigmond, 'Corona insulation'. IEEE Trans. Elec. Ins., EI. 12/2, pp.90-105, 1982.

[76] M. El Feddi, Z. Ren, A. Razek, and A. Bossavit, 'Homogenisation technique for Maxwell Equations in periodic structures', IEEE Trans. Magnet., Vol. 33, pp. 1382-1385, 1997.

[77] R. Courant, 'Varational methods for solution of problems of equilibrium and vibrations', Bull. Amer. Math. Soc., Vol. 49, pp. 1-23, 1943.

[78] P. Silvester, 'Finite elements for electrical engineers', Cambridge University Press, Cambridge, 1996.

CH3

[79] L.B. Loeb, 'Fundamental Processes of Electrical Discharge in Gases', John Wiley and Sons, 1939.

[80] L. Zhao, and K. Adamiak, 'Numerical simulation of the electrohydrodynamic flow in a single wire-plate electrostatic precipitator', IEEE Trans. Ind. Appl. Vol. 44, pp. 683-691, 2008.
https://doi.org/10.1109/TIA.2008.921453

[81] E. Kuffel, 'High Voltage Engineering', Pergamon Press, Oxford, UK, 1984.

[82] H. Nouri, N. Zouzou, E. Mreau, L. Dascalescu, and Y. Zebboudj, 'Effect of Relative Humidity on Current-Voltage Characteristics of an Electrostatic Precipitator', J. Electrostat, Vol. 70, pp.20-24, 2012.
https://doi.org/10.1016/j.elstat.2011.08.011

[83] K.R. Parker, 'Applied Electrostatic Precipitation', Edition Kluwer Academic Publishers, London, 1997.

[84] D. Zhang, Z. Chen, F. Zhong, and Z. Zhou, 'Experimental Study on Dust Removal Performance of Electrostatic Water Film Cyclone Dust Collector', Int. J. of Rotating Machinery, Vol. 3, pp. 1-9, 2023.
https://doi.org/10.1155/2023/9959052

[85] X. Zhou, M. Dong, J. Mi, and S. Du, 'Study of grounded pole atomized corona discharge coupled with screen dust collection pole laminated dust collector', J. Chem. Eng. of Japan, Vol. 56, pp. 1-11, 2023.
https://doi.org/10.1080/00219592.2023.2197461

[86] O. Anttalainen, E. Lattouf, P. Vanninen, H. Hakulinen, T. Kotiaho, and G. Eiceman, 'Computational analysis of an electrostatic separator design for removal of volatile organic compounds from indoor air', J. Air & Wast. Manag. Ass., Vol. 73, pp. 877–889, 2023.
https://doi.org/10.1080/10962247.2023.2265329

[87] H. Fu, W. Xu, S. Li, Z. Liu, and K. Yan, 'Convective heat transfer enhancement by corona discharge in a wire–cylinder electrostatic precipitator with the water-cooling system', J. Electrostat, Vol. 125, 103845, 2023.

[88] M. B. Fayyad, A. Asipuela, and T. Iváncsy, 'The effect of the corona wire distribution with W-type of collecting plate son the characteristics of electrostatic precipitators', J. Electrostat, Vol. 125, 103841, 2023.

[89] F. d. A. Lima, and V. G. Guerra, ''Influence of wire spacing and plate spacing on electrostatic precipitation of nanoparticles: An approach involving electrostatic shielding and diffusion charging', J. Particuology, Vol. 80, pp. 127-139, 2023. https://doi.org/10.1016/j.partic.2022.11.018

[90] Z. Long, and Q. Yao, 'Evaluation of various particle charging models for simulating particle dynamics in electrostatic precipitators', Journal of Aerosol Science, Vol. 41, pp. 702–718, 2010.

[91] M. Aissou, H. Ait said, H. Nouri, and Y. Zebboudj, 'Analysis of current density and electric field beneath a bipolar DC wires-to-plane corona discharge in humid air', Eur. Phys. J.Appl.Phys. Vol. 61, 30803, 2013.

[92] A. W. Yuen, 'Collector current density and dust collection in Wire-Plate Electrostatic Precipitators. PHD Thesis, School of Materials Science and Engineering', University of New South Wales, Australia, 2006.

[93] H. Nouri, N. Zouzou, L. Dascalescu, and Y. Zebboudj, 'Investigation of relative humidity effect on the particles velocity and collection efficiency of laboratory scale electrostatic precipitator', Process Safety and Environmental Protection, IchemE, Institution of Chemical Engineers Part A, Vol. 104, pp. 225–232, 2016.

[94] L. Dascalescu, R. Morar, A. Iuga, A. Samuila, and V. Neamtu, 'Electrostatic separation of insulating and conductive particles from granular mixes', Particulate Science and Technology, Vol. 16, pp. 25-42, 1998. https://doi.org/10.1080/02726359808906782

[95] L. Dascalescu, A. Mizuno, R. Tobazéon, A. Iuga, R. Morar, M. Mihailescu, A. Samuila, 'Charges and forces on conductive particles in roll-type corona-electrostatic separators', IEEE Trans. Ind. Appl., Vol. 31, pp. 947-956, 1995.

[96] S. R. Korzhenevskiy, A. A. Komarskiy, A. V. Ponomarev, A. S. Chepusov, and O. D. Krasniy, 'Application of a nanosecond corona discharge generator for electrical separation of ores', J. Phys.: Conf. Ser., IOP Publishing, Vol. 2064, P012089, 2021.

[97] A. J. Medelin, C. A. J. Fletche, and R. Morrow, 'A pseudo-transient approach to steady state solution of electric field-space charge coupled problems', J. Electrostat, Vol. 43, pp. 39-60, 1997.

[98] M. Al- Hamouz, 'A combined algorithm based on finite elements and a modified method of characteristics for the analysis of the corona in wire duct Electrostatic precipitators', IEEE Trans. Ind. Appl., Vol. 38, pp. 43-49, 2002. https://doi.org/10.1109/28.980343

[99] M. Abdel-Salam, and D. Wiitanen, 'Calculation of corona onset voltage for duct– type precipitators', IEEE Trans. Ind. Appl., Vol. 29, pp. 274-280, 1993. https://doi.org/10.1109/28.216532

[100] K. Adamiak, and P. Atten, 'Simulation of corona discharge in point–plane configuration', J. Electrostat, Vol. 61, pp. 85– 98, 2004.

[101] H. Nouri, H. Ait Said, Y. Zebboudj, N. Zouzou, and L. Dascalescu, 'Analysis of Electric Field and Current density in an Electrostatic Precipitator', IEEE Transactions on Dielectrics and Electrical Insulation, Vol. 23, pp. 665- 670, 2016.

[102] K. Adamiak, 'Adaptative approach to finite element modelling of corona fields', IEEE Trans. Industry. Appl., Vol. 30, pp. 387 – 393, 1994. https://doi.org/10.1109/28.287518

[103] O. Molchanov, K. Krpec, J. Horák, L. Kuboňová, and F. Hopan, ''Comparison of methods for evaluating particle charges in the electrostatic precipitation of fly-ash from small-scale solid fuel combustion'. Separation and Purification Technology, Vol. 248, 117057, 2020.

[104] H. Nouri, M. Aissou, H. Ait Said, and Y. Zebboudj, 'Finite Element Method Investigation of Electrostatic Precipitator Performance', International Journal of Numerical Modelling: Electronic Networks, Devices and Fields, John &Wiley, Vol. 28, pp. 138–154, 2015.

[105] K. Adamiak, and P. Atten, 'Numerical simulation of the 2-D gas flow modified by the action of charged fine particles in a single-wire ESP', IEEE Trans. Diel. Electr. Insul., Vol. 16, pp.608 – 614, 2009. https://doi.org/10.1109/TDEI.2009.5128495

[106] H. Nouri, M. Aissou, and Y. Zebboudj, 'Modeling and simulation of the effect of Pressure on the corona discharge for wire plane configuration'', IEEE Transactions on Dielectrics and Electrical Insul. Vol. 20, pp. 1547-1553, 2013.

[107] F.W. Peek, ''Dielectric Phenomena in High Voltage Engineering', McGraw-Hill Press, New York, 1929.

[108] A. Mizuno, 'Electrostatic precipitation', IEEE Trans. Dielectr. Electr. Insul., Vol. 7, pp. 615-624, 2000.

[109] J. P. Reynolds, L. Theodore, and J. Marino, 'Calculating collection efficiencies for electrostatic precipitators', Journal of the Air Pollution Control Association, Vol. 25, pp. 610-616, 1975.

[110] Z. Yang, C. Zheng, S. Liu, Y. Guo, C. Liang, X. Zhang, Y. Zhang, and X. Gao, 'Insights into the role of particle space charge effects in particle precipitation processes in electrostatic precipitator', Powder Technology, Vol. 339, pp. 606-614, 2018.

CH4

[111] K. Latreche, R. Taleb, A. Bentaallah, A.E. Toubal Maamar, M. Helaimi, and F. Chabni, 'Design and experimental implementation of voltage control scheme using the coefficient diagram method based PID controller for two-level boost converter with photovoltaic system', Electrical Engineering & Electromechanics, Vol. 1, pp. 3-9, 2024. https://doi.org/10.20998/2074-272X.2024.1.01

[112] H. Bounechba, A. Boussaid, and A. Bouzid, 'Experimental validation of fuzzy logic controller based on voltage perturbation algorithm in battery storage photovoltaic system', Electrical Engineering & Electromechanics, Vol. 5, pp. 20-27, 2024. https://doi.org/10.20998/2074-272X.2024.5.03

[113] A. Zorig, N. Hamouda, B. Babes, and S. Mouassa, 'Improving the efficiency of a non-ideal grid coupled to a photovoltaic system with a shunt active power filter using a self-tuning filter and a predictive current controller', Electrical Engineering & Electromechanics, Vol. 6, pp. 33-43, 2024. https://doi.org/10.20998/2074-272X.2024.6.05

[114] H. Salhi, S. Louarem, F. Z. Kebbab, and H. Nouri, 'Optimization of renewable source energy and FACT integration in distribution network based on Shark Smell method', Przegląd Elektrotechniczny, Vol. 101, no .9, 2025. ISSN: 00332097 http://pe.org.pl

[115] H. Salhi, 'Analyse technico-économique des solutions d'intégration des énergies renouvelables intermittentes dans le réseau de distribution'. PHD Thesis, University Setif 1, Algeria, 2025.

[116] N. Guettaf, Z. Anane, S. E. I. Guettaf, F. Hassaine, and H. Nouri, 'Study of the different parameter corona discharge in point-plane Electrostatic Separator', 2022 19th International Multi-Conference on Systems, Signals & Devices (SSD), pp.1831-1835, 2022. https://doi.org/10.1109/SSD54932.2022.9955502

[117] N. Guettaf, H. A. Said, M. Aissou, T. Zeghloul, and H. Nouri, 'Modeling a Corona Discharge Separation of Fine Particles for Different Materials Used in Electrical Engineering', Advanced Engineering Forum, Vol. 54, pp. 77–90, 2025. https://doi.org/10.4028/p-u8gcnx

[118] B-u. Kim, O-h. Han, H-s. Jeon, S-h. Baek, and C-h. Park 'Trajectory Analysis of Copper and Glass Particles in Electrostatic Separation for the Recycling of ASR', Metals, Vol. 7(10):434, 2017. https://doi.org/10.3390/met7100434

[119] Y. Qin, K. Gao, J. Li, and Z. Xu, 'Particle trajectory model for tribo-electrostatic separating mixed granular plastics', Cleaner Engineering and Technology, Vol. 4, 100219, 2021. https://doi.org/10.1016/j.clet.2021.100219

[120] P.M. Ireland, 'Modelling dense particle streams during free fall electrostatic separation', Powder Technology, Vol. 434,119290, 2024. https://doi.org/10.1016/j.powtec.2023.119290

[121] Z. M. Xu, J. Li, H. Z. Lu, and J. Wu, 'Dynamics of conductive and nonconductive particles under high-voltage electrostatic coupling fields',Telematique, Vol. 21 (1), pp. 2359–2366, 2009. https://doi.org/10.1007/s11431-008-0198-2

[122] H.K. Dhayef, and T.H. Khalaf, 'Simulation of a corona discharge in a wire-duct electrostatic precipitator'. Sci. China Ser. E-Technol. Sci, Vol. 52, pp. 4603–4614, 2022. https://doi.org/10.1007/s11431-008-0198-2

[123] N. Guettaf., S.E.I. Guettaf, T. Zeghloul, and H. Nouri, 'Numerical study of particles trajectories in a multifunctional electrostatic separator powered by photovoltaic system', Electrical Engineering & Electromechanics, Vol. 1, pp. 69-75, 2026. https://doi.org/10.20998/2074-272X.2026.1.09

ملخص:

يعتمد الفصل الكهروستاتيكي على تطبيق القوانين الأساسية للكهرباء الساكنة لفهم الظواهر الناتجة عن الشحنات الكهربائية . تُعد هذه التقنية الحديثة وسيلة فعّالة لجعل التفاعلات بين الشحنات مرئية للمراقب بشكل مباشر. كما أنها تتيح وصفًا دقيقًا للقوى المؤثرة بين الجسيمات المشحونة أثناء عملية الفصل. وتتميز هذه التقنية بانخفاض استهلاك الطاقة مقارنة بالطرق التقليدية ، إضافةً إلى ذلك، فإن تكاليف التشغيل والصيانة منخفضة، وهو ما يعزز جدواه الاقتصادية.
يركز هذا البحث على التحليل العددي للمعايير الرئيسية المؤثرة في أداء نظام فصل كهروستاتيكي متعدد الوظائف يعمل بنظام كهروضوئي.
في الفواصل الكهروستاتيكية، تختلف آليات الشحن الكهربائي باختلاف تركيب المخاليط المراد فصلها. وتشمل هذه الآليات: الشحن الاحتكاكي، التفريغ الإكليلي، والحث الكهروستاتيكي. ويمكن دمج اثنتين من هذه الآليات على التوالي على طول مسار حركة الجسيمات لتحقيق شحن أكثر فعالية. وتؤثران بشكل متبادل على المجال الكهربائي وكثافة التيار الكهربائي.

الكلمات المفتاحية: الفصل الكهروستاتيكي، آلية شحن الجسيمات, المجال الكهربائي، النظام الكهروضوئي، النمذجة العددية، مسارات الجسيمات، نفايات المعدات الكهربائية والإلكترونية.

Résumé :

La séparation électrostatique est basée sur l'application des lois fondamentales de l'électrostatique. C'est une technologie moderne qui introduit les phénomènes créés par des charges électriques statiques pour l'observateur et décrit les forces qu'exercent les charges électriques entre elles. Elle est caractérisée par une faible consommation d'énergie, ainsi que par des coûts réduits d'exploitation et d'entretien.
Cette recherche porte sur l'analyse numérique des paramètres principaux influençant le système de séparation électrostatique multifonctionnel alimenté par un système photovoltaïque.
Dans les séparateurs électrostatiques, selon la composition des mélanges à séparer, trois mécanismes physiques de chargement électrique sont mis en œuvre : le chargement triboélectrique, la décharge couronne et l'induction électrostatique. Deux de ces mécanismes peuvent être positionnés en série dans la trajectoire des particules et avoir des influences réciproques sur le champ électrique et la densité de courant électrique.

Mots-clés: Séparation électrostatique, Mécanisme de charge de particules, Champ électrique, Système photovoltaïque, Modélisation numérique, Trajectoires de particules, Déchets d'équipements électriques et électroniques.

Abstract:

Electrostatic separation is based on the application of the fundamental laws of electrostatics. It is a modern technology that makes the phenomena created by static electric charges visible to the observer and describes the forces exerted between electric charges. It is characterized by low energy consumption, as well as reduced operating and maintenance costs.
This research focuses on the numerical analysis of the main parameters influencing a multifunctional electrostatic separation system powered by a photovoltaic system.
In electrostatic separators, depending on the composition of the mixtures to be separated, three physical mechanisms of electrical charging are implemented: triboelectric charging, corona discharge, and electrostatic induction. Two of these mechanisms can be positioned in series along the particle trajectory and have reciprocal influences on the electric field and the electric current density.

Keywords: Electrostatic separation, Particle charging mechanism, Electric field, Photovoltaic system, Numerical modeling, Particle trajectories, Waste electrical and electronic equipment.